

AD _____

Award Number: DAMD17-02-1-0315

TITLE: Targeting Breast Cancer Vasculature

PRINCIPAL INVESTIGATOR: Erkki I. Ruoslahti, M.D., Ph.D.

CONTRACTING ORGANIZATION: The Burnham Institute
La Jolla, California 92037

REPORT DATE: March 2004

TYPE OF REPORT: Annual

PREPARED FOR: U.S. Army Medical Research and Materiel Command
Fort Detrick, Maryland 21702-5012

DISTRIBUTION STATEMENT: Approved for Public Release;
Distribution Unlimited

The views, opinions and/or findings contained in this report are those of the author(s) and should not be construed as an official Department of the Army position, policy or decision unless so designated by other documentation.

BEST AVAILABLE COPY

20040903 075

REPORT DOCUMENTATION PAGEForm Approved
OMB No. 074-0188

Public reporting burden for this collection of information is estimated to average 1 hour per response, including the time for reviewing instructions, searching existing data sources, gathering and maintaining the data needed, and completing and reviewing this collection of information. Send comments regarding this burden estimate or any other aspect of this collection of information, including suggestions for reducing this burden to Washington Headquarters Services, Directorate for Information Operations and Reports, 1215 Jefferson Davis Highway, Suite 1204, Arlington, VA 22202-4302, and to the Office of Management and Budget, Paperwork Reduction Project (0704-0188), Washington, DC 20503

1. AGENCY USE ONLY (Leave blank)		2. REPORT DATE March 2004	3. REPORT TYPE AND DATES COVERED Annual (1 Mar 2003 - 29 Feb 2004)	
4. TITLE AND SUBTITLE Targeting Breast Cancer Vasculature			5. FUNDING NUMBERS DAMD17-02-1-0315	
6. AUTHOR(S) Erkki I. Ruoslahti, M.D., Ph.D.				
7. PERFORMING ORGANIZATION NAME(S) AND ADDRESS(ES) The Burnham Institute La Jolla, California 92037 E-Mail: jyu@burnham.org			8. PERFORMING ORGANIZATION REPORT NUMBER	
9. SPONSORING / MONITORING AGENCY NAME(S) AND ADDRESS(ES) U.S. Army Medical Research and Materiel Command Fort Detrick, Maryland 21702-5012			10. SPONSORING / MONITORING AGENCY REPORT NUMBER	
11. SUPPLEMENTARY NOTES				
12a. DISTRIBUTION / AVAILABILITY STATEMENT Approved for Public Release; Distribution Unlimited			12b. DISTRIBUTION CODE	
13. ABSTRACT (Maximum 200 Words) <p>The main problems with current cancer therapies, including those for breast cancer, are that they are only partially effective and highly toxic. We work on a strategy that enhances the efficacy of anti-tumor therapies, while simultaneously decreasing the side effects. Our target is the vasculature of tumors. Tumor cells depend on blood supply and the tumor vasculature is accessible through the blood stream. An added advantage is that the vasculature is composed of normal cell, which are unlikely to develop resistance to treatments.</p> <p>We identify tumor-specific vascular markers by screening phage-displayed peptide libraries in mice bearing breast cancer xenografts or endogenous transgenic breast cancers. When the libraries are intravenously injected into the mice, the phage that have specific affinity for tumor vasculature home to the tumors. These peptides can then be used to carry drugs and other therapeutics into tumors. The receptors for the peptides are potential drug targets.</p> <p>During the past year, the main findings are: (1) The discovery of a novel protein, which we have named metadherin, as a breast cancer cell surface protein that mediates the binding of the tumor cells to the lung vasculature, facilitating metastasis. (2) The identification of cell surface nucleolin as the receptor for a previously identified tumor-homing peptide, and (3) the as yet unpublished observation that antibodies to nucleolin have an anti-angiogenic activity in vitro and in vivo. These findings may lead to new ways of combating metastasis and inhibiting tumor growth.</p>				
14. SUBJECT TERMS No Subject Terms			15. NUMBER OF PAGES 46	
			16. PRICE CODE	
17. SECURITY CLASSIFICATION OF REPORT Unclassified	18. SECURITY CLASSIFICATION OF THIS PAGE Unclassified	19. SECURITY CLASSIFICATION OF ABSTRACT Unclassified	20. LIMITATION OF ABSTRACT Unlimited	

NSN 7540-01-280-5500

Standard Form 298 (Rev. 2-89)
Prescribed by ANSI Std. Z39-18
298-102

Targeting Breast Cancer Vasculature

Progress Report (Year 2: 3/1/03 – 2/29/04)

TABLE OF CONTENTS

Cover.....	1
SF 298.....	2
Table of Contents.....	3
Introduction.....	4
Body.....	4
Key Research Accomplishments.....	6
Reportable Outcomes.....	6
Conclusions.....	7
References.....	7
Appendices.....	

DOD Breast Cancer Innovator Award Progress Report Yr 02 (3/1/03 – 2/29/04)

INTRODUCTION

Toxic side effects limit the usefulness of many of the existing anti-cancer drugs. If it were possible to selectively target the drug into the tumor tissue, the efficacy of anti-tumor therapies could be enhanced while simultaneously decreasing the side effects. We are working on a targeting strategy that aims at physically concentrating therapeutic agents in tumor tissue by making use of the unique features of tumor vasculature.

Directing a therapy at the tumor vasculature has advantages: First, the vasculature is available for the therapeutic agent through the blood stream. In contrast, agents directed at the tumor cells often do not adequately penetrate into the tumor. Second, tumor cells depend on blood supply; an average of 100 tumor cells depends on one endothelial cell, making vascular therapy potentially highly effective. Finally, the vasculature is composed of normal cells, which, because they do not possess the genetic instability that is characteristic of tumor cells, are unlikely to develop resistance to treatments.

Tumor vasculature grows as the tumor grows, and this process – angiogenesis – makes tumor blood vessels distinct from normal resting blood vessels. Several anti-angiogenic therapies are in pre-clinical and clinical development. The approach we are working on, while it also targets the blood vessels, differs from these anti-angiogenic therapies in many important ways. The therapeutic agent is concentrated in tumor vessels, but it acts both on the endothelial cells and the tumor cells. Furthermore, the therapy can be directed specifically to breast cancer vasculature – both the blood vessels and the lymphatic vessels – eliminating potential side effects from targeting angiogenesis in tissue repair. Finally, we can also target pre-malignant lesions for destruction.

We have identified tissue-specific and tumor-specific vascular markers by *in vivo* screening of libraries of peptides displayed on phage. The vasculature of normal breast tissue expresses specific markers that we can selectively target with the phage-derived peptides. Tumor vasculature can be targeted through its angiogenesis-associated markers, or through blood vessels and lymphatic markers specific for individual tumor types. In this project, we profile the specialization of the vasculature, both blood vessels and lymphatic, in pre-malignant and malignant breast lesions as well as metastases. The tools developed in this work can be used to design new therapies that specifically target such lesions.

BODY

The approved tasks for this project are:

Task 1: To identify peptides that specifically home to the blood and/or lymphatic vessels of MMTV-PyMT breast cancers.

Task 2: To validate the specific blood vessel and lymphatic vessel homing of the selected peptides.

Task 3: To identify and characterize receptors for the peptides that specifically home to the blood and/or lymphatic vessels of breast cancers.

Task 4: Study the specificity of vascular entry of tumor cells by using phage libraries.

Task 5: To study the use of homing peptides in breast cancer prevention and treatment in mouse models.

During the second year of grant support we have made substantial progress:

Tasks 1 and 2. The superior tumor-homing properties of the CREKA peptide that emerged from our PyMT tumor screens, and that was described in the previous progress report, has been confirmed by two collaborators, AntiCancer Inc. and dr. Gregory Lanza at the Washington University. Characterization of this peptide and other peptides that bind to breast cancer extracellular matrix is an ongoing project. In a separate project, we have shown that homing peptides can distinguish between the vasculature of premalignant lesions and fully developed tumors (Joyce et al., 2003).

We had previously shown that the lymphatic vessels in a human breast cancer xenograft model carry a specific marker detectable with a peptide isolated from a phage library (Laakkonen et al., 2002). A nonapeptide (LyP-1) homes to lymphatic vessels in the breast cancer xenografts and in some other tumors. However, some tumors (particularly xenografts obtained with the human melanoma C8161 cells), even though they contained lymphatic vessels, were negative. We screened phage libraries for peptides that would bind to the lymphatics in the C8161 tumors. We then developed a new screening procedure for this purpose that is based on isolation of lymphatic endothelial cells (and phage bound to them) with antibodies that specifically recognize these cells. We have identified two lymphatic homing peptides for this tumor, but they home poorly, or not at all to the MDA-MB-435 tumors. Thus, a lymphatic vessel "zip code" system of the kind predicted in the original application is beginning to emerge. A paper is being prepared on the peptides that define the first elements of this "zip code system" (L. Zhang, Hoffman, J.A. and E. Ruoslahti, in preparation).

The main discovery during this past grant period relates to a novel protein, metadherin. We have shown that metadherin mediates the binding and tissue-specific metastasis of experimental breast cancer to the lungs (Brown and Ruoslahti, *Cancer Cell*, in press). Parallel microarray analysis results from a large human breast cancer study show that elevated expression of an mRNA detected with an EST representing the metadherin mRNA is an excellent marker of aggressive breast cancer (van 't Veer et al., 2002). Gene expression profiling predicts clinical outcome of breast cancer. Our study, together with these microarray results, establishes metadherin as a novel metastasis-promoting protein that is likely to be clinically important. Future studies will aim at identifying the protein to which metadherin binds in lung vasculature.

Task 3. We have identified cell surface-expressed nucleolin as a receptor for a tumor-homing peptide on the MDA-MB-435 cells. The peptide, F3, is a fragment of the nuclear protein HMGN2 (Porkka et al., 2002). F3 binds to tumor blood vessel endothelial cells and tumor cells and it also recognizes a small subpopulation of cells in the bone marrow that may represent endothelial precursor cells. These results, being prepared for publication at the time of the last report, have now been published (Christian et al., 2003). The results in this paper establish nucleolin as a marker of tumor vessels.

We also have an excellent candidate for the cell surface molecule that binds the LyP-1 peptide to tumor lymphatics and tumor cells. Transfection experiments with cDNA are in progress to confirm the identification.

Task 4. Our initial studies on the use of phage libraries to study tumor intravasation were hampered by varying uptake of the phage by the liver and spleen (presumably by the reticuloendothelial

system). We were not able to reliably distinguish phage that were preferentially transported from tissue into the blood from phage that was not efficiently eliminated by the reticuloendothelial system. We selected phage that is not eliminated into the reticuloendothelial system, or does so inefficiently. We plan to use this phage to construct peptide libraries to screen for enhanced intravasation without interference from the short half-life of the phage. This project has been assigned a secondary priority this past year.

Task 5. The newest, as yet unpublished results show that antibodies against the F3-binding domain of nucleolin inhibit angiogenesis in mice. These results are being prepared for publication.

We have previously shown that the LyP-1 peptide, which homes to tumor lymphatics, accumulates in MDA-MB-435 xenografts with an extraordinary efficiency and selectivity. In fact, we are able to detect the fluorescein-labeled LyP-1 in tumors of intact mice after an intravenous injection. We have now found that the LyP-1 peptide has an apoptotic effect on cells that bind this peptide, and that treatment of nude mice bearing MDA-MB-435 human breast cancer xenografts significantly suppresses tumor growth. Thus, the LyP-1 receptor is not only a marker of tumor lymphatics, but is also important in tumorigenesis. Future studies will be directed at elucidating the mechanism of action of this peptide.

Finally, we have extended the in vivo tumor screening technology to include the screening of libraries of chemical compounds for accumulation in a specific tissue of live animals (Brown et al., *ChemBioChem*, in press). This technical advance will allow us to screen large numbers of compounds for tumor homing. We expect to find novel tumor-specific compounds, some of which may have anti-tumor activity, as we found to be the case with LyP-1 from an analogous peptide library screening.

KEY RESEARCH ACCOMPLISHMENTS

- Shown that homing peptides can distinguish the blood vessels of pre-malignant lesions from those of fully developed tumors (and from normal vessels).
- Started preparing a paper on peptides that home to lymphatic vessels in various tumors (including breast cancer xenografts).
- Identified a breast cancer cell receptor for a peptide that homes to tumor vasculature as cell surface-expressed nucleolin.
- Shown that anti-nucleolin is anti-angiogenic and that systemically administered tumor lymphatic homing peptide has an anti-tumor effect.
- Discovered a vascular address system that is involved in breast cancer metastasis.
- Developed a method for in vivo screening of small molecular weight chemical compounds.

REPORTABLE OUTCOMES

(1) Two original papers acknowledging this grant have been published and two are in press:

Published:

Joyce, J.A., Laakkonen P., Bernasconi, M., Bergers, G., Ruoslahti, E., and Hanahan, D. Stage-specific vascular markers revealed by phage display in a mouse model of pancreatic islet tumorigenesis. *Cancer Cell* 4:393-403 (2003).

Christian, S., Pilch, J., Porkka, K., Laakkonen, P., and Ruoslahti, E. Nucleolin expressed at the cell surface is a marker of endothelial cells in tumor blood vessels. *J Cell Biol.* 163: 871-878 (2003).

In Press:

Brown, D. M. and Ruoslahti, E. Metadherin, a novel cell-surface protein in breast tumors that mediates lung metastasis. *Cancer Cell.* (2004) In Press

Brown, D.M., Pellecchia, M., and Ruoslahti, E. Drug identification through *in vivo* screening of chemical libraries. *ChemBioChem.* (2004) In Press.

(2) Two patents filed:

Nucleolin application (PLJ 5662) and the Metadherin application (04-012-01PR)

CONCLUSIONS

This has been another productive year toward progress in completing the Tasks in the application. A "zip code" system for lymphatic vessels in tumors is beginning to emerge. This heterogeneity of the lymphatics is similar to what we have established and continue to establish for tumor blood vessels. In our current work, we have shown that it is possible to distinguish the vasculature of premalignant lesions from both the vasculature of the corresponding normal tissue and fully developed tumors of the same tumor system.

The discovery of metadherin, a tumor cell surface protein involved in lung metastasis of breast cancer has opened up a new avenue of research on factors that affect tissue-specific cancer metastasis and determine the aggressiveness of individual cancers.

One of the lymphatic homing peptides and the blood vessel homing peptide, F3, show remarkably efficient and specific accumulation in breast cancer xenografts. Latest results identify the receptor for the blood vessel homing peptide as cell surface nucleolin and indicate that antibodies against an appropriate domain of nucleolin have an anti-angiogenic/anti-tumor effect. Ongoing work has also identified a candidate receptor for the lymphatic homing peptide and suggests that this peptide has a systemic anti-tumor effect.

Finally, *in vivo* screening of chemical compounds developed under this program in the past year will greatly expand our ability to discover compounds that target tumors and have anti-tumor effects.

REFERENCES

Brown, D. and Ruoslahti, E. Metadherin, a novel cell-surface protein in breast tumors that mediates lung metastasis. *Cancer Cell.* (2004) In Press

Brown, D.M., Pellecchia, M., and Ruoslahti, E. Drug identification through *in vivo* screening of chemical libraries. *ChemBioChem.* (2004) In Press.

Christian, S., Pilch, J., Porkka, K., Laakkonen, P., and Ruoslahti, E. Nucleolin expressed at the cell surface is a marker of endothelial cells in tumor blood vessels. *J Cell Biol.* 163: 871-878 (2003).

Joyce, J.A., Laakkonen P., Bernasconi, M., Bergers, G., Ruoslahti, E., and Hanahan, D. Stage-specific vascular markers revealed by phage display in a mouse model of pancreatic islet tumorigenesis. *Cancer Cell* 4:393-403 (2003).

Laakkonen, P., Porkka, K., Hoffman, J. A., and Ruoslahti, E. A tumor-homing peptide with a lymphatic vessel-related targeting specificity. *Nature Med* 8: 743-751 (2002).

Porkka, K., Laakkonen, P., Hoffman, J.A., Bernasconi, M., and Ruoslahti, E. Targeting of peptides to the nuclei of tumor cells and tumor endothelial cells in vivo. *Proc. Natl. Acad. Sci. USA*. 99: 7444-7449. (2002).

van 't Veer, L. J., Dai, H., van de Vijver, M. J., He, Y. D., Hart, A. A., Mao, M., Peterse, H. L., van der Kooy, K., Marton, M. J., Witteveen, A. T., *et al.* Gene expression profiling predicts clinical outcome of breast cancer. *Nature* 415: 530-536 (2002).

Metadherin, a cell surface protein in breast tumors that mediates lung metastasis

Darren M. Brown and Erkki Ruoslahti*

Cancer Research Center, The Burnham Institute, 10901 North Torrey Pines Road, La Jolla, California 92037

*Correspondence: ruoslahti@burnham.org

Summary

We used a phage expression library of cDNAs from metastatic breast carcinoma to identify protein domains that bind to the vasculature of the lung, a frequent site of breast cancer metastasis. We found that one protein domain selectively targeted phage as well as cells to the lung. This domain is part of the protein metadherin, shown by gene expression profiling to be overexpressed in metastatic breast cancer. Immunostaining revealed that metadherin is overexpressed in breast cancer tissue and breast tumor xenografts. Antibodies reactive to the lung-homing domain of metadherin and siRNA-mediated knockdown of metadherin expression in breast cancer cells inhibited experimental lung metastasis, indicating that tumor cell metadherin mediates localization at the metastatic site.

Introduction

Tumor metastasis is a complex, multistep process in which cancer cells detach from the original tumor mass and establish metastatic foci at organ-specific sites (Fidler, 2001). The location of the metastatic site depends on the particular type of cancer and stage of disease. For example, breast cancer spreads first to the lungs and liver (Kamby et al., 1987; Rutgers et al., 1989; Tomin and Donegan, 1987). Later in the disease, breast cancer spreads to the central nervous system and bone (Amer, 1982; Boogerd, 1996). The metastatic phase of the disease is devastating, given that conventional treatments are usually ineffective and patients typically survive only a few years after diagnosis (Harris et al., 1997).

Several factors affect the location and growth of metastases. Depending on the bloodflow pattern from the primary tumor, certain tumor cells are carried preferentially to particular organs (Weiss, 1992). While in circulation, some tumor cells selectively recognize particular endothelial cell surface molecules that mediate cell adhesion to specific organs (Abdel-Ghany et al., 2001; Cheng et al., 1998; Johnson et al., 1993). The arrest of tumor cells at the metastatic site, be it through mechanical trapping in small capillaries or through adhesive interactions with the endothelium, is a necessary step for tumors to establish at a secondary site (Chambers et al., 2002; Orr and Wang, 2001). Once the tumor cells have seeded the target organ, the local microenvironment influences whether or not a particular cancer cell will proliferate (Fidler, 2001; Radinsky, 1995). Unfortunately,

many of the factors that contribute to organ-specific metastasis have yet to be elucidated.

To identify tumor cell surface molecules that mediate breast cancer metastasis, we have used *in vivo* phage screening. This screening method has been used by our group to identify peptides and proteins that are capable of mediating selective *in vivo* localization of phage to individual organs as well as tumors and that reveal tissue-specific vascular differences (Arap et al., 1998, 2002; Laakkonen et al., 2002; Pasqualini and Ruoslahti, 1996; Porkka et al., 2002; Rajotte et al., 1998).

In this study, we isolated from phage expression libraries of breast carcinoma cDNAs a domain in a protein we call metadherin (for metastasis adhesion protein) that causes the phage to home specifically to lung microvasculature after intravenous injection. We show that the lung-homing domain of metadherin is extracellular. Antibodies to metadherin revealed high amounts of metadherin throughout human breast tumors and breast tumor xenografts while drastically lower levels of metadherin were present in normal breast tissue. We also show that antibodies reactive to the lung-homing domain of metadherin inhibited experimental breast cancer lung metastasis, as did siRNA-mediated knockdown of metadherin expression. These results suggest that metadherin plays an important role in breast cancer metastasis.

Results

Identification of cDNA clones by phage display

To identify candidate cell adhesion proteins that mediate breast cancer metastasis, we used an *in vivo* phage screening ap-

SIGNIFICANCE

Adhesive interactions with the endothelium have been shown to contribute to the localization and growth of tumors at particular secondary sites in experimental animals. In this report, we show that metadherin, a protein greatly overexpressed in breast cancers, mediates lung-specific dissemination of metastatic cells. Independent microarray data have identified high metadherin gene expression as a prognostic indicator of clinical metastasis in human breast cancer patients. Our results provide a possible mechanistic explanation for the clinical findings. Our demonstration that metastasis can be inhibited by blocking the lung-homing domain of metadherin with an antibody or by reducing metadherin expression identifies metadherin as a candidate target for therapeutic intervention in breast cancer and perhaps other cancers as well.

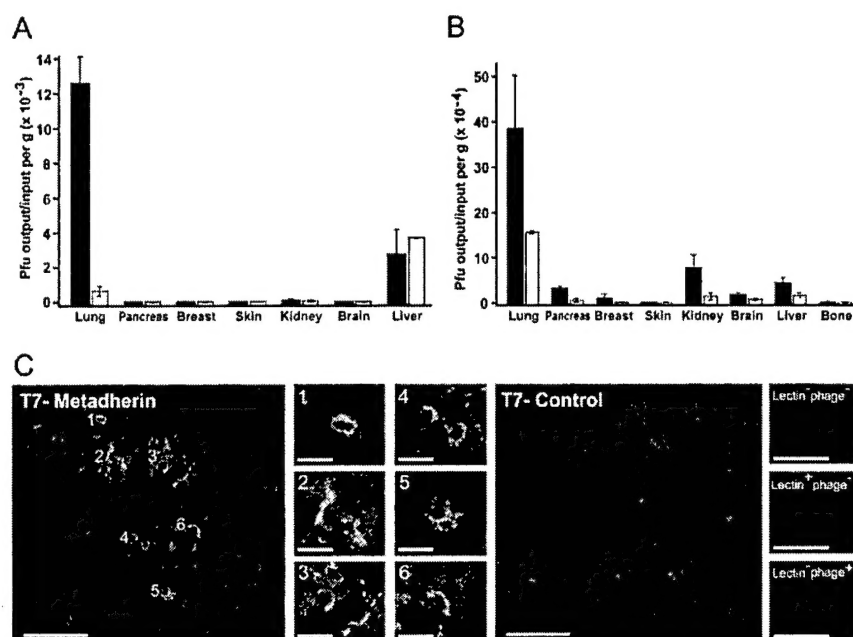


Figure 1. Homing specificity of metadherin phage

A: Metadherin (closed bars) and nonrecombinant (open bars) phage titers recovered from lung, pancreas, breast, skin, kidney, brain, and liver after injection into the tail vein of Balb/c mice and circulation for 5 min. Error bars represent mean \pm SD for 2–7 experiments per variable.

B: Metadherin (closed bars) and nonrecombinant (open bars) phage titers recovered from lung, pancreas, breast, skin, kidney, brain, liver, and bone (tibia) after injection into the left ventricle of the heart of Balb/c mice and circulation for 5 min. Error bars represent mean \pm SEM for 2–5 experiments per variable.

C: Confocal projections of anti-phage immunostained lungs from mice co-injected with fluorescein-labeled tomato lectin (green) and either metadherin phage (T7-metadherin) or T7-415 nonrecombinant phage (T7-Control). Control lungs were from noninjected mice (lectin⁺ phage⁻), mice injected with lectin alone (lectin⁺ phage⁻), or mice injected only with metadherin phage (lectin⁻ phage⁺). Anti-phage antibody was detected with Alexa 594 goat anti-rabbit IgG antibody (red). Nuclei were stained with DAPI (blue). The scale bars correspond to 50 μ m, except in panels 1–6, where the scale bars correspond to 10 μ m.

proach. We selected the highly metastatic, Balb/c-derived 4T1 mammary tumor cell line to study tumor metastasis because 4T1 cells and human mammary adenocarcinomas share similar sites of metastasis (Aslakson and Miller, 1992; Dexter et al., 1978; Miller et al., 1983). Human breast cancer spreads first to the lungs in 24%–77% of the cancers and to the liver in 22%–62% (Kamby et al., 1987; Rutgers et al., 1989; Tomin and Donegan, 1987). Similarly, 4T1 spreads in mice to the lungs and liver in >95% and >75% of the cancers, respectively (Pulaski and Ostrand-Rosenberg, 1998). We used the 4T1 cells to prepare a cDNA library enriched in transcripts that encode secreted and transmembrane proteins potentially involved in metastasis.

The 4T1 phage library was injected intravenously, and phage that localized to the lungs were isolated. After three rounds of selecting for lung-homing phage clones, 32 clones were initially isolated. We tested individual phage clones for their ability to specifically bind to lung vasculature. One of the five lung-specific clones we identified encoded a fragment of a protein recently deposited into GenBank (accession numbers AAL92861 and AAP30791).

The selected phage, when intravenously (i.v.) injected into mice and allowed to circulate for 5 min, bound to lungs almost 20-fold more than control phage (Figure 1A). In contrast, similar numbers of the selected phage and control phage accumulated in pancreas, breast, skin, kidney, brain, and liver. When injected into the left ventricle of the heart in mice, significantly more selected phage accumulated in the lungs, pancreas, kidney, brain, and liver than control phage (Figure 1B). Similar numbers of selected phage and control phage accumulated in breast, skin, and bone. The selected phage colocalized with blood vessels in the lungs (Figure 1C).

cDNA cloning and membrane topology of metadherin

The deduced amino acid sequence of the lung-homing domain of the lung-homing phage is shown in Figure 2A. Using BLAST

(Altschul et al., 1997), we found one cDNA clone (GenBank accession number AY082966) that encoded the putative full-length human protein corresponding to the phage clone. The GenBank entry refers to the protein as “LYRIC” and describes it as a putative CEACAM1-associated protein in colon carcinoma. These observations remain unpublished. Based on our results

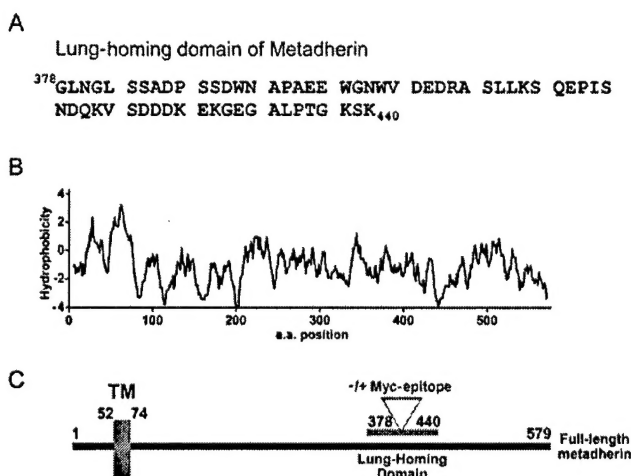


Figure 2. Sequence analysis of metadherin

A: Amino acid sequence of metadherin's lung-homing domain. This domain corresponds to residues 378–440 of the full-length mouse metadherin protein.

B: Hydrophobicity analysis of metadherin, using a window size of 9 amino acids.

C: Layout of the full-length metadherin protein. TM denotes the location of the putative transmembrane domain. The numbers denote the position of amino acids in the metadherin protein.

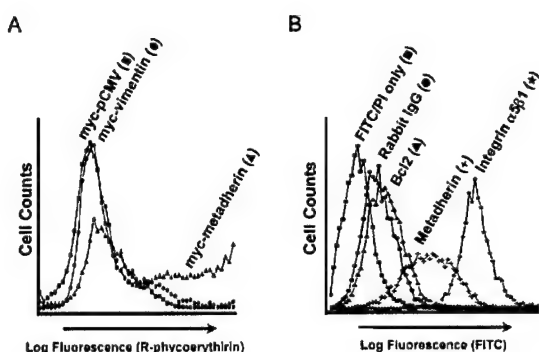


Figure 3. Lung-homing domain of metadherin is extracellular

A: HEK293T cells expressing full-length myc-tagged metadherin, myc-vimentin, or myc-pCMV were analyzed by flow cytometry. Anti-myc antibodies were applied to the cells and detected with a PE-labeled secondary Ab. **B:** Rabbit IgG, anti-Bcl2 polyclonal Ab (Bcl2), anti-integrin $\alpha 5\beta 1$ polyclonal antibody (Integrin $\alpha 5\beta 1$), or anti-metadherin₍₃₇₈₋₄₄₀₎ (metadherin) was applied to nonpermeabilized 4T1 tumor cells and detected with a FITC-labeled secondary Ab. Control cells were stained with FITC-labeled secondary Ab and propidium iodide alone (FITC/PI only).

that show the importance of this lung-homing protein in breast cancer metastasis, we have named this protein metadherin (metastasis adhesion protein). We used a reported mouse cDNA homolog of metadherin (GenBank accession number AK029915) to design oligonucleotides and amplified the full-length 1740 bp mouse metadherin cDNA by reverse transcription-polymerase chain reaction.

Analysis of the hydrophobic regions of metadherin (Kyte and Doolittle, 1982) revealed that amino acid residues 52–74 encode a putative transmembrane domain (Figure 2B). We did not find any domains in metadherin that were similar to other known proteins. Using a hidden Markov model to detect membrane helices and predict transmembrane topology in proteins (Glasgow, 1998; Krogh et al., 2001), we found that metadherin was predicted to be a type II transmembrane protein with an extracellular lung-homing domain. To confirm this prediction, we subcloned a c-myc epitope into the lung-homing domain of the metadherin cDNA, as shown in Figure 2C. This myc-tagged cDNA was expressed in HEK293T cells, and these cells were then stained with anti-myc antibodies. Using flow cytometry, we observed that intact myc metadherin-expressing cells were labeled with anti-myc antibodies (Figure 3A), indicating that the lung-homing domain of metadherin was extracellular. No cell surface labeling was detected in vector-transfected cells or nonpermeabilized cells expressing the intracellular protein myc-vimentin (Figure 3A). Anti-myc antibodies stained the myc vimentin-expressing cells when permeabilized, which confirms the expression of myc-vimentin, and permeabilized cells expressing vector alone were not stained with anti-myc antibodies (data not shown).

Metadherin expression in tumor cells and tumors

We also raised rabbit antibodies reactive to the lung-homing domain of metadherin to study endogenous metadherin in tumor cells and tumors. These antibodies bound to nonpermeabilized 4T1 cells in flow cytometry (Figure 3B). This result confirms the presence of the lung-homing domain of metadherin on tumor

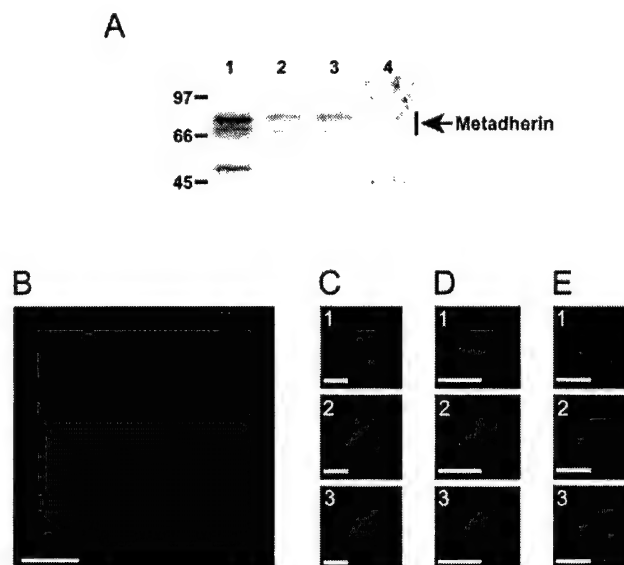


Figure 4. Metadherin expression in 4T1 tumor cells

A: Immunoblot of endogenous metadherin. Lanes 1 and 4, 4T1 cell extract; lane 2, KRIB cell extract; lane 3, MDA-MB-435 cell extract. Immunoblot detection of metadherin was performed with anti-metadherin₍₃₇₈₋₄₄₀₎ (lanes 1–3). Immunoblot detection of an unrelated protein, Clone D2, was performed with anti-Clone D2 polyclonal antibody (lane 4).

B: Confocal projection of permeabilized 4T1 cells stained with anti-metadherin₍₃₇₈₋₄₄₀₎. Scale bar corresponds to 50 μ m.

C: Confocal sections (0.15 μ m thick; panels 1–3) of nonpermeabilized 4T1 cells stained with anti-metadherin₍₃₇₈₋₄₄₀₎.

D and E: Nonpermeabilized 4T1 cells stained with anti-metadherin₍₃₇₈₋₄₄₀₎ that was pre-incubated with excess metadherin₍₃₇₈₋₄₄₀₎ peptide (**D**, panels 1–3) or excess control peptide (**E**, panels 1–3). In **B–E**, anti-metadherin₍₃₇₈₋₄₄₀₎ was detected with Alexa 594 goat anti-rabbit IgG antibody (red). Nuclei were stained with DAPI (blue). Images in **D** and **E** were captured using an inverted fluorescent microscope. The scale bars in **C–E** correspond to 5 μ m.

cells at the cell surface where it would be available to bind to vascular targets during metastasis. An antibody against a cytoplasmic protein (Bcl-2) and rabbit IgG did not bind to the surface of nonpermeabilized 4T1 cells, while the cells were strongly positive for integrin $\alpha 5\beta 1$ (Figure 3B).

In 4T1 tumor cell extracts, anti-metadherin₍₃₇₈₋₄₄₀₎ detected proteins with apparent molecular weights of approximately 80 kDa, 75 kDa, and 55 kDa (Figure 4A, lane 1). KRIB and MDA-MB-435 cell extracts also contained the 80 kDa and 75 kDa proteins (Figure 4A, lanes 2 and 3, respectively). A control, affinity-purified polyclonal antibody reactive to a nonrelated protein (Clone D2) did not detect the anti-metadherin₍₃₇₈₋₄₄₀₎ immunoreactive bands (Figure 4A, lane 4). The 80 kDa and 55 kDa proteins detected by anti-metadherin₍₃₇₈₋₄₄₀₎ were also produced by an in vitro transcription and translation reaction using an epitope-tagged metadherin cDNA as template (data not shown); this suggests that the 55 kDa protein may be a degradation product of metadherin.

In fixed and permeabilized 4T1 cells, metadherin immunoreactivity localized throughout the cytoplasm (Figure 4B). In nonpermeabilized cells, the staining was concentrated at the edges of the cells (Figure 4C). Controls showed that pre-incubation of anti-metadherin₍₃₇₈₋₄₄₀₎ with the metadherin₍₃₇₈₋₄₄₀₎ lung-homing

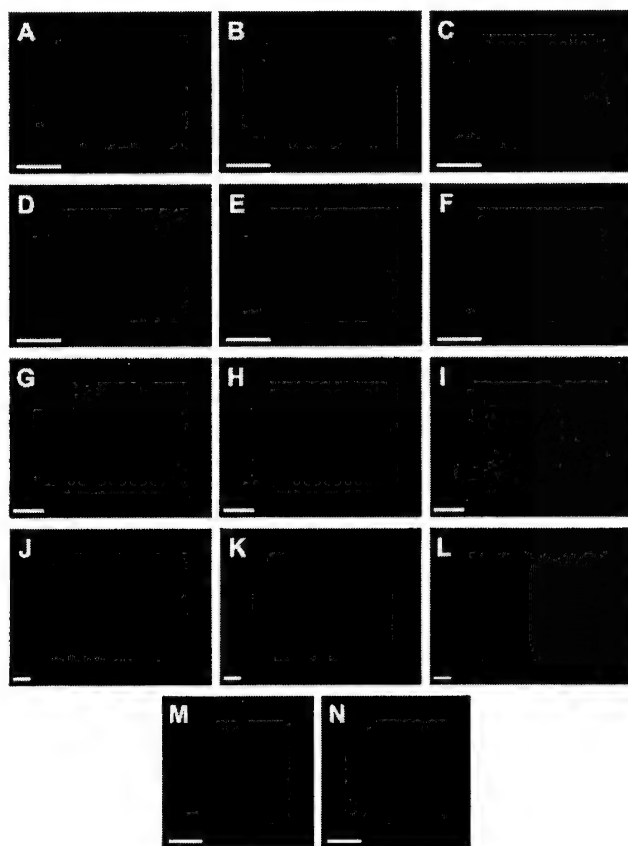


Figure 5. Metadherin expression in tumor xenografts and human breast cancer

MDA-MB-435 breast adenocarcinoma (A–C) or KRIB osteosarcoma (D–F) tumor xenografts grown in nude Balb/c mice were analyzed by immunostaining. Sections were stained with either anti-metadherin₍₃₇₈₋₄₄₀₎ alone (A and D) or anti-metadherin₍₃₇₈₋₄₄₀₎ pre-incubated with excess metadherin₍₃₇₈₋₄₄₀₎ peptide (B and E) or excess control peptide (C and F). Sections of human breast tumor (G–I) or normal human breast tissue (J–L) were stained with either anti-metadherin₍₃₇₈₋₄₄₀₎ alone (G and J) or anti-metadherin₍₃₇₈₋₄₄₀₎ pre-incubated with excess metadherin₍₃₇₈₋₄₄₀₎ peptide (H and K) or excess control peptide (I and L). Sections of mouse breast tissue were stained with either anti-metadherin₍₃₇₈₋₄₄₀₎ alone (M) or anti-metadherin₍₃₇₈₋₄₄₀₎ pre-incubated with excess metadherin₍₃₇₈₋₄₄₀₎ peptide (N). In all panels, anti-metadherin₍₃₇₈₋₄₄₀₎ was detected with Alexa 594 goat anti-rabbit IgG antibody (red) and nuclei were stained with DAPI (blue). The confocal projections in A–N were captured using a confocal microscope. The scale bars correspond to 50 μ m.

peptide inhibited the staining (Figure 4D), whereas a control peptide did not (Figure 4E).

We detected strong metadherin staining in sections of MDA-MB-435 and KRIB tumor xenografts (Figures 5A and 5D), which are two tumor models known to generate lung metastases (Berlin et al., 1993; Price et al., 1990). The anti-metadherin immunostaining was specific, since pre-incubation of antibody with the metadherin₍₃₇₈₋₄₄₀₎ lung-homing peptide (Figures 5B and 5E) inhibited the staining and control peptide (Figures 5C and 5F) had no inhibitory effect. Subcutaneous tissue or skin adjacent to the tumors showed no anti-metadherin staining (e.g., Figure 5D, lower left corner).

Several human breast cancer sections stained with anti-

metadherin₍₃₇₈₋₄₄₀₎ showed high amounts of metadherin throughout the tumor (Figure 5G). In contrast, we did not detect any cytoplasmic or cell surface-associated metadherin in normal human breast tissue, but nuclear staining was present (Figure 5J). The cell surface staining of breast cancer tissue could be inhibited with the metadherin₍₃₇₈₋₄₄₀₎ peptide (Figure 5H), but not with control peptide (Figure 5I). Neither peptide inhibited nuclear staining (Figures 5H, 5I, 5K, and 5L). The human sections were paraffin embedded and processed with heat-induced target retrieval. Apparently, the antibody nonspecifically stains nuclei in such sections. In frozen tissue sections of normal mouse mammary tissue, we found specific metadherin staining at the apical surface of epithelial cells lining ducts of the mammary glands (Figures 5M and 5N), and a small amount of metadherin was dispersed through the mammary fat pad. We detected no metadherin in the spleen, kidney, lung, or skin, but minute amounts were seen in the liver. Purkinje neurons in the early postnatal and adult cerebellum were strongly positive for metadherin staining (data not shown). Tissue array slides of human breast tissue and breast adenocarcinomas were also stained with anti-metadherin₍₃₇₈₋₄₄₀₎. We detected strong anti-metadherin₍₃₇₈₋₄₄₀₎ staining throughout the tissue sections in 17 out of 31 breast adenocarcinomas, while metadherin was absent in 18 out of 20 samples of normal breast tissue. The other two normal breast tissue samples stained positive for metadherin at epithelial cells lining ducts of the mammary glands. These immunostaining results show that metadherin is selectively overexpressed in tumors.

Effect of metadherin expression on the localization of injected cells

To test the effect of metadherin on tissue distribution of i.v.-injected tumor cells, we studied HEK293T cells transiently transfected with metadherin. The cells were cotransfected with DsRed2 and metadherin, and DsRed2-positive cells were isolated using fluorescence-activated cell sorting (FACS). The cells were then i.v.-injected into mice. Fluorescent cells were detected in the blood vessels of lungs examined 2 hr after the injection; cell counting showed 22% more metadherin-transfected cells than that of vector-transfected cells (Figures 6A and 6B; Student's *t* test; *p* < 0.001). We did not see significant numbers of DsRed2 HEK293T cells in the brain, skin, liver, kidney, heart, spleen, or pancreas (Figure 6A). This result supports the phage homing data indicating that metadherin preferentially binds to lung vasculature. The relatively small incremental effect of metadherin overexpression on the lung localization of HEK293T cells is probably due to endogenous expression of metadherin by these cells, which immunoblotting showed to be about 45% of that in the 4T1 cells (data not shown).

Anti-metadherin and metadherin siRNA inhibit 4T1 lung metastasis

To gain information on the role of metadherin in metastasis, we decided to inhibit metadherin activity in the 4T1 cells with antibodies reactive to the lung-homing domain of metadherin. When co-injected with the 4T1 cells, anti-metadherin₍₃₇₈₋₄₄₀₎ inhibited lung metastasis by about 40% (Figure 7, *p* < 0.01), compared to 4T1 cells treated with rabbit IgG. In a separate experiment, we did not observe any difference between the growth of mammary fat pad tumors formed from 4T1 cells pretreated with the anti-metadherin₍₃₇₈₋₄₄₀₎ or rabbit IgG (data not shown).

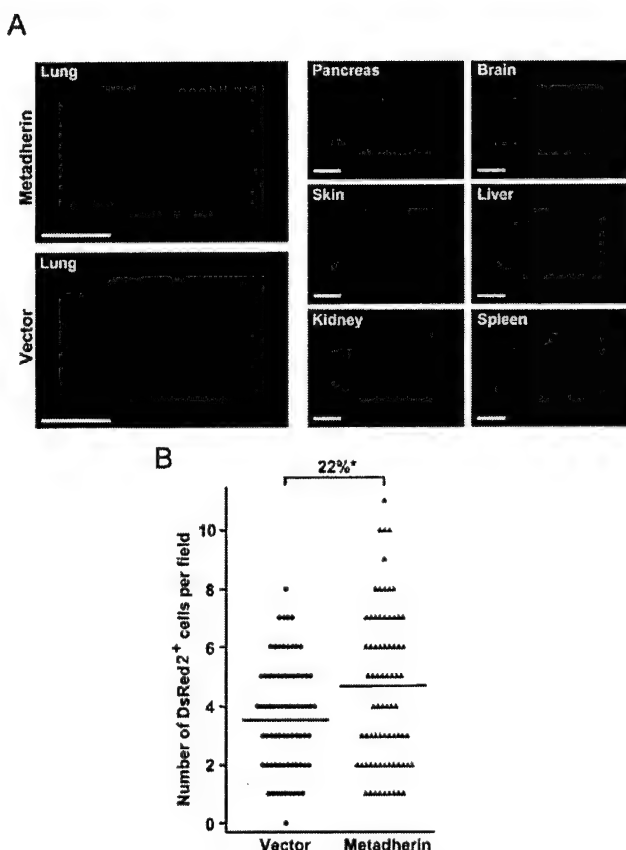


Figure 6. HEK293Ts overexpressing metadherin localize to lung

A: DAPI-stained (blue) lung sections from mice injected with HEK293T cells that were cotransfected with a DsRed2 expression vector (red) and either metadherin-pCMV or expression vector alone. Pancreas, skin, kidney, brain, liver, and spleen sections from mice injected with HEK293T cells that were transfected with a DsRed2 expression vector (red) and metadherin-pCMV. The scale bars correspond to 100 μ m.

B: Number of DsRed2-positive cells per viewing field in the lung sections ($n = 75$; one-tailed Student's t test; * $p < 0.001$).

As a second approach, we measured the metastatic potential of breast cancer cells expressing reduced levels of metadherin. As shown in Figure 8A, siRNA reactive to metadherin, but not siRNA to GAPDH or scrambled-siRNA, was able to knock down expression of transfected myc-metadherin in HEK293T cells. We were unable to generate stable cell lines that expressed reduced levels of metadherin because metadherin expression levels returned to normal after 2 weeks. Instead, we coexpressed green fluorescent protein (EGFP) and the metadherin-reactive siRNA or scrambled-siRNA in 4T1 cells and selected for siRNA-transfected cells by FACS. The transfection with metadherin-siRNA did not affect the expression of β -actin or the type II transmembrane protein, transferrin receptor (Figure 8B). However, metadherin protein expression in metadherin-siRNA cells was reduced by about 40% relative to the scrambled-siRNA cells (Figure 8B). Measured by real-time PCR, metadherin-siRNA cells expressed about 40% less metadherin mRNA than the scrambled-siRNA cells, when metadherin mRNA levels were normalized to β -actin mRNA levels (Figure 8C).

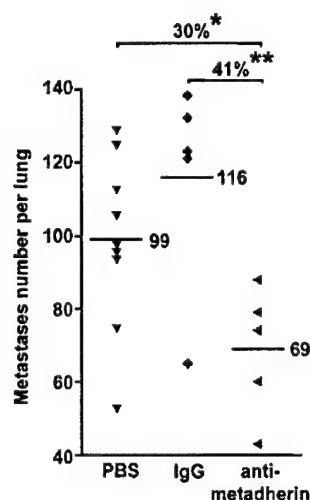


Figure 7. Anti-metadherin antibodies inhibit lung metastasis

Number of lung metastases from mice injected with 4T1 cells that were treated with anti-metadherin_[378-440], rabbit IgG, or PBS. Average number of metastases in each group is denoted with a horizontal line. The percent difference in average number of metastases between groups is denoted above the brackets, with significance measured using a one-tailed Student's t test (* $p < 0.02$, ** $p < 0.01$).

Using flow cytometry, the effects of metadherin-reactive siRNA and scrambled-siRNA on cell growth and viability were assessed. In 4T1 cells cotransfected with EGFP and metadherin-reactive siRNA or scrambled-siRNA expression plasmids, we did not detect any significant difference in propidium iodide staining between the EGFP-positive populations from the metadherin-reactive siRNA or scrambled-siRNA cells (4.52% versus 5%, see Supplemental Figure S1 at <http://www.cancercell.org/cgi/content/full/5/4/365/DC1>). This suggested metadherin-reactive siRNA did not affect 4T1 cell viability under these conditions. In addition, the number of EGFP-positive cells in the metadherin-reactive siRNA and scrambled-siRNA transfected 4T1 cells was not significantly different, suggesting the metadherin-reactive siRNA plasmid did not inhibit cell growth during the 2 day transfection period (9.55% versus 9.95%, Supplemental Figure S1). Also, we counted the number of cells before and 2 days after transfecting the siRNA expression plasmids and did not see any significant effect of the metadherin-siRNA on the growth rate of the cells (data not shown).

Immunostaining confirmed that metadherin-siRNA cells expressed less metadherin (Figure 8D, 1 and 2) than scrambled-siRNA cells (Figure 8D, 3 and 4). Using FACS, we isolated EGFP-positive cells that excluded propidium iodide to select for viable siRNA-transfected cells (Figure 8D, 5–8). When injected into mice, the 4T1 cells expressing metadherin-reactive siRNA formed about 80% fewer experimental lung metastases than cells expressing scrambled-siRNA (Figure 8E, Student's t test, $p < 0.001$).

Discussion

We report here that a protein, metadherin, is overexpressed in breast tumors and binds to lung vasculature through a C-ter-

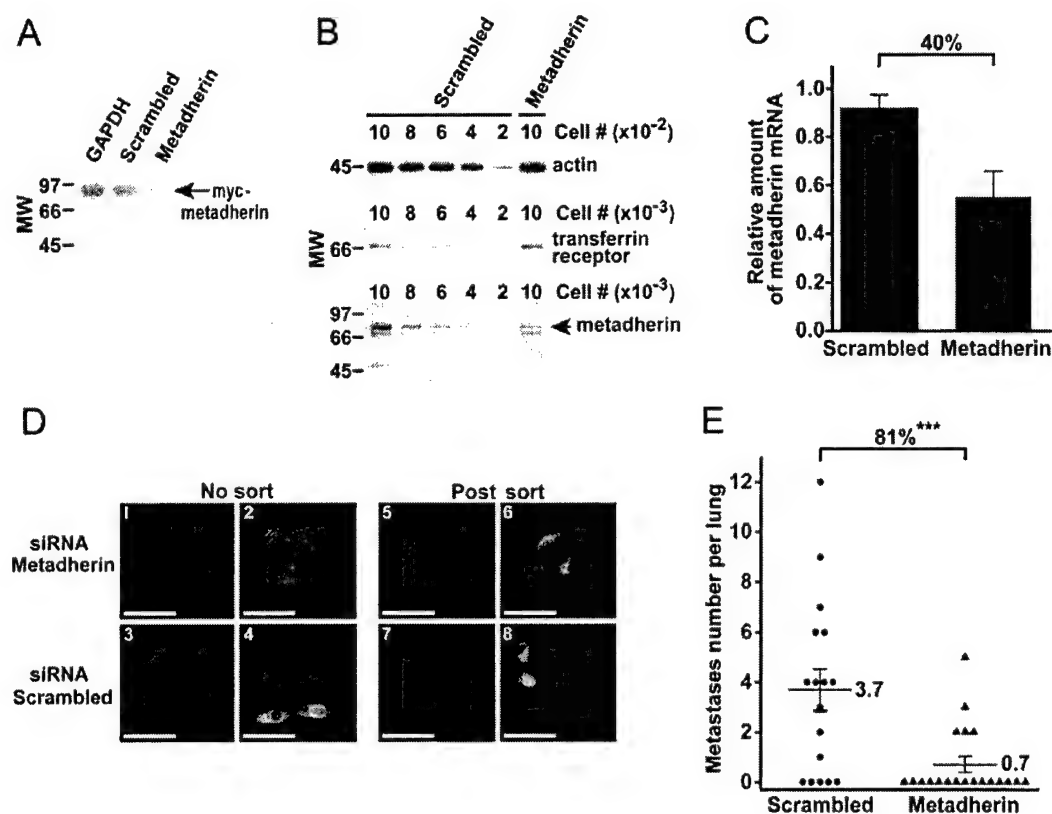


Figure 8. siRNA reactive to metadherin mRNA inhibits lung metastasis

A: Anti-myc immunoblot of HEK293T cell extracts expressing myc-tagged metadherin and siRNA reactive to GAPDH or metadherin, or scrambled-siRNA. **B:** Immunoblot quantitation of β -actin, transferrin receptor, or metadherin protein levels in 4T1 cells expressing siRNA reactive to metadherin or scrambled-siRNA. The arrow in B denotes the 80 kDa metadherin protein band quantified by densitometry.

C: Quantitation of metadherin mRNA in 4T1 cells expressing siRNA reactive to metadherin or scrambled-siRNA. The relative amount of metadherin mRNA was normalized to the abundance of β -actin mRNA, also detected by real-time PCR. Error bars represent mean \pm SD.

D: 4T1 cells were cotransfected with an EGFP expression vector and a vector expressing siRNA reactive to metadherin (panels 1, 2, 5, and 6) or scrambled-siRNA (panels 3, 4, 7, and 8). The cells were sorted by FACS to select for EGFP-expressing cells (Post sort). Nonsorted cells (No sort; panels 1–4) and postsorted cells (panels 5–8) were stained with anti-metadherin_[378–440]. Panels 2, 4, 6, and 8 show the EGFP-expressing cells (green) displayed in panels 1, 3, 5, and 7, respectively. In all panels, anti-metadherin_[378–440] was detected with Alexa 594 goat anti-rabbit IgG antibody (red). Nuclei were stained with DAPI (blue). The scale bars correspond to 50 μ m.

E: siRNA reactive to metadherin transcripts inhibits 4T1 cell experimental lung metastasis. Values are expressed as the number of tumor foci per 10,000 cells injected. Bars represent mean \pm SEM (one-tailed Student's *t* test; ****p* < 0.001). In C and E, percentages indicate relative suppression compared to control group.

minimal segment in the extracellular domain. We also show that blocking the lung-homing domain with antibodies or inhibiting the expression of metadherin with siRNA can inhibit breast cancer metastasis. These results identify metadherin as a potential mediator of cancer metastasis.

Metadherin appears to detect a specific marker of lung vasculature. Metadherin phage accumulated in lung vasculature after either tail-vein or intracardiac injection, suggesting that among the various vascular beds, it primarily binds to lung endothelium. In this regard, metadherin is similar to lung-specific homing peptides isolated by *in vivo* phage display (Rajotte and Ruoslahti, 1999) and antibodies that specifically bind to lung vasculature (McIntosh et al., 2002). The ability of metadherin phage to specifically target lung vasculature suggests that among the various vascular beds, the molecule(s) metadherin binds ("metadherin receptor") is primarily expressed on lung endothelium. The identity of the receptor is currently unknown.

Tissue-specific expression of vascular markers is not limited to lung vasculature; recent data suggest that each tissue puts a specific signature on its vasculature (Ruoslahti, 2002). Thus, the binding of tumor cells to tissue-specific vascular markers may play a role in selective tumor metastasis to other tissues as well.

Metadherin appears to primarily mediate metastasis to one of the four sites commonly affected by human breast cancer: the lungs. The fact that metadherin phage primarily targeted the lungs after either intravenous or intracardiac injection and was not detected in substantial amounts in the liver, brain, or bone suggests that metadherin mediates specific adhesion to lung vasculature, even after passing through capillary networks of other organs. The ability of metadherin phage to accumulate in the lungs even after intracardiac injection suggests that metadherin also promotes selective binding of tumor cells to lung

- vasculature, rather than helping them adhere to the first capillary bed the cells encounter.

Metadherin may be important to the pathogenesis of cancer. We found high expression of metadherin in cultured tumor cells, and its expression was higher in both experimental and clinical breast cancers than in normal breast tissue and in other normal tissues, as detected with specific metadherin antibodies. The only exception to the relatively low expression in the normal tissues we studied were the Purkinje cells in the cerebellum; metadherin may have a specific function in these cells.

A recent gene expression profiling study on breast cancer patients revealed that metadherin is overexpressed in many metastatic breast cancers. van 't Veer et al. (2002) found that metadherin mRNA expression levels (described as GenBank entry AK000745) in breast cancer patients were significantly correlated with a poor prognosis due to metastasis. Out of 25,000 genes analyzed, metadherin was ranked 25th when correlating gene expression levels with metastasis. Most of the patients who expressed high levels of these "poor prognosis" classified genes developed distant metastases within 5 years of observation. Thus, metadherin is overexpressed in breast cancer both at the protein and mRNA levels and is associated with increased malignancy of these cancers. Our results suggest that the association of metadherin overexpression with poor prognosis of breast cancer is due to an ability of metadherin to specifically promote tumor metastasis to the lungs.

There are other examples of adhesive interactions that are required in order for lung metastases to form. Dipeptidyl dipeptidase IV on lung endothelial cells was found to be an adhesion receptor for fibronectin on metastasizing breast and prostate carcinoma cells in a mouse model (Cheng et al., 1998; Johnson et al., 1993). In another mouse model, Ca²⁺-sensitive chloride channel, hCLCA2, expressed on lung endothelial cells was reported to be a ligand for β 4 integrins on metastasizing breast cancer cells (Abdel-Ghany et al., 2001; Elble et al., 1997). Most recently, the secreted chemokine, CXCL12, which is highly expressed in the lung, liver, and lymph nodes, was shown to bind to CXCR4 receptors on the surface of metastasizing breast cancer cells (Muller et al., 2001). Moreover, interfering with only one of these interactions was sufficient to inhibit metastasis (Abdel-Ghany et al., 2001; Cheng et al., 1998; Muller et al., 2001). Although there is no evidence available on the significance of these interactions in breast cancer, it seems that multiple interactions of cell adhesion molecules and growth factor receptors may be required for the attachment and growth of circulating tumor cells in the lung. Similar mechanisms based on unique vascular addresses may play a role in organ-specific metastasis to other organs.

The importance of metadherin in tumor cell metastasis might not only be limited to breast cancer. Using SAGEmap (Lal et al., 1999; Lash et al., 2000), a component of The Cancer Genome Anatomy Project at the National Center for Biotechnology Information, we found that metadherin is significantly overexpressed not only in breast cancers, but also in cancers of the brain and prostate ($p < 0.05$). This suggests that metadherin might also play a role in the metastasis of these cancers. Metadherin is conserved among mammals, and with the BLAST algorithm (Altschul et al., 1997), we found additional mouse and human metadherin-like molecules in the GenBank databases. It will be important to determine what role, if any, these related molecules might play in cancer.

Metadherin is a potential target for tumor diagnosis and preventative therapy. Given the cell surface localization of metadherin in tumor cells and the discrete overexpression of metadherin in primary tumors, therapeutics that target metadherin might prove to be selective for metastasis-prone tumors. Our results showing the antimetastatic activity of anti-metadherin antibodies and siRNA reactive to metadherin mRNA suggest that antibody or siRNA-based therapies that target metadherin might be effective in preventing certain tumors from metastasizing.

Experimental procedures

Cell lines, mice, and tumors

4T1, a cell line derived from a Balb/c breast adenocarcinoma, was obtained from ATCC and maintained as described by Pulaski and Ostrand-Rosenberg (1998). MDA-MB-435 and KRII cell lines were maintained as described before (Laakkonen et al., 2002). Nude Balb/c mice were subcutaneously injected with 1×10^6 tumor cells and kept for 5 weeks (KRII) or 10 weeks (MDA-MB-435). Tumors were then removed, frozen in OCT embedding medium (Tissue-Tek, Elkhart, IN), and sectioned. The Burnham Institute Animal Research Committee approved the animal experimentation.

Phage library and screening

A cDNA library was prepared from membrane bound polyribosomal mRNA of 4T1 cells. Briefly, RNA from membrane bound polysomes of 3.2×10^8 4T1 cells was prepared using the methods described by Mechler (1987). Approximately 1 μ g of this RNA was used to generate 6 μ g of amplified antisense mRNA (aRNA), using the methods described by Luo et al. (1999). Using aRNA as template, mRNA was synthesized as described by Luo et al. (1999), except the primer, 5'-TTNNNNNN-3', was used instead of random hexamer primer, and methylated dNTPs were used instead of dNTPs. A cDNA library was prepared from the mRNA, as described in the manufacturer's protocol (OrientExpress Random Primer cDNA synthesis kit; Novagen, Madison, WI).

T7 phage vectors, designed to express cDNA library-encoded proteins fused at the N terminus to phage 10B coat protein and to a myc epitope at the C terminus, were then assembled. Oligonucleotides encoding myc epitopes in all three reading frames, internal EcoRI and HindIII restriction enzyme cleavage sites and flanking EcoRI/HindIII adapters, were synthesized. The oligonucleotides were then individually phosphorylated, annealed, and ligated to EcoRI/HindIII-digested T7Select 1-2a, 1-2b, or 1-2c vector arms (Novagen) to generate myc epitope phage vectors.

To prevent myc epitope expression in phage vectors that were unsuccessfully ligated to cDNA during library construction, a linker encoding stop codons in all three reading frames was inserted upstream of the myc epitope and downstream of the 10B coat protein in the phage vector. Oligonucleotides encoding stop codons in all three reading frames were synthesized, phosphorylated, annealed, and ligated to EcoRI/HindIII-digested myc epitope phage vectors to form myc-T7 vectors. A map of the myc epitope phage vector is shown in Supplemental Figure S2 at <http://www.cancercell.org/cgi/content/full/5/4/365/DC1>. The cDNA libraries were then ligated to EcoRI/HindIII-digested myc-T7 vector, phage were packaged, and libraries were amplified in *E. coli* BLT5615 cells (according to the manufacturer's protocol; Novagen). As measured by plaque assay, the library contained 4.7×10^6 primary recombinants.

Phage clones that expressed cDNA inserts with open reading frames were enriched by three rounds of selection with anti-myc mAb (3.1 μ g/ml MAB8864; Chemicon, Temecula, CA) bound to rat anti-mouse IgG1 magnetic beads (3.1 μ l per 1 ml of buffer; Miltenyi Biotec, Auburn, CA). Selections were performed with 10^{11} plaque forming units (pfu) of phage in 10 ml of Dulbecco's phosphate buffered saline containing 0.5% bovine serum albumin (PBSB). Phage were applied to a magnetized LS MACS column (Miltenyi Biotec), washed with buffer (50 mM Tris-HCl [pH 7.5], 150 mM NaCl, 1% NP-40, 0.5% sodium deoxycholate, 0.1% sodium dodecyl sulfate), eluted with PBSB after demagnetizing the column, and transferred to a second column for more washes. Phage were amplified in BLT5615 *E. coli* using the liquid lysate method after each anti-myc selection round and supernatants clarified by centrifugation were supplied with 1% vol/vol of *E. coli* protease

inhibitors cocktail (P-8465; Sigma-Aldrich, St. Louis, MO). After three rounds of myc antibody sorting, over 90% of the phage clones in the 4T1 library were found to contain open reading frame cDNA inserts. On average, the phage clones expressed protein fragments that were 75 amino acids long.

Ex vivo and in vivo screenings with the 4T1 phage library were performed as previously described (Hoffman et al., 2004). Briefly, cell suspensions were prepared from mouse lungs and incubated overnight at 4°C with 10^9 pfu of 4T1 phage library. The cells were washed to remove unbound phage, and the bound phage were rescued and amplified by adding BLT5615 *E. coli*. The amplified 4T1 phage library was applied to a lung cell suspension for a second ex vivo selection round, as before. The ex vivo preselected phage pool (200 μ l, or approximately 10^9 pfu) was injected intravenously into 2-month-old Balb/c mice through the tail vein, allowed to circulate for 5 min, and heart-perfused with PBS to remove unbound intravascular phage. Cell suspensions of tissue were prepared by mechanical disruption and washed to remove unbound phage, and the bound phage were rescued and amplified by adding BLT5615 *E. coli*. The phage pool was reinjected into Balb/c mice, and the cycle repeated twice. For each selection round, the number of phage recovered from the tissue was normalized to the number of injected phage and tissue mass. After three rounds of in vivo selections, cDNA inserts were sequenced from 32 phage clones as described before (Hoffman et al., 2004).

Cloning of full-length metadherin cDNA

The following primers were synthesized to amplify the full-length mouse metadherin cDNA: 5'-ACCATGGCTGCACGAAGCTGGCAGGACGAGCTG-3' and 5'-TCACGTTTCCCGCTGCTGGCCTTTTCTCTTTTAA-3'. RNA was isolated from 4T1 cells using a Total RNA Isolation Kit (Qiagen, Valencia, CA). The metadherin cDNA was amplified by RT-PCR using a Superscript One-Step RT-PCR Kit for Long Templates (according to manufacturer's protocol; Invitrogen, Carlsbad, CA) and subcloned into the TOPO-TA vector, pcDNA3.1-V5/His (according to the manufacturer's protocol; Invitrogen).

A myc epitope was added to metadherin protein by first inserting an *EcoRI* restriction enzyme site in the metadherin cDNA after nucleotide 1222 with a QuickChange site-directed mutagenesis kit (Stratagene, La Jolla, CA). Then, oligonucleotides encoding a myc epitope (EQKLISEEDL) and flanking *EcoRI* adapters were synthesized, phosphorylated, and ligated into the *EcoRI*-digested metadherin cDNA. The myc-metadherin cDNA was subcloned into the pCMV vector (Clontech, Palo Alto, CA). Human myc-vimentin cDNA was generated by reverse transcription-polymerase chain reaction, using vimentin-specific primers and human mRNA as template, and then subcloned into the pCMV-Myc vector (Clontech, Palo Alto, CA).

Antibodies, immunoblotting, and immunohistology

Anti-T7 phage affinity purified antibody was previously described (Laakkonen et al., 2002). A polyclonal antibody was generated in New Zealand White rabbits against the recombinant metadherin lung-homing domain that was fused to glutathione-S transferase. The initial immunization was done in complete Freund's adjuvant and boosters were with incomplete Freund's adjuvant. The antibody was affinity purified on recombinant hexahistidine-tagged metadherin₍₃₇₈₋₄₄₀₎ peptide coupled to SulfoLink Gel (Pierce, Rockford, IL) via a cysteine residue added to the amino terminus of the metadherin₍₃₇₈₋₄₄₀₎ peptide.

Blood vessel localization of metadherin phage was examined by i.v. injection of 2.5×10^{10} pfu metadherin phage (in 200 μ l M9LB) into the tail vein of a mouse. Blood vessels were visualized by co-injection of phage with 200 μ g of *Lycopersicon esculentum* (tomato) lectin conjugated to fluorescein. The injected materials were allowed to circulate for 10 min. Lungs were removed and frozen in OCT embedding medium (Tissue-Tek).

Tumor cell lysates were prepared in 2.5 \times Laemmli's sample buffer (Laemmli, 1970) at a ratio of 10^6 cells per 150 μ l and subjected to SDS-PAGE on 4%–20% acrylamide gradient gels. Proteins were transferred to PVDF membrane and immunoblots were performed with anti-metadherin₍₃₇₈₋₄₄₀₎ (0.1 μ g/ml) and goat anti-rabbit IgG-HRP (diluted 1:10,000; Bio-Rad, Hercules, CA) and developed using ECL+ plus chemiluminescence reagent (Amersham Biosciences, Piscataway, NJ), according to the manufacturer's instructions. The relative amount of metadherin detected by immunoblot was quantitated using an AlphaMager (Alpha Innotech, San Leandro, CA). β -actin was detected with an anti-actin monoclonal antibody (10 μ g/ml, Chemicon). Transferrin receptor was detected with an anti-transferrin receptor polyclonal antibody (2 μ g/ml, Santa Cruz Biotech, Santa Cruz, CA). Affinity-purified

polyclonal antibody reactive to a 175 kDa protein, Clone D2, was prepared as described for anti-metadherin₍₃₇₈₋₄₄₀₎. Control immunoblots were performed with anti-Clone D2 (0.1 μ g/ml) and goat anti-rabbit IgG-HRP (described above).

For cell surface labeling, anti-metadherin₍₃₇₈₋₄₄₀₎, diluted to 20 μ g/ml in ice-cold IMEM (Invitrogen) with 10% fetal bovine serum (FBS), was added to cells cultured on chamber slides and incubated for 1 hr on ice. The cells were washed with IMEM and fixed with cold 4% paraformaldehyde in PBS for 15 min. Anti-metadherin antibodies were detected with Alexa 594 goat anti-rabbit IgG (diluted 1:500 in PBS with 1% FBS and 3% goat serum). Slides were mounted with Vectashield fluorescence mounting medium (Vector, Burlingame, CA). For permeabilized cell labeling, cells were first fixed with 4% paraformaldehyde (described above) and then treated with 0.1% Triton X-100 in PBSB for 15 min. The cells were washed with PBSB and incubated with anti-metadherin₍₃₇₈₋₄₄₀₎ (diluted to 20 μ g/ml in IMEM with 10% FBS) for 1 hr at room temperature. Anti-metadherin₍₃₇₈₋₄₄₀₎ was detected with Alexa 594 goat anti-rabbit IgG, as described above.

Paraffin-embedded human tissue sections (Spring Biosciences, Fremont, CA) and breast adenocarcinoma tissue array sections (InnoGenex, San Ramon, CA; NCI, Frederick, MD) were deparaffinized and then treated with Target Retrieval Solution (according to the manufacturer's instructions; DAKO, Carpinteria, CA). For immunofluorescence imaging, the sections were stained as described above, except PBSB was substituted for 0.5% Blocking Reagent (NEN Life Sciences, Boston, MA) in 0.1 M Tris/150 mM NaCl. The tissue array sections were stained as described above, except anti-metadherin₍₃₇₈₋₄₄₀₎ was detected with the EnVision + System (according to the manufacturer's instructions; DAKO) and cells were counterstained with hematoxylin (DAKO). To determine specificity, anti-metadherin₍₃₇₈₋₄₄₀₎ (20 μ g/ml) was pre-incubated overnight with 200 μ g/ml recombinant metadherin lung-homing protein or unrelated recombinant control protein (72 amino acid, lung-homing Clone D2) in blocking buffer before immunostaining the sections.

FACS analysis

Transiently transfected HEK293T cells expressing myc-vimentin, myc-metadherin, or myc-pCMV vector alone (Clontech) were detached from their culture dishes by gently washing with PBS containing 1% BSA (PBSB). The cells were then stained with anti-myc mAb (2 μ g/ml in PBSB; Chemicon) for 20 min at 4°C. The cells were washed with PBSB, stained with goat anti-mouse IgG PE-labeled antibody (4 μ g/ml in PBSB; Pharmingen, San Diego, CA), washed again with PBSB, fixed with 2% paraformaldehyde in PBS, resuspended in PBS, and analyzed using a FACScan flow cytometer (BD, San Jose, CA).

To analyze the 4T1 cells by FACS, the cells were detached from culture plates by incubating with PBS with 2 mM EDTA (PBSE) for 10 min. The cells were then washed with PBSB and incubated with 40 μ g/ml (in PBSB) of the following antibodies: anti-Bcl2 (SL-492, Santa Cruz Biotechnology, Santa Cruz, CA), normal rabbit IgG (Sigma, St. Louis, MO), anti-integrin $\alpha_5\beta_1$ (Protein G-purified from rabbit serum containing antibodies raised against human fibronectin receptor), and anti-metadherin₍₃₇₈₋₄₄₀₎. To detect bound antibodies, cells were incubated with goat anti-rabbit IgG-FITC (40 μ g/ml in PBSB; Molecular Probes, Eugene, OR). After the final wash, the cells were resuspended with PBS containing 2 μ g/ml of propidium iodide (PI) and analyzed by FACS.

HEK293T cell homing

HEK293T cells were cotransfected with DsRed2 (Clontech) and either metadherin-pCMV or empty myc-pCMV vector. 2 days posttransfection, the cells were detached with PBSE and filtered through a 40 μ m nylon filter. DsRed2-expressing cells were isolated using a FACS Vantage flow cytometer (BD Biosciences, San Jose, CA). 2.5×10^5 DsRed2-positive cells were injected into the tail vein of nude Balb/c mice. Five mice were injected with each cell type. After 2 hr, the mice were sacrificed, organs were removed and fixed with 4% paraformaldehyde in PBS, and 10 μ m thick frozen tissue sections were prepared. For each lung section, three different fields were counted. Clumps of DsRed2-positive cells with three or more cells were excluded from the count. Five sections per lung were counted.

Tumor metastasis studies

The 4T1 cells were detached from plates with PBSE, washed once with PBS, resuspended to 5×10^5 cells/ml in PBS, and placed on ice. Anti-

metadherin₃₇₈₋₄₄₀ or rabbit IgG (200 µg) was added to 5×10^4 cells and the cells were then injected via the lateral tail vein into female Balb/c nu/nu mice. Animals were sacrificed 7 days after tumor cell injection. Lungs were recovered and fixed with Bouin's solution, and the tumor foci on the surface of the left lobe were counted under a dissecting microscope.

siRNA knockdown of metadherin expression

For the siRNA-mediated knockdown of metadherin expression, nucleotides 1597–1615 of the mouse metadherin cDNA (5'-GTGCCACCGATGTTAC AAG-3') were used as the target sequence. Oligonucleotides containing this target sequence were synthesized and subcloned into the pSilencer 3.0-H1 plasmid (Ambion, Austin, TX) according to the manufacturer's instructions. 4T1 cells were transfected with the metadherin or a negative control siRNA pSilencer vector together with an EGFP-expression vector (Clontech), using a 4:1 ratio of pSilencer to EGFP vectors. 2 days posttransfection, 4T1 cells that were labeled with EGFP and excluded propidium iodide were isolated by FACS. 10,000 or 50,000 of these selected 4T1 cells in 100 µl of PBS were injected into the tail vein of anesthetized nude Balb/c mice. The mouse lungs were harvested 22 days postinjection and fixed with Bouin's solution. The tumor foci on the lung surface were counted under a dissecting microscope. Data were recorded as the number of tumor foci formed per 10,000 cells injected. The levels of β -actin and metadherin mRNA in siRNA-transfected cells were determined using a one-step RT-PCR RNA Amplification Kit and LightCycler Instrument (according to manufacturer's protocol; Roche, Indianapolis, IN).

GenBank accession number

The nucleotide sequence of the mouse metadherin cDNA has been deposited in GenBank and received accession number AY553638.

Acknowledgments

We thank Drs. Kathryn Ely, Eva Engvall, and Yu Yamaguchi for comments on the manuscript. We also thank Yoav Altman for excellent technical assistance and Roslind Varghese for editing. This work was supported by grants PO1 CA 82713 and Cancer Center Support Grant CA 30199 from the NCI and DAMD17-02-1-0315 from the DOD. D.M.B. was supported by Postdoctoral training grant T32 CA 09579 from the NCI.

Received: September 5, 2003

Revised: February 13, 2004

Accepted: March 8, 2004

Published: April 19, 2004

References

- Abdel-Ghany, M., Cheng, H.C., Eible, R.C., and Pauli, B.U. (2001). The breast cancer beta 4 integrin and endothelial human CLCA2 mediate lung metastasis. *J. Biol. Chem.* 276, 25438–25446.
- Altschul, S.F., Madden, T.L., Schaffer, A.A., Zhang, J., Zhang, Z., Miller, W., and Lipman, D.J. (1997). Gapped BLAST and PSI-BLAST: a new generation of protein database search programs. *Nucleic Acids Res.* 25, 3389–3402.
- Amer, M.H. (1982). Chemotherapy and pattern of metastases in breast cancer patients. *J. Surg. Oncol.* 19, 101–105.
- Arap, W., Pasqualini, R., and Ruoslahti, E. (1998). Cancer treatment by targeted drug delivery to tumor vasculature in a mouse model. *Science* 279, 377–380.
- Arap, W., Haedicke, W., Bernasconi, M., Kain, R., Rajotte, D., Krajewski, S., Ellerby, H.M., Bredesen, D.E., Pasqualini, R., and Ruoslahti, E. (2002). Targeting the prostate for destruction through a vascular address. *Proc. Natl. Acad. Sci. USA* 99, 1527–1531.
- Aslakson, C.J., and Miller, F.R. (1992). Selective events in the metastatic process defined by analysis of the sequential dissemination of subpopulations of a mouse mammary tumor. *Cancer Res.* 52, 1399–1405.
- Berlin, O., Samid, D., Donthineni-Rao, R., Akeson, W., Amiel, D., and Woods, V.L., Jr. (1993). Development of a novel spontaneous metastasis model of human osteosarcoma transplanted orthotopically into bone of athymic mice. *Cancer Res.* 53, 4890–4895.
- Boogerd, W. (1996). Central nervous system metastasis in breast cancer. *Radiother. Oncol.* 40, 5–22.
- Chambers, A.F., Groom, A.C., and MacDonald, I.C. (2002). Dissemination and growth of cancer cells in metastatic sites. *Nat. Rev. Cancer* 2, 563–572.
- Cheng, H.C., Abdel-Ghany, M., Eible, R.C., and Pauli, B.U. (1998). Lung endothelial dipeptidyl peptidase IV promotes adhesion and metastasis of rat breast cancer cells via tumor cell surface-associated fibronectin. *J. Biol. Chem.* 273, 24207–24215.
- Dexter, D.L., Kowalski, H.M., Blazar, B.A., Fligiel, Z., Vogel, R., and Heppner, G.H. (1978). Heterogeneity of tumor cells from a single mouse mammary tumor. *Cancer Res.* 38, 3174–3181.
- Eible, R.C., Widom, J., Gruber, A.D., Abdel-Ghany, M., Levine, R., Goodwin, A., Cheng, H.C., and Pauli, B.U. (1997). Cloning and characterization of lung-endothelial cell adhesion molecule-1 suggest it is an endothelial chloride channel. *J. Biol. Chem.* 272, 27853–27861.
- Fidler, I.J. (2001). Seed and soil revisited: contribution of the organ microenvironment to cancer metastasis. *Surg. Oncol. Clin. N. Am.* 10, 257–269.
- Glasgow, J. (1998). Proceedings, Sixth International Conference on Intelligent Systems for Molecular Biology: June 28–July 1, 1998, Montreal, Quebec (Menlo Park, CA: AAAI Press).
- Harris, J., Morrow, M., and Norton, L. (1997). Malignant tumors of the breast. In *Cancer: Principles and Practice of Oncology* (Philadelphia: Lippincott-Raven), pp. 1557–1616.
- Hoffman, J.A., Laakkonen, P., Porkka, K., Bernasconi, M., and Ruoslahti, E. (2004). *In vivo* and *ex vivo* selections using phage-displayed libraries. In *Phage Display: A Practical Approach*, T. Clackson and H. Lowman, eds. (Oxford, UK: Oxford University Press).
- Johnson, R.C., Zhu, D., Augustin-Voss, H.G., and Pauli, B.U. (1993). Lung endothelial dipeptidyl peptidase IV is an adhesion molecule for lung-metastatic rat breast and prostate carcinoma cells. *J. Cell Biol.* 121, 1423–1432.
- Kamby, C., Dirksen, H., Vejborg, I., Daugaard, S., Guldhammer, B., Rossing, N., and Mouridsen, H.T. (1987). Incidence and methodologic aspects of the occurrence of liver metastases in recurrent breast cancer. *Cancer* 59, 1524–1529.
- Krogh, A., Larsson, B., von Heijne, G., and Sonnhammer, E.L. (2001). Predicting transmembrane protein topology with a hidden Markov model: application to complete genomes. *J. Mol. Biol.* 305, 567–580.
- Kyte, J., and Doolittle, R.F. (1982). A simple method for displaying the hydrophobic character of a protein. *J. Mol. Biol.* 157, 105–132.
- Laakkonen, P., Porkka, K., Hoffman, J.A., and Ruoslahti, E. (2002). A tumor-homing peptide with a targeting specificity related to lymphatic vessels. *Nat. Med.* 8, 751–755.
- Laemmli, U.K. (1970). Cleavage of structural proteins during the assembly of the head of bacteriophage T4. *Nature* 227, 680–685.
- Lal, A., Lash, A.E., Altschul, S.F., Velculescu, V., Zhang, L., McLendon, R.E., Marra, M.A., Prange, C., Morin, P.J., Polyak, K., et al. (1999). A public database for gene expression in human cancers. *Cancer Res.* 59, 5403–5407.
- Lash, A.E., Tolstoshev, C.M., Wagner, L., Schuler, G.D., Strausberg, R.L., Riggins, G.J., and Altschul, S.F. (2000). SAGEmap: a public gene expression resource. *Genome Res.* 10, 1051–1060.
- Luo, L., Salunga, R.C., Guo, H., Bittner, A., Joy, K.C., Galindo, J.E., Xiao, H., Rogers, K.E., Wan, J.S., Jackson, M.R., and Elander, M.G. (1999). Gene expression profiles of laser-captured adjacent neuronal subtypes. *Nat. Med.* 5, 117–122.
- McIntosh, D.P., Tan, X.Y., Oh, P., and Schnitzer, J.E. (2002). Targeting endothelium and its dynamic caveolae for tissue-specific transcytosis in vivo: a pathway to overcome cell barriers to drug and gene delivery. *Proc. Natl. Acad. Sci. USA* 99, 1996–2001.

- Mechlér, B.M. (1987). Isolation of messenger RNA from membrane-bound polysomes. *Methods Enzymol.* 152, 241–248.
- Miller, F.R., Miller, B.E., and Heppner, G.H. (1983). Characterization of metastatic heterogeneity among subpopulations of a single mouse mammary tumor: heterogeneity in phenotypic stability. *Invasion Metastasis* 3, 22–31.
- Muller, A., Horney, B., Soto, H., Ge, N., Catron, D., Buchanan, M.E., McClanahan, T., Murphy, E., Yuan, W., Wagner, S.N., et al. (2001). Involvement of chemokine receptors in breast cancer metastasis. *Nature* 410, 50–56.
- Orr, F.W., and Wang, H.H. (2001). Tumor cell interactions with the microvasculature: a rate-limiting step in metastasis. *Surg. Oncol. Clin. N. Am.* 10, 357–381.
- Pasqualini, R., and Ruoslahti, E. (1996). Organ targeting in vivo using phage display peptide libraries. *Nature* 380, 364–366.
- Porkka, K., Laakkonen, P., Hoffman, J.A., Bernasconi, M., and Ruoslahti, E. (2002). A fragment of the HMGN2 protein homes to the nuclei of tumor cells and tumor endothelial cells in vivo. *Proc. Natl. Acad. Sci. USA* 99, 7444–7449.
- Price, J.E., Polyzos, A., Zhang, R.D., and Daniels, L.M. (1990). Tumorigenicity and metastasis of human breast carcinoma cell lines in nude mice. *Cancer Res.* 50, 717–721.
- Pulaski, B.A., and Ostrand-Rosenberg, S. (1998). Reduction of established spontaneous mammary carcinoma metastases following immunotherapy with major histocompatibility complex class II and B7.1 cell-based tumor vaccines. *Cancer Res.* 58, 1486–1493.
- Radinsky, R. (1995). Modulation of tumor cell gene expression and phenotype by the organ-specific metastatic environment. *Cancer Metastasis Rev.* 14, 323–338.
- Rajotte, D., and Ruoslahti, E. (1999). Membrane dipeptidase is the receptor for a lung-targeting peptide identified by in vivo phage display. *J. Biol. Chem.* 274, 11593–11598.
- Rajotte, D., Arap, W., Hagedorn, M., Koivunen, E., Pasqualini, R., and Ruoslahti, E. (1998). Molecular heterogeneity of the vascular endothelium revealed by in vivo phage display. *J. Clin. Invest.* 102, 430–437.
- Ruoslahti, E. (2002). Specialization of tumour vasculature. *Nat. Rev. Cancer* 2, 83–90.
- Rutgers, E.J., van Slooten, E.A., and Kluck, H.M. (1989). Follow-up after treatment of primary breast cancer. *Br. J. Surg.* 76, 187–190.
- Tomin, R., and Donegan, W.L. (1987). Screening for recurrent breast cancer—its effectiveness and prognostic value. *J. Clin. Oncol.* 5, 62–67.
- van 't Veer, L.J., Dai, H., van de Vijver, M.J., He, Y.D., Hart, A.A., Mao, M., Peterse, H.L., van der Kooy, K., Marton, M.J., Witteveen, A.T., et al. (2002). Gene expression profiling predicts clinical outcome of breast cancer. *Nature* 415, 530–536.
- Weiss, L. (1992). Comments on hematogenous metastatic patterns in humans as revealed by autopsy. *Clin. Exp. Metastasis* 10, 191–199.

Stage-specific vascular markers revealed by phage display in a mouse model of pancreatic islet tumorigenesis

Johanna A. Joyce,^{1,3} Pirjo Laakkonen,^{2,3,4} Michele Bernasconi,^{2,5} Gabriele Bergers,^{1,6} Erkki Ruoslahti,^{2,*} and Douglas Hanahan^{1,*}

¹Department of Biochemistry and Biophysics, Diabetes and Comprehensive Cancer Centers, University of California, San Francisco, 513 Parnassus Avenue, San Francisco, California 94143

²Cancer Research Center, The Burnham Institute, 10901 North Torrey Pines Road, La Jolla, California 92037

³These authors contributed equally to this work.

⁴Present address: Molecular/Cancer Biology Laboratory, Biomedicum Helsinki, University of Helsinki, P.O.B. 63 (Haartmaninkatu 8), FIN-00014 Helsinki, Finland.

⁵Present address: Functional Genomics Unit, Divisions of Infectious Diseases and Oncology, The University Children's Hospital of Zürich, August-Forel Strasse 1 CH-8008 Zürich, Switzerland.

⁶Present address: Department of Neurological Surgery, University of California, San Francisco, 513 Parnassus Avenue, San Francisco, California 94143.

*Correspondence: dh@biochem.ucsf.edu (D.H.); ruoslahti@burnham.org (E.R.)

Summary

The vasculature in the angiogenic stages of a mouse model of pancreatic islet carcinogenesis was profiled *in vivo* with phage libraries that display short peptides. We characterized seven peptides distinguished by their differential homing to angiogenic progenitors, solid tumors, or both. None homed appreciably to normal pancreatic islets or other organs. Five peptides selectively homed to neoplastic lesions in the pancreas and not to islet β cell tumors growing subcutaneously, xenotransplant tumors from a human cancer cell line, or an endogenously arising squamous cell tumor of the skin. Three peptides with distinctive homing to angiogenic islets, tumors, or both colocalized with markers that identify endothelial cells or pericytes. One peptide is homologous with pro-PDGF-B, which is expressed in endothelial cells, while its receptor is expressed in pericytes.

Introduction

Angiogenesis, the formation of new blood vessels, is essential for tumor growth. The transition from normal to neoplastic vasculature during tumorigenesis has been termed the "angiogenic switch," and both positive and negative regulators of the switch have been identified (Hanahan and Folkman, 1996). The vascular anatomy of tumors is typically distinct from that of normal tissues (Carmeliet and Jain, 2000). In contrast to their normal counterparts, tumor vessels are tortuous and dilated and show reduced vessel integrity. Tumor vessels often have numerous fenestrae or discontinuities, loose interendothelial junctions, and a discontinuous or absent basement membrane, collectively resulting in vessel leakiness (Carmeliet and Jain, 2000; Hashizume et al., 2000).

We are only beginning to understand the molecular events underlying the pronounced abnormalities evident in the angiogenic vasculature of tumors and progenitor lesions. Previous

studies have shown that a number of genes are upregulated during the transition from normal to tumor blood vessels, including the integrins $\alpha v\beta 3$, $\alpha v\beta 5$, and $\alpha 5\beta 1$; several matrix metalloproteinases; and various endothelial growth factor receptors (Hanahan and Folkman, 1996; Ruoslahti, 2002). Recently, St. Croix et al. further showed, using a comparative RNA expression profiling technology (SAGE), that a number of genes or EST's were selectively expressed or upregulated in the tumor endothelium of human colorectal cancer, relative to the corresponding normal colonic vasculature (St. Croix et al., 2000). This approach relied on substantive differences in gene expression to identify tumor-specific endothelial markers, which will likely only reveal a subset of alterations that distinguish normal and tumor blood vessels. Specific binding of phage from libraries that can display more than a billion random peptide sequences offers a complementary approach for comparative screening. *In vivo* phage display screening has proven to be a powerful method for un-

SIGNIFICANCE

While there is abundant evidence that tumor vasculature is functionally and morphologically aberrant, we show herein using a peptide epitope profiling technology that the angiogenic vasculature in premalignant lesions is distinguishable from normal as well as tumor vessels in a model of multistage tumorigenesis. Moreover, both angiogenic progenitor and tumor vessels in the pancreas have molecular signatures distinct from tumors growing in or under the skin, even of the analogous cell type. The stage and organ specificities of particular homing peptides may prove instructive about mechanisms regulating the neovasculature in different pathways of tumorigenesis, suggest means to detect and distinguish premalignant and malignant lesions noninvasively, and predict differential sensitivity to therapeutic agents targeting angiogenesis.

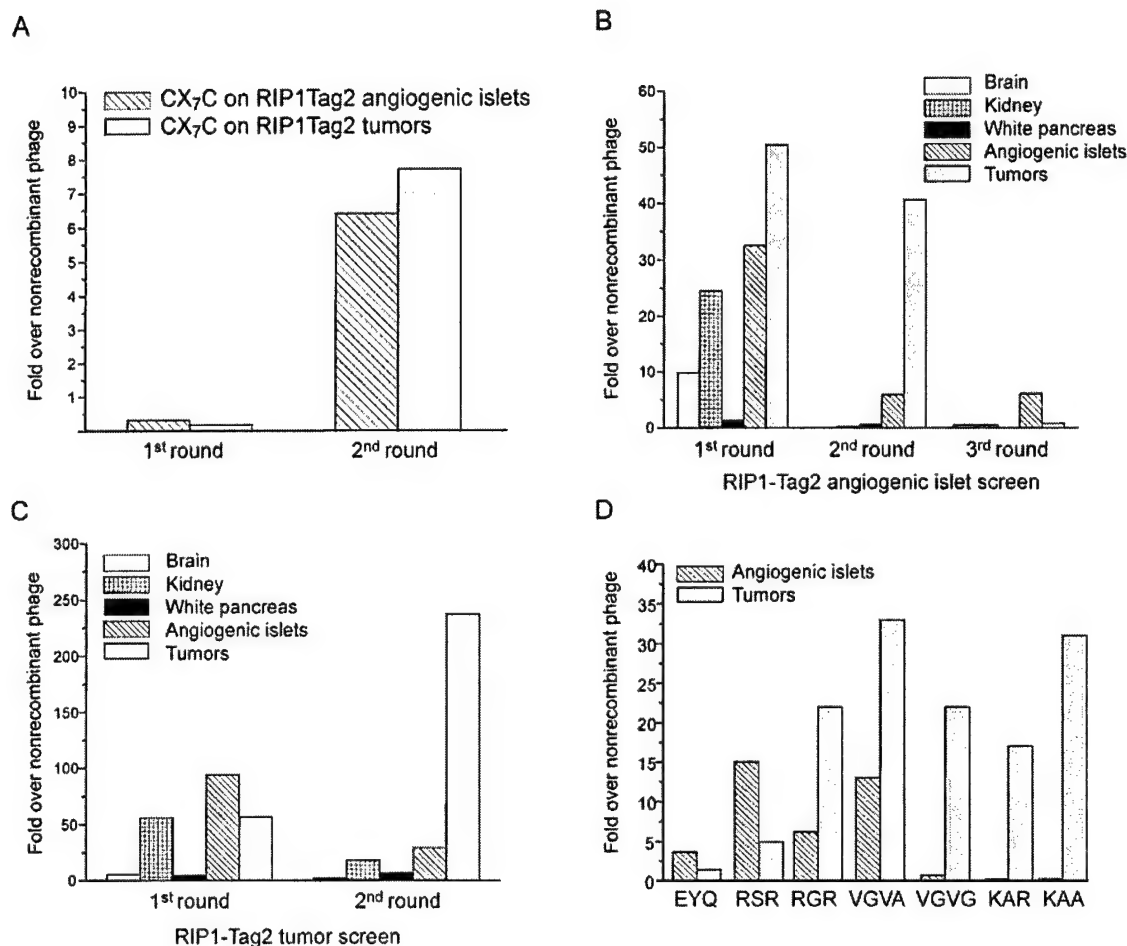


Figure 1. Isolation of stage-specific phage using ex vivo and in vivo phage display

A: Ex vivo screening on cells derived from RIP1-Tag2 angiogenic islets or tumors using the CX₇C peptide library displayed on T7 phage. The enriched phage pools were used for subsequent in vivo homing to RIP1-Tag2 angiogenic islets (three rounds of selection) (**B**) and tumors (two rounds of selection) (**C**). **D:** In vivo homing of individual phage to RIP1-Tag2 angiogenic islets and tumors.

covering differences among individual vascular beds in normal organs (Pasqualini and Ruoslahti, 1996; Rajotte et al., 1998) and has also yielded peptides that specifically home to blood vessels or lymphatics in tumors (Arap et al., 1998; Laakkonen et al., 2002; Porkka et al., 2002). The targets for these peptides in blood vessels include the $\alpha v \beta 3$ and $\alpha v \beta 5$ integrins (Arap et al., 1998) and aminopeptidase N (Pasqualini et al., 2000).

In this and a companion study (Hoffman et al., 2003 [this issue of *Cancer Cell*]), we set out to use phage-display profiling to ask whether additional levels of neoplastic vascular specialization might exist in tumor development. We sought to distinguish the vessels of premalignant angiogenic lesions from those of angiogenic solid tumors and to examine whether differences exist between angiogenic vessels of tumors developing in different organs. Previous studies have profiled differences between normal blood vessels and the vasculature of transplanted tumors in immunodeficient mice. Unlike these transplanted tumors, transgenic tumor models provide an opportunity to examine pre-neoplastic changes unfolding in different organs in a more physiologically relevant microenvironment.

We used a prototypical mouse model of multistage tumorigenesis, the RIP1-Tag2 transgenic model of islet cell carcinoma (Hanahan, 1985), to address our hypothesis that the vasculature of pre-neoplastic lesions differs from that of established tumors. RIP1-Tag2 transgenic mice express the SV40 T antigens (Tag) under the control of the insulin gene promoter, which elicits the sequential development of tumors in the islets of Langerhans over a period of 12–14 weeks. Hyperplastic islets begin to appear at around 4 weeks of age, and angiogenesis is activated a few weeks later in a subset of the hyperplastic islets, producing angiogenic (dysplastic) islets (Bergers et al., 1998; Folkman et al., 1989). Solid tumors form beginning at 9 to 10 weeks, initially presenting as small nodules that grow and progress to large islet tumors with well-defined margins, as well as two classes of invasive carcinoma (Lopez and Hanahan, 2002). We set out to identify stage-specific molecular markers accessible via the circulation, either on the surface of endothelial cells, their periendothelial support cells (pericytes and smooth muscle cells), or even tumor cells themselves (as a result of the hemorrhagic,

-leaky angiogenic vasculature). We successfully selected phage pools that homed preferentially to different stages during RIP1-Tag2 tumorigenesis. In addition to "pan-angiogenic" markers shared by many types of tumors, we identified vascular target molecules that are characteristic of this tumor's tissue of origin and are not expressed in the vessels of several tumor types growing in or under the skin. We have begun to investigate the binding partners for these peptides and present evidence linking one peptide to a vascular signaling circuit involving PDGF ligands expressed in endothelial cells and their receptor PDGFR β , expressed in pericytes of the angiogenic vasculature.

Results

Isolation of stage-specific phage from RIP1-Tag2 mice

RIP1-Tag2 mice develop multifocal angiogenic islet progenitors and then solid tumors in a stepwise manner, such that at 12 weeks of age, each mouse will typically have approximately 50 angiogenic islets and 2–6 small tumors. This circumstance allowed us to use 12-week-old mice to select for phage binding to angiogenic islet progenitors and/or tumors in the same mouse. In order to enrich for phage that bind to RIP1-Tag2 target cells (endothelial, perivascular, and tumor), we included a pre-selection step (Laakkonen et al., 2002; Porkka et al., 2002) on cell suspensions prepared from pancreatic lesions. Two rounds of *ex vivo* selection from a CX₇C peptide library on cell suspensions from angiogenic islets or solid tumors yielded phage pools that bound 7- to 8-fold over a control, nonrecombinant phage to their respective target cells (Figure 1A). These enriched phage pools were used in subsequent *in vivo* rounds to select for phage that would home specifically to either angiogenic islets or tumors in RIP1-Tag2 mice.

Three rounds of *in vivo* selection on angiogenic islets resulted in a phage pool that selectively homed to angiogenic islets. The homing to the islets was 7-fold higher than to tumors in the same mouse (Figure 1B). There was no homing to control organs. The tumor selection yielded a pool that showed an 8-fold preference for tumors versus angiogenic islets in the same mouse following two rounds of *in vivo* selection (Figure 1C).

Sequencing of phage from the selected pools identified a number of peptide sequences that were represented more than once, and these were tested for their ability to bind cell suspensions prepared from angiogenic islets and tumors. Six of the phage selected for further analysis were from the tumor screen (referred to as KAA, RGR, RSR, VGVA, VGVG, and KAR), and one (EYQ) was picked from the angiogenic screen. Peptide sequences corresponding to each of these peptide motifs are shown in Table 1. All of these peptides are linear, although the phage library used here (CX₇C) was designed to express peptides cyclized by a covalent bond between two cysteine residues. However, a library of this design does contain a minority of linear peptides. A stop codon occurring within the random insert will cause truncation of the peptide, and a frameshift mutation frequently changes the second cysteine into valine. It may be that the target molecules in the RIP1-Tag2 tumors selected for linear peptides. In the companion study (Hoffman et al., 2003), the same library yielded cyclic homing peptides. The RIP1-Tag2 homing phage fall into three classes based on their homing either to angiogenic islets or to tumors *in vivo* (Figure 1D) and their *ex vivo* binding patterns: tumor-selective phage

(KAA, KAR, and VGVG), angiogenic islet-selective phage (RSR and EYQ), and phage that home to both types of angiogenic lesions (VGVA and RGR). Some of the selected peptides that share similar peptide motifs also display similar homing patterns. For example, KAA and KAR (CKAAKNK and CKGAKAR = XBXXBXB, where B represents basic residues and X denotes uncharged residues) both preferentially home to tumors over angiogenic islets. However, other related peptides such as RGR and RSR (CRGRRST and CRSRKG = XBXXBX) have quite different homing capabilities. Interestingly, all of these peptides are distinct from those found previously in phage display screens of transplant tumors (Arap et al., 1998; Laakkonen et al., 2002; Porkka et al., 2002).

Stage-specific homing of fluorescein-conjugated peptides

To confirm that the selective phage homing was due to the displayed peptide sequences, we studied the localization of fluorescein-conjugated peptides after intravenous injection; one peptide from each homing class was selected for detailed analysis. We used 8-week-old RIP1-Tag2 mice to examine peptide localization during the angiogenic switch and 12-week-old RIP1-Tag2 mice to visualize both angiogenic islets and tumors.

The observed peptide localization profiles in each case closely mimicked that of the cognate phage, as shown in Figure 1D, with each peptide falling into the same of the three homing classes. Figure 2 illustrates the peptide localization for these three representative fluorescein-conjugated peptides: RSR (angiogenic-selective), KAA (tumor-selective), and RGR (angiogenic- and tumor-homing). RSR shows abundant accumulation in RIP1-Tag2 angiogenic islets (Figure 2B) but little or no localization in tumors (Figure 2C) or normal islets (Figure 2A). KAA shows abundant localization in RIP1-Tag2 tumors (Figure 2F) but little or no localization in angiogenic islets (Figure 2E) or normal islets (Figure 2D). Finally, RGR localizes in both RIP1-Tag2 angiogenic islets (Figure 2H) and tumors (Figure 2I) but there is little or no peptide in normal islets (Figure 2G). It was somewhat unexpected that RSR, which was selected from the tumor phage screening, preferentially bound to angiogenic islets. It seems that the epitope this peptide binds to is present both in tumors and angiogenic islets, but is more abundant in angiogenic islets. This result could also be indicative of the heterogeneity of the pools of angiogenic islets or tumors isolated by gross examination, in which there are multiple lesions of differing grades within each group. Hence, a gross selection of the tumor pool may in fact include some large, advanced angiogenic islets that can only be definitively distinguished by histological grading, which was performed in conjunction with the peptide homing to the different lesions.

Homing of the peptides to the pancreatic islet lesions was specific: little or no homing was detected in normal islets, brain, liver, lung, and spleen (Figures 2K and 2L and data not shown). Fluorescence was detected in kidney, presumably as a result of uptake from glomerular filtrate (Figure 2J). Representative figures of control tissues from a RIP1-Tag2 mouse injected with fluorescein-conjugated RGR peptide are shown in Figures 2J–2L. A similar absence of fluorescence in control tissues was observed for all other injected peptides (data not shown). In addition, control peptides did not show specific homing to any of the RIP1-Tag2 lesion stages or to a number of normal tissues.

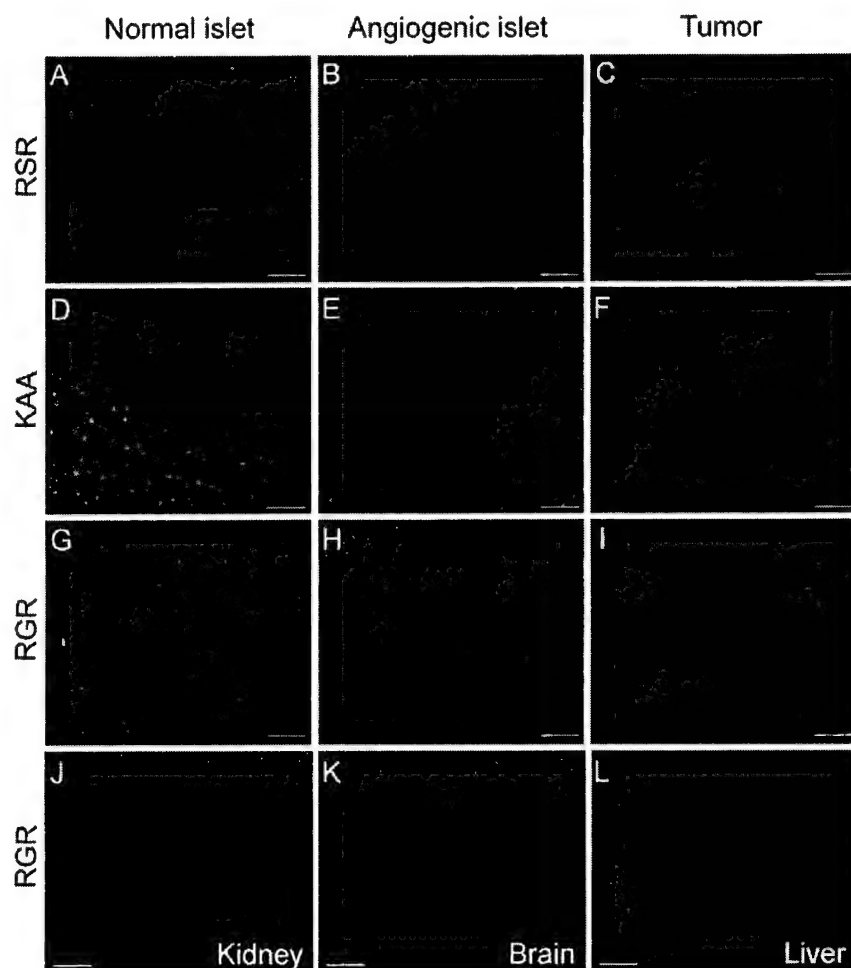


Figure 2. Stage-specific homing of fluorescein-conjugated peptides in RIP1-Tag2 model

Visualization of an angiogenic islet-selective peptide (RSR) homing is shown in normal islet (A), angiogenic islet (B), and tumor (C). Homing profiles are also shown for a tumor-selective peptide (KAA) to normal islet (D), angiogenic islet (E), and tumor (F), as well as of a peptide (RGR) that homes to both angiogenic islets and tumors (G, normal islet; H, angiogenic islet; and I, tumor). Control tissues (J, kidney; K, brain; and L, liver) from a RIP1-Tag2 mouse injected with fluorescein-conjugated RGR peptide are also presented. Similar absence of fluorescence in control tissues was observed for all other injected peptides, indicative of a lack of specific homing. The scale bar corresponds to 50 μ M.

Fluorescein-conjugated peptides colocalize with vascular markers

We reasoned that intravenous administration of the phage libraries would select for phage carrying peptides that bind to endothelial molecules specific for the target vasculature. The expectation of endothelial selectivity is based upon the preferential exposure of phage to luminal cells of the vasculature, as well as the appreciable size of the phage and the short time the phage are allowed to circulate (Pasqualini and Ruoslahti, 1996). In order to test this expectation, tissues were collected following i.v. infusion with the various fluorescein-conjugated peptides, sectioned, and evaluated with endothelial cell markers. The primary analysis involved immunostaining with a mouse pan-endothelial cell antigen (MECA32) antibody that recognizes a dimer of 50–55 kDa protein subunits present on all endothelial cells (Hallman et al., 1995; Leppink et al., 1989) (Figures 3B, 3C, 3H, 3I, 3N, and 3O). Additional analyses (not shown) involved immunostaining to reveal CD31/PECAM or systemic infusion of a fluorescent-labeled lectin that binds to the endothelial lumen. In addition, tissue sections from peptide-infused mice were stained with an antibody recognizing NG2, a marker of the neovascular pericytes (Schlingemann et al., 1990, 1991) (Figures 3E, 3F, 3K, 3L, 3Q, and 3R). Remarkably, all three peptides (RSR, KAA, and RGR) show some colocalization both with endo-

thelial cell and pericyte markers, indicating that each homes to and binds moieties associated with both cell types (Figure 3 and data not shown). Again, there was no colocalization of these peptides with those same markers in the adjacent exocrine pancreas or in normal pancreatic islets; tissue sections stained with MECA32 and NG2 showed some colocalization, consistent with the proximity of endothelial cells and pericytes (Figures 3S–3U).

The apparent homing of peptides representing all three classes of stage specificity to both pericytes and endothelial cells was unexpected. It may be pertinent that the RIP1-Tag2 tumor vasculature is known to be leaky, as evidenced by extensive microhemorrhaging (Parangi et al., 1995) and morphometric analysis (Hashizume et al., 2000; Morikawa et al., 2002; Thurston et al., 1998), such that the circulating phage pool likely had access to the extraluminal vascular microenvironment, where receptors on pericytes and in the extracellular matrix could be accessible. It is known that the vasculature of both angiogenic islets and tumors is leaky (Morikawa et al., 2002). However, reciprocal homing of the peptides that recognize the angiogenic islet but not tumor vessels, and vice versa, excludes the possibility that the recognition of angiogenic islet versus tumor vessels would simply be caused by differences in the leakiness of the

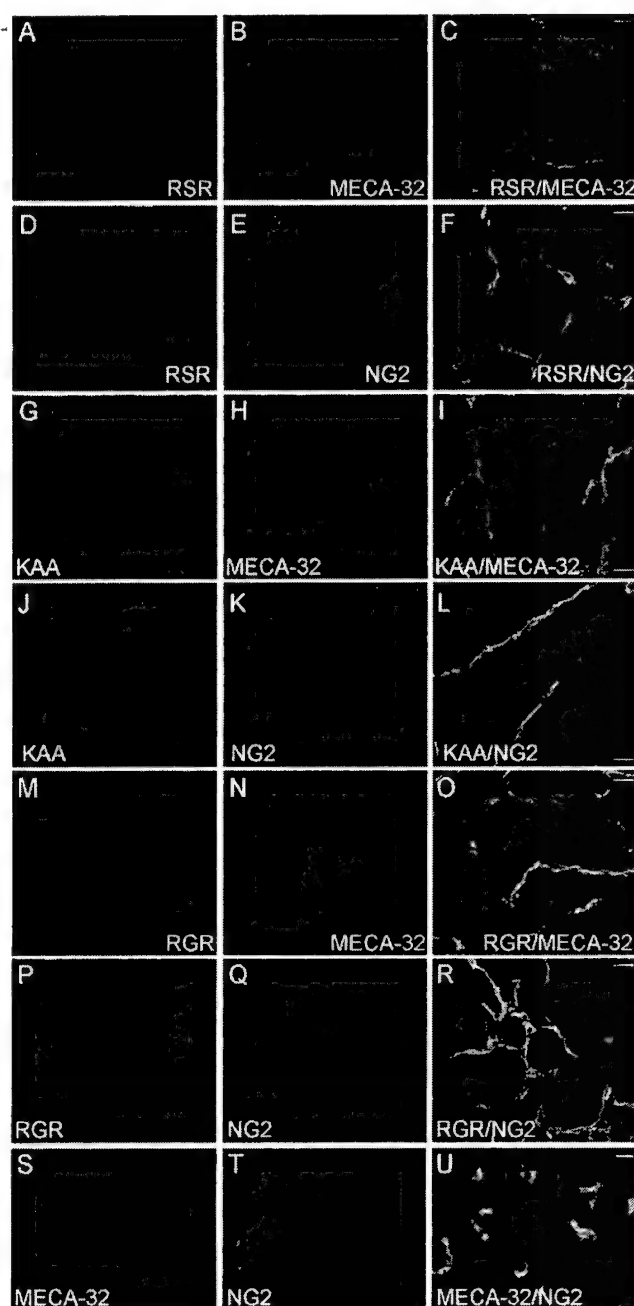


Figure 3. Colocalization of fluorescein-conjugated peptides with vascular markers in RIP1-Tag2 islet lesions

RSR peptide localization in an angiogenic islet is shown in (A) and (D) (green), while co-staining for MECA32 (red) and the merge are shown in (B) and (C). Co-staining for NG2 (red) is shown in (E), with the merge in (F). KAA peptide localization in a tumor is shown in (G) and (J) (green), while co-staining for MECA32 (red) and the merge are shown in (H) and (I). Co-staining for NG2 (red) is shown in (K), with the merge in (L). RGR peptide localization in an angiogenic islet is shown in (M) and (P) (green), while co-staining for MECA32 (red) and the merge are shown in (N) and (O). Co-staining for NG2 (red) is shown in (Q), with the merge in (R). Staining for endothelial cells (MECA32) (S) and pericytes (NG2) (T) in tumor sections demonstrated their close association (U). Scale bar: 10 μ m.

vessels. The ex vivo pre-selection step we used to enrich for RIP1-Tag2-specific targets may have similarly selected for non-luminal endothelial binding partners, but it should be emphasized that any peptide selected ex vivo must also have been accessible via the circulation during the in vivo selections. Consistent with this logic, phage-displaying peptides that bind to the pericyte marker, NG2, have previously been shown to home to a transplant tumor in vivo (Burg et al., 1999).

Specificity of in vivo homing to islet tumors in the pancreas

Selection of phage that home to the vasculature of neoplastic lesions in RIP1-Tag2 mice can be envisioned to identify two classes of peptides: those whose cognate receptors are specific to angiogenic islets and/or tumors in the pancreas and those that also home to the angiogenic vasculature in other tumor types. Therefore, we asked whether phage and peptides selected in pancreatic neoplasias would home to two different transplant tumors growing subcutaneously or to de novo skin tumors induced in another transgenic mouse model.

β TC3 transplant tumors arise following subcutaneous inoculation of nude mice with cultured islet tumor-derived (β TC3) cells (Efrat et al., 1988), allowing the study of islet tumors and their vasculature outside of their natural environment in the pancreas. Because the vasculature of a subcutaneously grown β TC3 tumor derives from skin, we also tested another subcutaneous transplant tumor, arising from inoculation of the MDA-MB-435 human breast carcinoma cell line. Finally, K14-HPV16 mice, another well-studied transgenic mouse model of cancer that develop tumors of the squamous epithelial cells of the skin (Arbeit et al., 1994; Coussens et al., 1996), allowed us to compare RIP1-Tag2 islet tumors to a tumor with similar multistage pathogenesis arising in a different tissue. The relative homing efficiencies in the various tumor models of the phage from the RIP1-Tag2 tumor screen fall broadly into two categories: those that selectively home to RIP1-Tag2 tumors (KAA, RGR, VGVA) and those that show a more general homing to other tumors in addition to RIP1-Tag2 (VGVG, KAR) (Figure 4A). The phage homing data were supported by i.v. injection of fluorescein-conjugated peptides corresponding to the phage. Results for the three representative peptides are summarized in Figure 4B, and an example of the tissue fluorescence produced following injection of the KAR peptide in different tumors is shown in Figures 4C–4E.

Homing during non-tumor angiogenesis was examined using angiogenesis in subcutaneously implanted matrigel plugs. All peptides except one showed no homing to the matrigel plugs. The RGR peptide appeared in a punctate manner in some blood vessels. However, the intensity was much lower and the pattern quite different than in RIP-Tag lesions (data not shown). This indicates that this set of peptides are selective for neovascularization during tumorigenesis and are not general markers of neovessel formation.

Identification of candidate vascular receptors

The set of peptides homing to angiogenic neoplasias in the pancreas were applied to database searches, seeking to identify mouse proteins with sequences homologous to the peptides. Table 1 lists candidate proteins with such homologies that were deemed to be of interest. In theory, these proteins could correspond to putative ligands mimicked by the phage-displayed

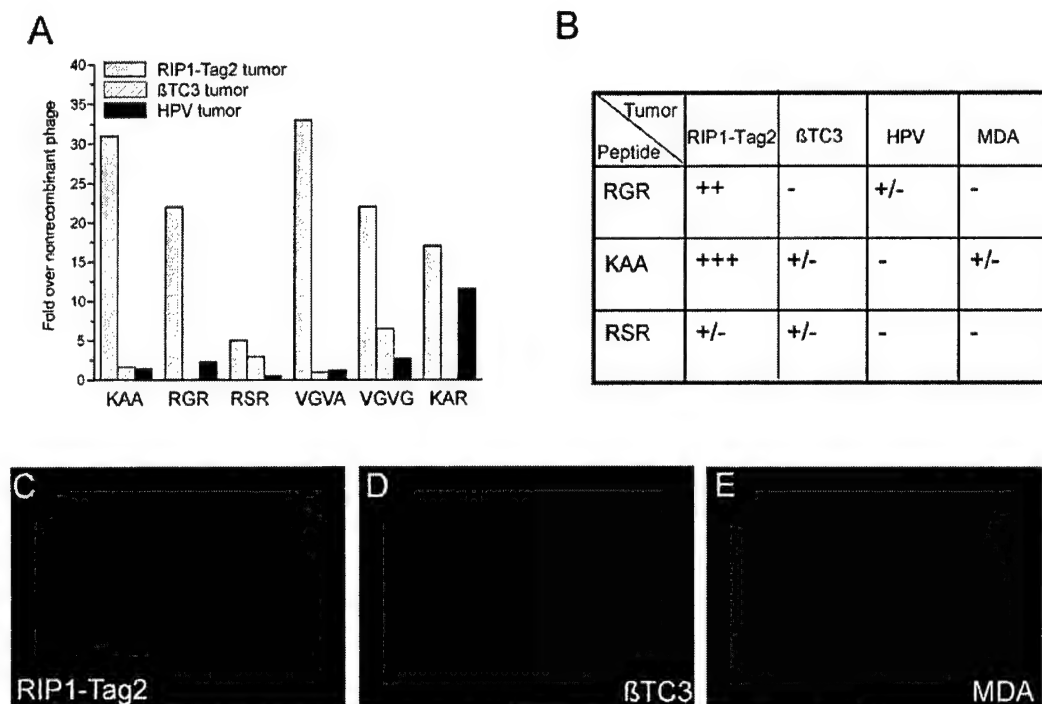


Figure 4. Evaluation of the neoplastic specificity of selected homing phage and peptides

A: Bar graph showing homing efficiency of individual phage to a pancreatic islet tumor in a RIP1-Tag2 mouse, a βTC3-derived subcutaneous transplant tumor in a nude mouse, and a squamous cell carcinoma in a K14-HPV16 mouse.

B: Table summarizing the relative homing of fluorescein-conjugated peptides to different tumor models. +++ indicates strong homing, as revealed by the fluorescent intensity of i.v. injected peptide, ++ indicates moderate homing, + indicates weak homing, - indicates absence of homing. Representative images of fluorescein-conjugated KAR peptide homing to a RIP1-Tag2 pancreatic islet tumor (**C**), a βTC3 subcutaneous tumor (**D**), and an MDA subcutaneous tumor (**E**) are also shown. Magnification 200×.

peptides. Many of the candidate proteins have been previously associated with the vasculature. One protein, collagen XII, was found to share homology with two peptides: KAR (CKGAKAR) and VGVA (FRVGVADV), though in different structural domains. It is interesting to note that collagen XII was also identified by gene expression profiling as a gene that is overexpressed in tumor endothelial cells (St. Croix et al., 2000; and <http://mendel.imp.univie.ac.at/SEQUENCES/TEMS/mainpgs/temtable.html>).

It was somewhat surprising that homologies to peptide se-

quences in two cell surface receptors, fibroblast growth factor receptor 1 (FGFR1) and Tie-1, were revealed by homology searching, as phage-displayed peptides have traditionally been thought to mimic ligands not receptors. However, in the case of FGFR1, the particular peptide sequence (YQLDV) has been reported to be in the ligand binding domain D2 (Plotnikov et al., 1999), suggesting the possibility that the phage displaying this peptide may in fact be binding to FGFR1 ligands, i.e., the fibroblast growth factors (FGFs). It is well known that many of the

Table 1. Candidate mouse proteins sharing motifs with homing peptides

Peptide	Peptide sequence	Extended motif	Mouse protein with the motif	Accession number
RGR	CRGRRST	RGRRS RGRR	PDGF-B Stromal interaction molecule 2	P31240 Q9P246
RSR	CRSRKG	CRSR-G	Cadherin EGF LAG receptor 1	O35161
KAA	CKAAKNK	CKA-K	WNT-2	NPO76142
KAR	CKGAKAR	CKGAKA AKAR GAKAR	Collagen XII Collagen XII Claudin 9	Q60847 Q60847 Q9ZOS7
VGVA	FRVGVADV	F-VGVADV RVGV	Collagen XII Collagen XII	Q60847 Q60847
EYQ	CEYQLDVE	CEYQL YQLDV YQLDV	Semaphorin 4C FGFR1 Tie-1	Q64151 P16092 Q06806

Peptides were analyzed using a BLAST (NCBI) search against the SWISSPROT database, using the option for short nearly exact matches, to identify mouse proteins with homologous sequences.

heparin binding FGFs are sequestered in the extracellular matrix and basement membrane by binding to heparan sulfate proteoglycans (Ornitz and Itoh, 2001), which is consistent with phage homing to these FGF depots in vivo. As the Tie-1 receptor is an orphan receptor tyrosine kinase, ligand binding information is not currently available; however, the peptide sequence homology is in the extracellular domain (Sato et al., 1993).

Another provocative homology was seen for the RGR peptide (CRGRRST), which is contained within the B chain of the pro-form of platelet-derived growth factor (PDGF-B), a known ligand for the transmembrane receptor tyrosine kinase PDGFR β . The RGR sequence homology (RGRRS) spans the pro-peptide cleavage site of pro-PDGF-B (Johnsson et al., 1984). To investigate the hypothesis that the RGR peptide was homing to PDGFR β by virtue of this homology, we transfected 293T cells with a fusion gene designed to overexpress PDGFR β . The binding of RGR phage was 20-fold more efficient to PDGFR β -transfected cells than nontransfected cells. In contrast, no binding above the background was detected toward cells transfected with vascular endothelial growth factor receptor 2 (VEGFR2) (Figure 5A). Moreover, when we tested the RSR phage, which has a peptide sequence similar to RGR, no specific binding was observed either to PDGFR β - or VEGFR2-transfected cells (Figure 5A). The association of RGR with PDGFR β was further substantiated when intravenously injected fluorescein-conjugated RGR peptide was shown to colocalize with PDGFR β , visualized by subsequent immunostaining of tissue sections from RIP1-Tag2 tumors. Merging of the RGR-FITC image (Figure 5B, panel a) with the antibody staining for PDGFR β (Figure 5B, panel b) revealed almost complete colocalization (Figure 5B, panels c and d).

Discussion

We set out in this and the companion study (Hoffman et al., 2003) to characterize the vasculature during the discrete stages of organ-specific carcinogenesis, using a profiling technology based on peptide libraries displayed on the surface of bacteriophage. Phage that display a peptide with an appropriate binding specificity home via the circulation to the site of binding affinity. As such, phage profiling can reveal differences in the composition and properties of the vasculature of different organs and pathological lesions. Using as a target the RIP1-Tag2 mouse model of multistage tumorigenesis involving the pancreatic islets of Langerhans, we have identified peptides that discriminate between the vasculature of the premalignant angiogenic islets and the fully developed tumors. Most of the identified homing peptides appear to selectively detect vascular changes induced during tumorigenesis in the endocrine pancreas, but not in other tumors growing in or under the skin. Remarkably, three peptides representing one of the distinctive homing classes (to angiogenic progenitors, to tumors, or to both) each colocalized with markers separately identifying endothelial cells and pericytes in the angiogenic lesions. The sequences of the homing peptides suggest candidate proteins containing homologous sequences that are mimicked by peptide binding to the angiogenic vasculature.

Insights into organ-specific differences in neoplastic vasculature

The influence of tissue microenvironment in tumor development is increasingly appreciated (Coussens and Werb, 2002; Liotta

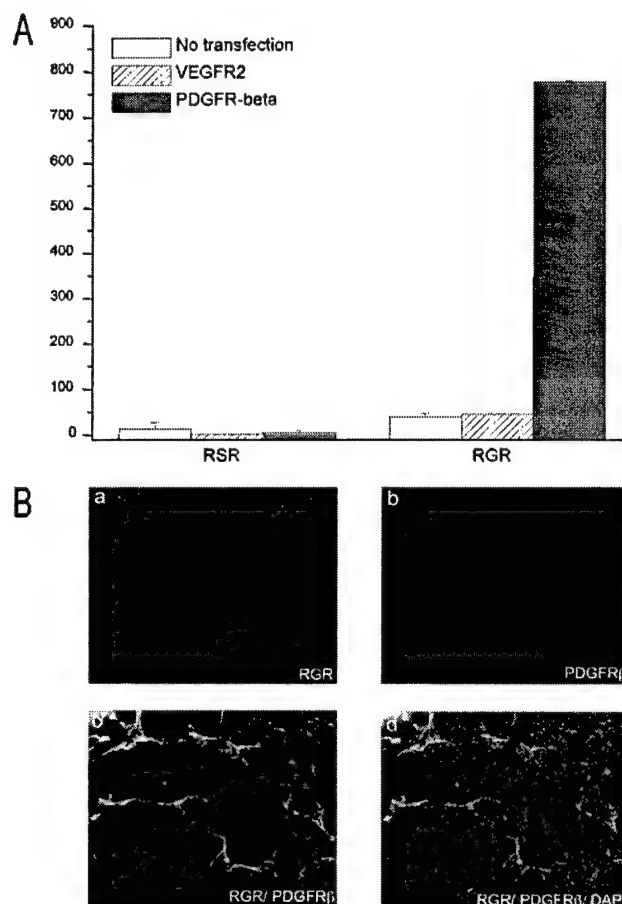


Figure 5. PDGFR β is a candidate receptor for RGR peptide

A: Bar graph showing binding of RGR or RSR phage to 293T cells transfected with either the PDGFR β , the related VEGFR2, or nontransfected cells. Y axis = fold over nonrecombinant phage.

B: Colocalization of fluorescein-conjugated RGR peptide (**a**, green) with the PDGFR β antibody (**b**, red) and merged images (**c** and **d**) in RIP1-Tag2. Magnification 400 \times .

and Kohn, 2001). As developing neoplasias activate angiogenesis and recruit a neovasculature from the surrounding tissue microvascular bed, the organ microenvironment may influence the morphology and physiology of the tumor neovasculature. Evidence in support of organ-specific differences has come, for example, by comparing permeability in the vessels of transplant tumors as a function both of tumor type and the host tissue site (Hobbs et al., 1998; Roberts et al., 1998).

We asked whether tumors arising in their natural microenvironment are different from those developing in another "foreign" location by comparing endogenously arising RIP1-Tag2 tumors in the pancreas with β TC3 cell-derived tumors grown subcutaneously (the β TC3 cell line was established from a RIP1-Tag2 pancreatic islet tumor; Efrat et al., 1988). The results from both phage and peptide binding (Figure 4 and data not shown) indicate that some phage/peptides home to β TC3 subcutaneous tumors in addition to RIP1-Tag2 endogenous tumors, albeit less efficiently (e.g., VGVG). However, most of the other phage/

peptides do not show any appreciable homing to β TC3 tumors by comparison to RIP1-Tag2 tumors (e.g., KAA and VGVA), supporting the predominant role of the tissue microenvironment in influencing some of the receptors that are displayed on the cell surface.

Similar results were found for the two other tumor types we studied: squamous cell carcinomas of the epidermis arising in K14-HPV16 transgenic mice and subcutaneous xenograft tumors of the human MDA-MB-435 breast cancer cell line. KAR and VGVG were the only phage/peptides that homed appreciably to these models, whereas the other peptides showed a similar lack of homing, as for β TC3 tumors. Thus, the majority of phage-displayed and soluble peptides homed selectively to the tumor vasculature of RIP1-Tag2 tumors arising in their natural environment in the endocrine pancreas, showing little affinity for tumors growing subcutaneously or in the skin itself. By contrast, in the aforementioned study of tumor endothelial genes revealed by expression profiling (St. Croix et al., 2000), a number of the tumor-specific endothelial genes identified as upregulated in a colorectal cancer screen were also found in the tumor endothelium of other cancers (lung, brain, pancreas, and breast primary tumors; and a colorectal metastasis to the liver). Our method has clearly revealed a partially overlapping but distinctive set of markers. These results support the existence of both tumor-specific and tumor-generic vascular markers and may have implications for interpretation of data forthcoming from xenograft tumor models. If vascular markers are not recapitulated in transplant models representing a particular organ-specific cancer, then aspects of its phenotypic behavior and response to therapy (particularly targeted antiangiogenic and antivascular agents) may differ as well. Similar results have been seen in the companion study (Hoffman et al., 2003) comparing *de novo* epidermal squamous cell carcinomas in the K14-HPV16 mice with transplant tumors in the adjacent subcutaneous microenvironment.

Homing peptides revealing molecular anatomy of tumor vasculature

We have begun to investigate candidate binding moieties ("receptors") for the RIP1-Tag2 homing peptides, initially by searching protein databases for proteins that contain the homing peptide sequences and thus might represent the endogenous protein mimicked by the peptide. It is striking that a number of the candidate proteins revealed by the search have been implicated in some aspect of angiogenesis (PDGFs, WNTs, claudins, collagen XII, FGFR1, Tie-1). We chose to evaluate the PDGF-B homology in light of recent evidence implicating PDGF signaling in the angiogenic phenotype in the RIP-Tag2 model: three PDGF ligand genes are expressed in the tumor endothelial cells, while PDGF receptor β is expressed in tumor pericytes (Bergers et al., 2003). Pharmacological inhibition of PDGFR signaling in RIP1-Tag2 mice disrupted pericyte association with the tumor endothelium, inhibited angiogenesis, and reduced the vascularity of the islet tumors (Bergers et al., 2003). The results add to a knowledge base implicating PDGF signaling in pericyte-endothelial cell homeostasis, both in developing vessels (Betsholtz et al., 2001; Leveen et al., 1994; Lindahl et al., 1997; Soriano, 1994) and in tumors (Heldin and Westermark, 1999; Ostman and Heldin, 2001).

The evaluation of RGR in light of its homology to PDGF-B clearly suggests its homing is associated with PDGFR expres-

sion and/or signaling. The most compelling evidence comes from overexpressing PDGFR β in cultured cells. There was a striking increase in the binding of the RGR phage to cells transfected with PDGFR β , whereas transfection with a structurally related receptor tyrosine kinase, VEGFR2, had no effect on the binding. Moreover, systemically infused RGR colocalizes with virtually all of the PDGFR β detected by immunostaining in angiogenic islets and tumors. Both lines of evidence support the model that RGR binds to PDGFR β . There are, however, other data that complicate this simple conclusion. First, RGR colocalizes not only with a pericyte marker, NG2, consistent with PDGFR β expression in pericytes, but also with an endothelial cell marker, MECA32, indicative of homing to endothelial cells (which do not typically express PDGFR β —see Bergers et al., 2003). Second, the RGR peptide sequence overlaps the pro-peptide processing site and is thus only partially represented in mature PDGF-B ligand; moreover, the sequences for PDGF homo- and heterodimerization and for receptor binding are not at the N terminus of the mature ligand (Clements et al., 1991; Heldin and Westermark, 1999; Ostman et al., 1991). Thus it is not clear how RGR might bind either to PDGF ligands or receptors. These data lead us to suggest that RGR mimics a protein-protein interaction site in pro-PDGF-B that mediates its specific homing and mimics bona fide associations of pro-PDGF-B. One possible association for RGR is either with PDGFR β itself or with a protein induced by its expression, given the enhanced binding seen in the transfected cells overexpressing PDGFR β as well as the observed colocalization of RGR with PDGFR β in angiogenic islets and tumors. It is interesting to note that a similar sequence is found in PDGF-D, a related PDGF ligand that also signals through PDGFR β . The sequence RGRS is located in the secreted PDGF-D at the site of processing from the inactive to active form of PDGF-D (Bergsten et al., 2001; LaRochelle et al., 2001).

The additional colocalization of RGR with the endothelial cell marker MECA32 suggests that an RGR binding moiety is also expressed by endothelial cells or shared between pericytes and endothelial cells. While there is no obvious coimmunostaining of either endothelial cell marker (CD31, MECA32) with any of several pericyte markers (desmin, SMA, NG2) in the angiogenic islets or tumors (J.J. and G.B., unpublished observations), a small subset of FAC-sorted cells within RIP1-Tag2 tumors are positive for both CD31 and NG2 (G.B., unpublished observations). In addition, both cell types contribute to the vascular basement membrane and the extracellular matrix that separates and envelops them, and these structures could contain RGR binding motifs produced by one or both cell type and localized amongst them. Indeed, purified PDGF-B has been shown to bind various ECM and BM proteins, including collagens I-IV (Somasundaram and Schuppan, 1996), laminin-1, nidogen, and perlecan (Gohring et al., 1998). Another attractive candidate for RGR binding is the predicted prohormone processing enzyme that binds and cleaves pro-PDGF-B within the RGR homology. Interestingly, while the RGR phage and peptide homed effectively to angiogenic progenitor islets and solid tumors in RIP1-Tag2 mice, neither homed to angiogenic dysplasias or tumors in the HPV16 transgenic mice nor to the MDA-MB-435 subcutaneous tumors. These results suggest that PDGF signaling and the resultant vessel stabilization by pericytes may differ among tumors or that there are differences in pericyte activation and/or maturation (Morikawa et al., 2002). Alternatively, the blood

vessels in the squamous cell carcinomas, being less hemorrhagic, may limit the accessibility of the blood-borne phage and labeled peptides to the perivascular cells (see below).

Other homologies between homing peptides and endogenous proteins listed in Table 1 may also be significant. The fact that many of these proteins have been implicated in angiogenesis, or related biological processes, supports this prediction. For example, two of the peptides, KAR and VGVA, show homology to collagen XII, which is associated with blood vessels in the developing embryo (Bohme et al., 1995; Oh et al., 1993). Colocalization of both peptides with vascular markers (data not shown) is consistent with the predicted localization of collagen XII.

Lessons from profiling different tumor types

It is of interest to compare and contrast the results reported here to that of the companion study (Hoffman et al., 2003), which similarly used phage display libraries to profile the angiogenic dysplasias and squamous cell carcinomas that arise in the skin of K14-HPV16 transgenic mice. That study produced a series of homing peptides that were selective for angiogenic progenitors or solid tumors. And again, both tumor type-selective and tumor-generic phage were identified; their analysis focused on skin tumor-specific phage that did not home to the angiogenic vasculature in the stages of pancreatic islet carcinogenesis in RIP1-Tag2 mice. The skin-tumor homing peptides had different sequences from those identified herein, and their candidate cellular homologs (and prospective binding moieties) were distinctive. In sum, each study identified both tumor type-specific and stage-specific vascular homing peptides, further supporting the proposition that organ microenvironment imparts distinctive constraints on neoplastic development that affects the characteristics of the neovasculature induced to sustain tumor development and progression.

It is intriguing that the two organ sites of neoplastic development (skin and pancreas) preferentially selected phage with different cellular specificity. The HPV phage all homed exclusively to endothelial cells, whereas each of the RIP1-Tag2 phage representing the three homing classes (angiogenic progenitor, tumor, or both) chosen for analysis homed both to pericytes and to endothelial cells. This suggests significant differences in the vascular morphology and/or functionality in the skin and pancreas. One difference may be in vascular permeability. The islet tumors are blood red from hemorrhaging and the angiogenic vasculature is permeable to a variety of macromolecules (Hashizume et al., 2000; Thurston et al., 1998). By contrast, the skin tumors are white, indicative of less hemorrhagic vessels or higher interstitial pressure. Thus the phage population circulating through the vascular system in RIP1-Tag2 mice may have had ready access to the perivascular microenvironment, whereas the "tighter" vessels in the skin lesions may limit such accessibility. Future studies on the expression of the "receptors" identified by these distinctive classes of homing peptides should clarify whether their binding moieties are differentially expressed and/or differentially accessible via the vasculature in these distinctive tumor types and their angiogenic progenitor lesions, providing further insight into the dynamics and tissue-specific qualities of the angiogenic phenotype.

The selective accumulation of fluorescein-conjugated peptides in the RIP-Tag lesions indicates that a monovalent peptide-receptor interaction is robust enough to carry a payload to the

target. As such, these peptides could be used as biomarkers or for imaging, particularly of pre-neoplastic lesions, which are notoriously difficult to detect. The peptides homing to angiogenic islets, for example, could be used both as markers of the angiogenic switch and to monitor therapeutic response to antiangiogenic agents, in much the same way as parameters such as microvessel density are currently employed. Future experiments will test the efficacy of targeting of imaging agents and active drugs to multiple stages of tumorigenesis.

In conclusion, we have used phage display to profile the vasculature during the distinctive stages of multistep tumorigenesis in a prototypical mouse model of cancer. We have identified three different classes of stage-specific peptides suggestive of distinctive characteristics of the neovasculature in premalignant and malignant lesions. We expect that the selectivity in peptide homing will help us understand the stage-specific differences in efficacy observed for angiogenesis inhibitor therapy in the RIP1-Tag2 model (Bergers et al., 1999). In addition, it may be possible to selectively target antitumor therapies to individual or multiple cell types during RIP-Tag tumorigenesis using these homing peptides conjugated to, for example, proapoptotic sequences, as previously reported (Ellerby et al., 1999). It will be of further interest to ask whether these homing peptides can similarly characterize the neovasculature of stages in human pancreatic islet carcinogenesis, as well as in other organ-specific cancers in mouse models and humans.

Experimental procedures

Generation of mice and tissue isolation

The generation of RIP1-Tag2 mice (Hanahan, 1985) and K14-HPV16 mice (Arbeit et al., 1994; Coussens et al., 1996) has been reported. Angiogenic islets were isolated from 8- and 12-week-old RIP1-Tag2 mice by collagenase digestion of the excised pancreas and selected based on their red, hemorrhagic appearance (Parangi et al., 1995). Tumors were microdissected from the excised pancreas of 12-week-old RIP1-Tag2 mice and the surrounding exocrine tissue was carefully removed. The synchronicity of tumorigenesis in the RIP1-Tag2 model allowed us to simultaneously isolate pools of angiogenic islets and tumors from the same mouse at 12 weeks of age, thus affording us the opportunity to directly compare homing of individual phage to different stages in an individual mouse/pancreas. Tumors were dissected from the ear or chest of K14-HPV16 mice. For the β TC3 allograft models, 10^5 β TC3 tumor cells (Efrat et al., 1988) were inoculated under the skin of the rear flank of *nu/nu* mice in a BALB/c background and allowed to grow until approximately 5 mm in size, and then used for experimental analysis. MDA-MB-435 xenograft models were generated by inoculating 10^6 tumor cells subcutaneously in the chest of *nu/nu* BALB/c mice. Tumors were used for the homing/binding experiments at 8–12 weeks after injection of the tumor cells. Matrigel plug angiogenesis was induced as previously described (Fulgham et al., 1999; Ngo et al., 2000; Yi et al., 2003). Briefly, 100 μ l of Matrigel containing 80 ng/ml bFGF was injected subcutaneously in the abdominal area of BALB/c/*nu/nu* mice, and at day 8, the mice were injected with fluorescein-conjugated peptides as detailed below.

Phage libraries and library screening

The screening process involved two *ex vivo* selection rounds followed by 2–3 *in vivo* selection rounds. For the *ex vivo* selections, cell suspensions were prepared from the different RIP1-Tag2 lesions in 12-week-old RIP1-Tag2 mice and incubated overnight at 4°C with 10^8 plaque forming units (p.f.u.) of a T7 phage (Novagen) displayed CX₂C peptide library. The cells were washed to remove unbound phage and the bound phage rescued and amplified in *E. coli*. This procedure enriches for phage that bind to tumor, endothelial, and other stromal cells present in the suspension. The *ex vivo* pre-selected phage pool was injected intravenously into 12-week-old RIP1-Tag2 mice through the tail vein, allowed to circulate for 7 min, and heart-perfused with PBS to remove unbound intravascular phage. As the vascula-

ture is preferentially available for the phage to bind in this selection, there is an enrichment of phage that bind to the endothelium of the target tissue. The RIP1-Tag2 lesions and control tissues (brain, kidney, spleen, lung, "white" pancreas [i.e., not containing any hemorrhagic lesions], and liver) were excised to allow for comparison of homing efficiencies. Cell suspensions were prepared by mechanical disruption of the tissues, washed to remove unbound phage, and the bound phage rescued and amplified by adding *E. coli*. The phage pool was reinjected into mice at a similar disease stage, and the cycle repeated. In each experiment, nonrecombinant control phage was used as a control for relative selectivity. Sets of 96 phage clones were randomly collected from each homing phage population. The peptide-encoding DNA inserts were amplified by PCR, and the PCR products sequenced. Phage representing the most frequently appearing peptide motifs were individually tested for their ability to selectively home to the lesions on which they were selected, relative to other stages in the tumorigenesis pathway and to control organs. Fluorescein-conjugated peptides corresponding to these phage insert sequences were synthesized using an automated peptide synthesizer with standard solid-phase fluorenylmethoxycarbonyl (Fmoc) chemistry. One hundred micrograms of each individual fluorescein-conjugated peptide was injected intravenously into the tail vein of RIP1-Tag2 mice at 8 or 12 weeks of age and into normal BL/6 mice. The peptide was allowed to circulate for 7 min, followed by heart perfusion first with PBS and then with Zn-buffered formalin. The RIP1-Tag2 pancreas and control organs (brain, kidney, liver, lung, and spleen) were removed, fixed for 1 hr in formalin, washed with 1× PBS, placed in 30% sucrose for several hours, washed with 1× PBS, and embedded in OCT (Tissue-Tek). Each peptide was injected into at least three individual RIP1-Tag2 or normal mice at each of the different stages.

Histology and immunohistochemistry

To examine the localization of injected fluorescein-conjugated peptides, frozen sections (10 µm thick) were cut on a cryostat, mounted in Vectashield Mounting Medium with DAPI (Vector Laboratories), and visualized under an inverted fluorescent microscope or a confocal microscope (Zeiss LSM 510 META). For immunohistochemistry, frozen slides were preincubated with blocking buffer (1× PNB from NEN Biosciences) for 1 hr, washed several times in 1× PBS, and incubated with the primary antibody of interest overnight at 4°C. The cell-specific antibodies used were rat monoclonal anti-mouse CD31 (1:200; BD Pharmingen), rat monoclonal anti-mouse MECA32 (1:200; BD Pharmingen), rabbit polyclonal anti-mouse NG2 (1:200; Chemicon), and rat monoclonal anti-mouse PDGFRβ (CD140b) (1:200; eBioscience). The corresponding secondary antibodies; Cy-3 donkey anti-rabbit IgG and Rhodamine Red donkey anti-rat IgG (Jackson ImmunoResearch), were used at a 1:200 dilution and incubated for 1 hr at room temperature. The following species-matched immunoglobulins were used as negative controls: rabbit IgG (Vector Laboratories) and rat IgG (Jackson ImmunoResearch) at a 1:200 dilution. The slides were washed several times in 1× PBS and mounted in Vectashield Mounting Medium with DAPI (Vector Laboratories). Hematoxylin and eosin (H&E) staining was performed for histological grading of adjacent sections by standard methods, and lesions were graded as previously described (Lopez and Hanahan, 2002).

Transfection and phage binding assay

293T cells were transfected with plasmids encoding PDGFRβ or VEGFR2 (Borges et al., 2000) using Fugene transfection reagent (Roche Diagnostics). Briefly, 10 µg of plasmid was mixed with 700 µl of DMEM without serum and 30 µl of Fugene and incubated for 15 min at room temperature before adding the mixture to the cells. Forty-eight hours posttransfection, the cells were detached from the culture plates using EDTA and washed 1× with PBS. RSR, RGR, and the control nonrecombinant phage (about 1×10^8 pfu) were incubated with the transfected cells for 2 hr at 4°C, followed by five washes with 1% BSA in PBS to remove the unbound phage. The bound phage were rescued by adding bacteria, and the binding efficiencies were determined by plaque assay.

Acknowledgments

We thank Cherry Concengco for excellent technical assistance and Fernando Ferrer for peptide synthesis. We thank Dr. Kristian Pietras for reading the manuscript and for helpful suggestions. This study was supported by a grant

from the National Cancer Institute CA82713 (to E.R. and D.H.) and by grants from the Department of Defense DAMD 17-02-1-0315 (E.R.) and the N.C.I. (D.H.). J.A.J. received support from the Leukemia and Lymphoma Society. P.L. received support from the Academy of Finland and the Finnish Cultural Foundation.

Received: June 5, 2003

Revised: September 10, 2003

Published: November 24, 2003

References

- Arap, W., Pasqualini, R., and Ruoslahti, E. (1998). Cancer treatment by targeted drug delivery to tumor vasculature in a mouse model. *Science* 279, 377–380.
- Arbeit, J., Munger, K., Howley, P.M., and Hanahan, D. (1994). Progressive squamous epithelial neoplasia in K14-human papillomavirus type 16 transgenic mice. *J. Virol.* 68, 4358–4368.
- Bergers, G., Hanahan, D., and Coussens, L.M. (1998). Angiogenesis and apoptosis are cellular parameters of neoplastic progression in transgenic mouse models of tumorigenesis. *Int. J. Dev. Biol.* 42, 995–1002.
- Bergers, G., Javaherian, K., Lo, K.M., Folkman, J., and Hanahan, D. (1999). Effects of angiogenesis inhibitors on multistage carcinogenesis in mice. *Science* 284, 808–812.
- Bergers, G., Song, S., Meyer-Morse, N., Bergsland, E., and Hanahan, D. (2003). Benefits of targeting both pericytes and endothelial cells in the tumor vasculature with kinase inhibitors. *J. Clin. Invest.* 111, 1287–1295.
- Bergsten, E., Uutela, M., Li, X., Pietras, K., Ostman, A., Heldin, C.-H., Alitalo, K., and Eriksson, U. (2001). PDGF-D is a specific protease-activated ligand for the PDGF β-receptor. *Nat. Cell Biol.* 3, 512–516.
- Betsholtz, C., Karlsson, L., and Lindahl, P. (2001). Developmental roles of platelet-derived growth factors. *Bioessays* 23, 494–507.
- Bohme, K., Li, Y., Oh, P.S., and Olsen, B.R. (1995). Primary structure of the long and short splice variants of mouse collagen XII and their tissue-specific expression during embryonic development. *Dev. Dyn.* 204, 432–445.
- Borges, E., Jan, Y., and Ruoslahti, E. (2000). Platelet-derived growth factor receptor beta and vascular endothelial growth factor receptor 2 bind to the beta 3 integrin through its extracellular domain. *J. Biol. Chem.* 275, 39867–39873.
- Burg, M.A., Pasqualini, R., Arap, W., Ruoslahti, E., and Stallcup, W.B. (1999). NG2 proteoglycan-binding peptides target tumor neovasculature. *Cancer Res.* 59, 2869–2874.
- Carmeliet, P., and Jain, R. (2000). Angiogenesis in cancer and other diseases. *Nature* 407, 249–257.
- Clements, J.M., Bawden, L.J., Bloxidge, R.E., Catlin, G., Cook, A.L., Craig, S., Drummond, A.H., Edwards, R.M., Fallon, A., Green, D.R., et al. (1991). Two PDGF-B chain residues, arginine 27 and isoleucine 30, mediate receptor binding and activation. *EMBO J.* 10, 4113–4120.
- Coussens, L.M., and Werb, Z. (2002). Inflammation and cancer. *Nature* 420, 860–867.
- Coussens, L.M., Hanahan, D., and Arbeit, J.M. (1996). Genetic predisposition and parameters of malignant progression in K14-HPV16 transgenic mice. *Am. J. Pathol.* 149, 1899–1917.
- Efrat, S., Linde, S., Kofod, H., Spector, D., Delannoy, M., Grant, S., Hanahan, D., and Baekkeskov, S. (1988). Beta-cell lines derived from transgenic mice expressing a hybrid insulin gene-oncogene. *Proc. Natl. Acad. Sci. USA* 85, 9037–9041.
- Ellerby, H.M., Arap, W., Ellerby, L.M., Kain, R., Andrusiak, R., Rio, G.D., Krajewski, S., Lombardo, C.R., Rao, R., Ruoslahti, E., et al. (1999). Anti-cancer activity of targeted pro-apoptotic peptides. *Nat. Med.* 5, 1032–1038.
- Folkman, J., Watson, K., Ingber, D., and Hanahan, D. (1989). Induction of

- angiogenesis during the transition from hyperplasia to neoplasia. *Nature* 339, 58–61.
- Fulgham, D.L., Widhalm, S.R., Martin, S., and Coffin, J.D. (1999). FGF-2 dependent angiogenesis is a latent phenotype in basic fibroblast growth factor transgenic mice. *Endothelium* 6, 185–195.
- Gohring, W., Sasaki, T., Heldin, C.H., and Timpl, R. (1998). Mapping of the binding of platelet-derived growth factor to distinct domains of the basement membrane proteins BM-40 and perlecan and distinction from the BM-40 collagen-binding epitope. *Eur. J. Biochem.* 255, 60–66.
- Hallman, R.D., Mayer, D.N., Berg, E.L., Broermann, R., and Butcher, E.C. (1995). Novel mouse endothelial cell surface marker is suppressed during differentiation of the blood brain barrier. *Dev. Dyn.* 202, 325–332.
- Hanahan, D. (1985). Heritable information of pancreatic beta-cell tumors in transgenic mice expressing recombinant insulin/simian virus 40 oncogenes. *Nature* 315, 115–122.
- Hanahan, D., and Folkman, J. (1996). Patterns and emerging mechanisms of the angiogenic switch during tumorigenesis. *Cell* 86, 353–364.
- Hashizume, H., Baluk, P., Morikawa, S., McLean, J.W., Thurston, G., Roberge, S., Jain, R.K., and McDonald, D.M. (2000). Openings between defective endothelial cells explain tumor vessel leakiness. *Am. J. Pathol.* 156, 1363–1380.
- Heldin, C.H., and Westermark, B. (1999). Mechanism of action and in vivo role of platelet-derived growth factor. *Physiol. Rev.* 79, 1283–1316.
- Hobbs, S.K., Monsky, W.L., Yuan, F., Roberts, W.G., Griffith, L., Torchilin, V.P., and Jain, R.K. (1998). Regulation of transport pathways in tumor vessels: Role of tumor type and microenvironment. *Proc. Natl. Acad. Sci. USA* 95, 4607–4612.
- Hoffman, J.A., Giraudo, E., Singh, M., Zhang, L., Inoue, M., Porkka, K., Hanahan, D., and Ruoslahti, E. (2003). *Cancer Cell* 4, this issue, 383–391.
- Johnsson, A., Heldin, C.H., Wasteson, A., Westermark, B., Deuel, T.F., Huang, J.S., Seeburg, P.H., Gray, A., Ullrich, A., Scrace, G., et al. (1984). The *c-sis* gene encodes a precursor of the B chain of platelet-derived growth factor. *EMBO J.* 3, 921–928.
- Laakkonen, P., Porkka, K., Hoffman, J.A., and Ruoslahti, E. (2002). A tumor-homing peptide with a targeting specificity related to lymphatic vessels. *Nat. Med.* 8, 751–755.
- LaRochelle, W.J., Jeffers, M., McDonald, W.F., Chillakuru, R.A., Giese, N.A., Lokker, N.A., Sullivan, C., Boldog, F.L., Yang, M., Vemet, C., et al. (2001). PDGF-D, a new protease-activated growth factor. *Nat. Cell Biol.* 3, 517–521.
- Leppink, D.M., Bishop, D.K., Sedmak, D.D., Henry, M.L., Ferguson, R.M., Streeter, P.R., Butcher, E.C., and Orosz, C.G. (1989). Inducible expression of an endothelial cell antigen on murine myocardial vasculature in association with interstitial cellular infiltration. *Transplantation* 48, 874–877.
- Leveen, P., Pekny, M., Gebre-Medhin, S., Swolin, B., Larsson, E., and Betsholtz, C. (1994). Mice deficient for PDGF-B show renal, cardiovascular and hematological abnormalities. *Genes Dev.* 8, 1875–1887.
- Lindahl, P., Johansson, B.R., Leveen, P., and Betsholtz, C. (1997). Pericyte loss and microaneurysm formation in PDGF-B deficient mice. *Science* 277, 242–245.
- Liotta, L.A., and Kohn, E.C. (2001). The microenvironment of the tumour-host interface. *Nature* 411, 375–379.
- Lopez, T., and Hanahan, D. (2002). Elevated levels of IGF-1 receptor convey invasive and metastatic capability in a mouse model of pancreatic islet tumorigenesis. *Cancer Cell* 7, 339–353.
- Morikawa, S., Baluk, P., Kaidoh, T., Haskell, A., Jain, R.K., and McDonald, D.M. (2002). Abnormalities in pericytes on blood vessels and endothelial sprouts in tumors. *Am. J. Pathol.* 160, 985–1000.
- Ngo, C.V., Gee, M., Akhtar, N., Yu, D., Volpert, O., Auerbach, R., and Thomas-Tikhonenko, A. (2000). An in vivo function for the transforming Myc protein: elicitation of the angiogenic phenotype. *Cell Growth Differ.* 11, 201–210.
- Oh, S.P., Griffith, C.M., Hay, E.D., and Olsen, B.R. (1993). Tissue-specific expression of type XII collagen during mouse embryonic development. *Dev. Dyn.* 196, 37–46.
- Ornitz, D.M., and Itoh, N. (2001). Fibroblast growth factors. *Genome Biol.* 2, 3005.1–3005.12.
- Ostman, A., and Heldin, C.H. (2001). Involvement of platelet-derived growth factor in disease: development of specific antagonists. *Adv. Cancer Res.* 80, 1–38.
- Ostman, A., Andersson, M., Hellman, U., and Heldin, C.H. (1991). Identification of three amino acids in the platelet-derived growth factor (PDGF) B-chain that are important for binding to the PDGF- β receptor. *J. Biol. Chem.* 266, 10073–10077.
- Parangi, S., Dietrich, W., Christofori, G., Lander, E.S., and Hanahan, D. (1995). Tumor suppressor loci on mouse chromosomes 9 and 16 are lost at distinct stages of tumorigenesis in a transgenic model of islet cell carcinoma. *Cancer Res.* 55, 6071–6076.
- Pasqualini, R., and Ruoslahti, E. (1996). Organ targeting *in vivo* using phage display peptide libraries. *Nature* 380, 364–366.
- Pasqualini, R., Koivunen, E., Kain, R., Lahdenranta, J., Sakamoto, M., Stryhn, A., Ashmun, R.A., Shapiro, L.H., Arap, W., and Ruoslahti, E. (2000). Amino-peptidase N is a receptor for tumor-homing peptides and a target for inhibiting angiogenesis. *Cancer Res.* 60, 722–727.
- Plotnikov, A.N., Schlessinger, J., Hubbard, S.R., and Mohammadi, M. (1999). Structural basis for FGF receptor dimerization and activation. *Cell* 98, 641–650.
- Porkka, K., Laakkonen, P., Hoffman, J.A., Bernasconi, M., and Ruoslahti, E. (2002). A fragment of the HMGN2 protein homes to the nuclei of tumor cells and tumor endothelial cells *in vivo*. *Proc. Natl. Acad. Sci. USA* 99, 7444–7449.
- Rajotte, D., Arap, W., Hagedorn, M., Koivunen, E., Pasqualini, R., and Ruoslahti, E. (1998). Molecular heterogeneity of the vascular endothelium revealed by *in vivo* phage display. *J. Clin. Invest.* 102, 430–437.
- Roberts, W.G., Delaat, J., Nagane, M., Huang, S., Cavenee, W.K., and Palade, G.E. (1998). Host microvasculature influence on tumor morphology and endothelial gene expression. *Am. J. Pathol.* 153, 1239–1248.
- Ruoslahti, E. (2002). Specialization of tumour vasculature. *Nat. Rev. Cancer* 2, 83–90.
- Sato, T.N., Qin, Y., Kozak, C.A., and Audus, K.L. (1993). Tie-1 and Tie-2 define another class of putative receptor tyrosine kinase genes expressed in early embryonic vascular system. *Proc. Natl. Acad. Sci. USA* 90, 9355–9358.
- Schlingemann, R.O., Rietveld, F.J., de Waal, R.M., Ferrone, S., and Ruiter, D.J. (1990). Expression of the high molecular weight melanoma-associated antigen by pericytes during angiogenesis in tumors and in healing wounds. *Am. J. Pathol.* 136, 1393–1405.
- Schlingemann, R.O., Rietveld, F.J., Kwaspen, F., van de Kerkhof, P.C., de Waal, R.M., and Ruiter, D.J. (1991). Differential expression of markers for endothelial cells, pericytes, and basal lamina in the microvasculature of tumors and granulation tissues. *Am. J. Pathol.* 138, 1335–1347.
- Somasundaram, R., and Schuppan, D. (1996). Type I, II, III, IV, V, and VI collagens serve as extracellular ligands for the isoforms of platelet-derived growth factor (AA, BB, and AB). *J. Biol. Chem.* 271, 26884–26891.
- Soriano, P. (1994). Abnormal kidney development and hematological disorders in PDGF β -receptor mutant mice. *Genes Dev.* 8, 1888–1896.
- St. Croix, B., Rago, C., Velculescu, V., Traverso, G., Romans, K.E., Montgomery, E., Lal, A., Riggins, G.J., Lengauer, C., Vogelstein, B., and Kinzler, K.W. (2000). Genes expressed in human tumor endothelium. *Science* 289, 1197–1202.
- Thurston, G., McLean, J.W., Rizen, M., Baluk, P., Haskell, A., Murphy, T.J., Hanahan, D., and McDonald, D.M. (1998). Cationic liposomes target angiogenic endothelial cells in tumors and chronic inflammation in mice. *J. Clin. Invest.* 101, 1401–1413.
- Yi, M., Sakai, T., Fassler, R., and Ruoslahti, E. (2003). Antiangiogenic proteins require plasma fibronectin or vitronectin for in vivo activity. *Proc. Natl. Acad. Sci. USA*, in press.

Nucleolin expressed at the cell surface is a marker of endothelial cells in angiogenic blood vessels

Sven Christian,¹ Jan Pilch,¹ Maria E. Akerman,^{1,2} Kimmo Porkka,^{1,3} Pirjo Laakkonen,¹ and Erkki Ruoslahti¹

¹Cancer Research Center, The Burnham Institute, La Jolla, CA 92037

²Department of Bioengineering, University of California, San Diego, La Jolla, CA 92093

³Department of Medicine, Division of Hematology, Stem Cell and Basic Science Laboratory, Helsinki University Central Hospital, FIN-00029 HUS, Helsinki, Finland

A tumor-homing peptide, F3, selectively binds to endothelial cells in tumor blood vessels and to tumor cells. Here, we show that the cell surface molecule recognized by F3 is nucleolin. Nucleolin specifically bound to an F3 peptide affinity matrix from extracts of cultured breast carcinoma cells. Antibodies and cell surface biotin labeling revealed nucleolin at the surface of actively growing cells, and these cells bound and internalized fluorescein-conjugated F3 peptide, transporting it into the nucleus. In contrast, nucleolin was exclusively nuclear

in serum-starved cells, and F3 did not bind to these cells. The binding and subsequent internalization of F3 were blocked by an antinucleolin antibody. Like the F3 peptide, intravenously injected antinucleolin antibodies selectively accumulated in tumor vessels and in angiogenic vessels of implanted "matrigel" plugs. These results show that cell surface nucleolin is a specific marker of angiogenic endothelial cells within the vasculature. It may be a useful target molecule for diagnostic tests and drug delivery applications.

Introduction

Tumor growth is critically dependent on angiogenesis, which is the sprouting of new blood vessels from existing ones (Hanahan and Folkman, 1996). Angiogenic vessels differ from normal vessels in their morphological and molecular characteristics. The molecular markers of angiogenic vessels include endothelial growth factor receptors, integrins, proteolytic enzymes, and extracellular matrix components (Ruoslahti, 2002), as well as membrane proteins of unknown function (St Croix et al., 2000; Christian et al., 2001a). A specific marker for tumor lymphatics has also been described previously (Laakkonen et al., 2002).

The molecular markers that distinguish tumor vasculature from that of normal tissues are important in a number of ways. Many of the molecules that are selectively expressed in tumor blood vessels play a functional role in development and maintenance of new blood vessels. Examples include endothelial cell growth factor receptors and integrins (Eliceiri

and Cheresch, 1999; Ferrara and Alitalo, 1999; Hynes, 2002), matrix metalloproteases (Brooks et al., 1998; Bergers et al., 2000), and aminopeptidase N (Pasqualini et al., 2000). Blocking the function of these proteins inhibits angiogenesis. Furthermore, these and other molecules selectively expressed in tumor vasculature can be made use of in targeting diagnostic and therapeutic agents in tumors (Arap et al., 1998; Nilsson et al., 2001; El-Sheikh et al., 2002; Hood et al., 2002).

The identification of additional tumor blood vessel markers helps in the understanding of angiogenesis and could be useful for tumor targeting. We set out to identify the molecule, "receptor," that is recognized by a tumor-homing peptide recently identified by our laboratory. This peptide, F3, was discovered in a screening procedure that used a phage-displayed cDNA library and combined *ex vivo* screening on cell suspensions prepared from mouse bone marrow and *in vivo* screening for tumor homing. F3 is a 34-amino acid fragment of a high mobility group protein, HMG2N (Porkka et al., 2002). F3 homes to the vasculature of various types of tumors by binding to the endothelial cells. F3 also binds to a subpopulation of bone marrow cells that may be precursors for endothelial cells. In some tumors, the F3

Address correspondence to Erkki Ruoslahti, The Burnham Institute, 10901 North Torrey Pines Rd., La Jolla, CA 92037. Tel.: (858) 646-3125. Fax: (858) 646-3198. email: ruoslahti@burnham.org

Pirjo Laakkonen's present address is Molecular/Cancer Biology Laboratory, Biomedicum Helsinki, University of Helsinki, P.O. Box 63, Haartmaninkatu 8, FIN-00014 Helsinki, Finland.

Key words: angiogenesis; bone marrow; cell-penetrating peptides; nuclear proteins

Abbreviation used in this paper: HUVEC, human umbilical vein endothelial cell.

peptide also recognizes the tumor cells. A striking property of the F3 peptide is that it is internalized by its specific target cells and transported to the nucleus.

We have now identified cell surface-expressed nucleolin as the receptor for F3 on tumor cells and angiogenic endothelial cells. Cell surface nucleolin expression is a novel angiogenesis marker. It provides a tool for studying tumor angiogenesis, including the contribution of precursor cells to this process, and for targeting drugs into tumors.

Results

Nucleolin binds to F3 in affinity chromatography

The F3 peptide binds to and accumulates within both tumor endothelial cells and tumor cells *in vivo* (Porkka et al., 2002). Because F3 also binds to cultured tumor cells such as the human breast carcinoma cell line MDA-MB-435, we decided to use this cell line to identify a receptor for F3. Affinity chromatography of MDA-MB-435 cell extracts on an F3 peptide affinity matrix revealed a major F3-binding band at a molecular mass of 110 kD and several bands in the 20-kD range that did not bind to a control peptide matrix (Fig. 1 A). Mass spectrometry analysis indicated that the 110-kD band is nucleolin. Although the calculated mass of nucleolin is 76 kD, it migrates at 110 kD in SDS-PAGE, most likely because of posttranslational modifications and high content of negatively charged amino acids in the NH₂-terminal region of the protein (Harms et al., 2001). The 20-kD range bands were identified as various histones.

The identification of the 110-kD protein as nucleolin was confirmed by immunoblotting. A monoclonal antinucleolin antibody, MS-3, revealed a major 110-kD band and faint lower molecular mass bands in the F3-bound material (Fig. 1 B, a). These bands were not present in eluates from the control peptide matrix. The faint bands are probably fragments of nucleolin, as they aligned with some of the several lower molecular mass bands detected by the antibody in a whole cell extract. These results show that the F3 peptide can specifically interact with nucleolin, suggesting nucleolin as a candidate receptor for F3.

We prepared antisera against nucleolin by immunizing rabbits with two different synthetic peptides from the human nucleolin sequence. Affinity-purified antibodies recognized a band that aligned with the 110-kD nucleolin band defined by the MS-3 antibody (Fig. 1 B, b). Like MS-3, the rabbit antibodies also detected smaller molecular mass bands that presumably represent nucleolin fragments. As expected, based on the fact that the immunizing peptides came from different regions of the nucleolin molecule, the sets of minor bands detected by each antibody did not overlap. Immunoblotting showed that the NCL3 antibody also recognizes a 110-kD protein in extracts of mouse cells. (Fig. 1 B, c).

Nucleolin is expressed at the cell surface

To serve as an F3 receptor, nucleolin would have to be present at the cell surface. Nucleolin is primarily known as a nuclear and cytoplasmic protein, but recent studies have shown that a cell surface form of nucleolin also exists (Said et al., 2002; Sinclair and O'Brien, 2002). To determine if F3-binding nucleolin in the MDA-MB-435 cells is ex-

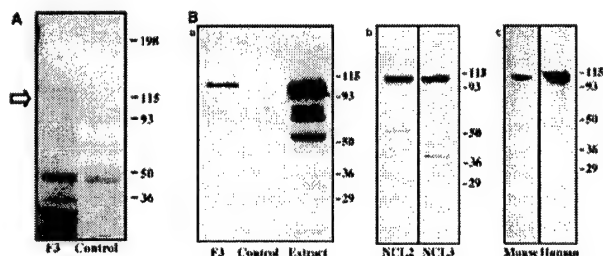


Figure 1. Nucleolin binds to immobilized F3 peptide. (A) SDS gel electrophoresis of Coomassie blue-stained proteins isolated from MDA-MB-435 cell extracts on F3 affinity matrix (F3) or control peptide matrix (Control). The arrow indicates a specific 110-kD band, which was identified as nucleolin by mass spectrometry. (B) Immunoblotting of eluates from F3 and control affinity matrices with a monoclonal mouse antinucleolin antibody (a); immunoblotting of MDA-MB-435 cell extracts with polyclonal rabbit antinucleolin antibodies NCL2 and NCL3 (b); immunoblotting of extracts generated from the human cell line C8161 and the mouse cell line 4T1 with NCL3 (c). The F3 bound material (a, F3) contains full-length nucleolin and a faintly staining 75-kD band. In the original cell extract (a, Extract), the antibody recognizes full-length nucleolin at 110 kD, along with several faster migrating bands (presumably nucleolin fragments), including one at 75 kD. No antinucleolin reactive bands are detected in eluates from the control matrix (a, Control). Affinity-purified polyclonal antibodies NCL2 and NCL3 recognize a band that aligns with the 110-kD nucleolin band in human extracts, and NCL3 crossreacts with mouse nucleolin (c, Mouse). Both antibodies also detect smaller bands that presumably represent nucleolin fragments.

pressed at the cell surface, exponentially growing cells were biotinylated with a cell-impermeable biotin reagent, and cell extracts were subjected to affinity chromatography on immobilized F3. Two biotinylated bands at 110 and 75 kD specifically bound to F3 (Fig. 2 A, a). The surface biotinylated 75-kD band was stronger than the 110-kD band, whereas the opposite was true in the affinity chromatography, possibly because the cell surface expression or accessibility to biotinylation may be different for the two forms. Notably, the histones that bound to the F3 matrix from the cell extract did not become biotin-labeled in intact cells, but were the most prominent F3-binding bands from cell surface-biotinylated serum-starved cultures, which contain many dead cells (Fig. 2 A, b). No nucleolin band was detectable in the serum-starved cells, suggesting a lack of cell surface nucleolin expression.

Nucleolin was also detected at the cell surface of growing MDA-MB-435 in FACS[®] analysis using antibodies. Both the polyclonal NCL3 and monoclonal MS-3 antibodies bound to MDA-MB-435 cells, producing a distinct shift of the fluorescence peak relative to control IgG and nonsurface reactive antibody, respectively. That result was consistent in repeated experiments (Fig. 2 B, a and b). Gating for cells that were negative for propidium iodide uptake showed that the antinucleolin-positive cells were alive and their cell membranes were intact. We used the polyclonal antibody, which gave a stronger signal with the MDA-MB-435 cells than the monoclonal, to test cultured human umbilical vein endothelial cells (HUEVCs) for cell surface nucleolin. A small shift in the fluorescence peak was observed (Fig. 2 B, c). These results show that nucleolin is expressed on the surface of the MDA-MB-435

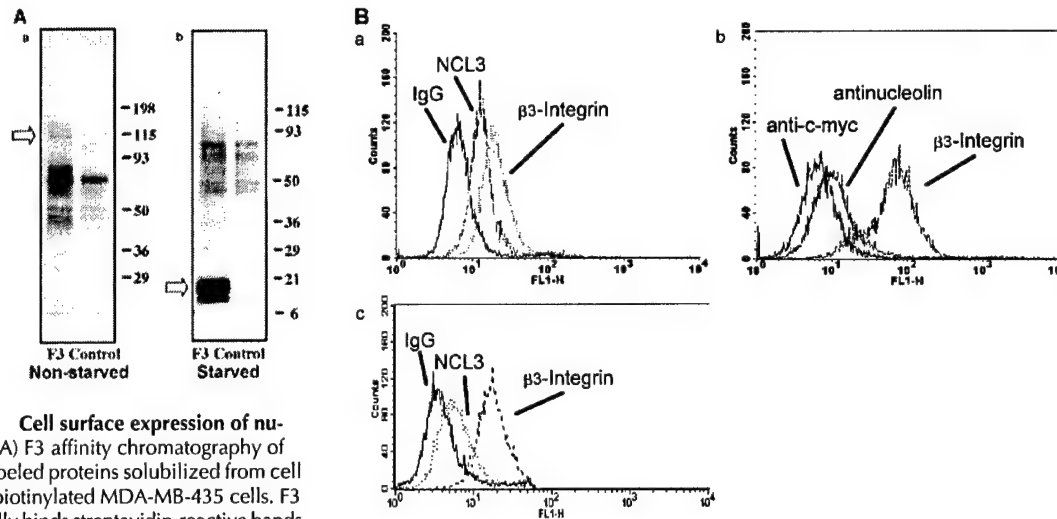


Figure 2. Cell surface expression of nucleolin. (A) F3 affinity chromatography of biotin-labeled proteins solubilized from cell surface-biotinylated MDA-MB-435 cells. F3 specifically binds streptavidin-reactive bands at 110 (arrow) and 75 kD in nonstarved cells (a). These bands are not detectable in serum-starved cells, but a set of low molecular mass bands is prominent (b, arrow). (B) FACS[®] analysis of antibody binding to MDA-MB-435 cells (a and b) and HUVECs (c). Propidium iodide-negative (living) cells were gated for the analysis. Polyclonal antinucleolin NCL3 (a and c) and monoclonal antinucleolin antibody MS-3 (b) cause a shift of the FACS[®] peak compared with controls (rabbit IgG and an isotype-matched monoclonal antibody with an unrelated specificity, respectively), indicating cell surface expression of nucleolin on the MDA-MB-435 and HUVECs. A positive control, an anti- β 3 integrin, gives a strong shift, reflecting a high cell surface expression of this integrin subunit in both types of cells.

cells and that HUVECs may also express some cell surface nucleolin. Because the presence of many dead cells prevented a FACS[®] analysis on serum-starved MDA-MB-435 cells, we used immunostaining to study their subcellular nucleolin distribution. The NCL3 antibody stained the surface of MDA-MB-435 cells when the cells were actively growing, but there was no surface staining of these cells after they were rendered stationary by serum withdrawal (Fig. 3). Nuclear nucleolin was detected in permeabilized cells under both conditions. These results agree with the cell surface biotinylation data shown in Fig. 2 and suggest that cell surface expression of nucleolin is a characteristic of actively growing cells.

Antinucleolin antibodies inhibit internalization of F3 by cells

Nucleolin has been reported to shuttle between the cytoplasm and the nucleus (Shibata et al., 2002) and between the cell surface and the nucleus (Said et al., 2002). We used antibodies to study whether nucleolin is involved in the internalization and nuclear transport of F3. As shown previously (Porkka et al., 2002), fluorescein-labeled F3 was taken up by the MDA-MB-435 cells and localized in the cytoplasm and nucleus of 100% of the cells (Fig. 4, a–c). Coincubation of the cells with the NCL3 antibody inhibited the appearance of F3 in the cytoplasm and nucleus of the cells (Fig. 4, e–g). Instead, the antibody was internalized into the MDA-MB-435 cells and transported into the nucleus. NCL2, although it bound to the MDA-MB-435 cells, was not internalized and did not inhibit the cytoplasmic and nuclear localization of F3 (Fig. 4, i–k). Neither antibody affected the internalization of the cell-penetrating peptide from the Tat protein (Fig. 4, d, h, and l). These results indicate that F3 binds to cells and is internalized by them in a nucleolin-dependent manner that involves the NH₂-terminal acidic domain of nucleolin.

Internalization of the F3 peptide into cultured cells is independent of heparan sulfates

Next, we determined whether glycosaminoglycans play a role in the internalization of F3 into cells. The F3 peptide is a highly basic peptide and, as such, has an affinity for negatively charged glycosaminoglycans. Previous studies have shown that binding to heparan sulfates can be sufficient for the internalization of a heparan sulfate-binding protein (Roghani and Mos-

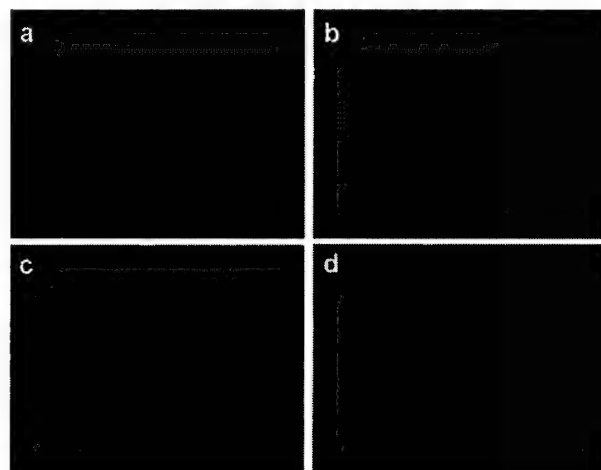
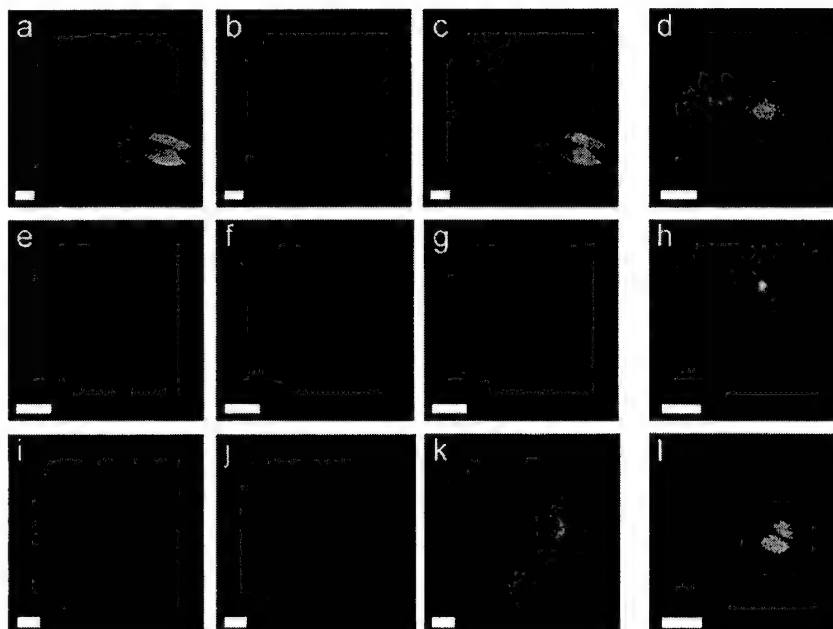


Figure 3. Subcellular distribution of nucleolin in dividing and stationary cells. MDA-MB-435 cells were cultured in standard culture media (a and c) or in media lacking serum (b and d). Nucleolin was detected using polyclonal NCL3 antibody in fixed cells without permeabilizing the cells (a and b) or after permeabilization with Triton X-100 (c and d). Nucleolin appears both on the surface and in the nuclei of the actively growing cells cultured in the standard media, but is exclusively nuclear in serum-starved cells.

Figure 4. Antinucleolin antibodies inhibit F3 internalization by cells.

Exponentially growing MDA-MB-435 cells were incubated with 1 μ M FITC-F3 or FITC-Tat peptide for 2 h at 37°C. FITC-F3 is internalized and transported into the nucleus (a, FITC-F3, green; b, red channel; c, merge). Coincubation with antinucleolin antibody NCL3 inhibits the cellular uptake and subsequent nuclear transport of the peptide (e, F3-FITC, green; f, NCL3, red; g, merge). NCL2 has no influence on uptake of F3 (i, F3-FITC, green; j, NCL2, red; k, merge). Internalization of FITC-Tat peptide (d) is not affected by NCL3 (h) or NCL2 (l). The antibodies were detected with Alexa-594 anti-rabbit IgG (red). Nuclei were stained with DAPI (blue). The images were obtained by confocal microscopy. Bars, 10 μ m.



catelli, 1992). CHO cells that produce no glycosaminoglycans because of a mutated xylosyl transferase gene (pgsA-745 cells; Esko et al., 1985) internalized fluorescein-conjugated F3 and transported it into the nucleus as efficiently as the wild-type cells (Fig. 5). Neither cell type internalized a fluorescein-conjugated control peptide. Thus, glycosaminoglycans do not seem to be involved in the uptake of the F3 peptide into cells.

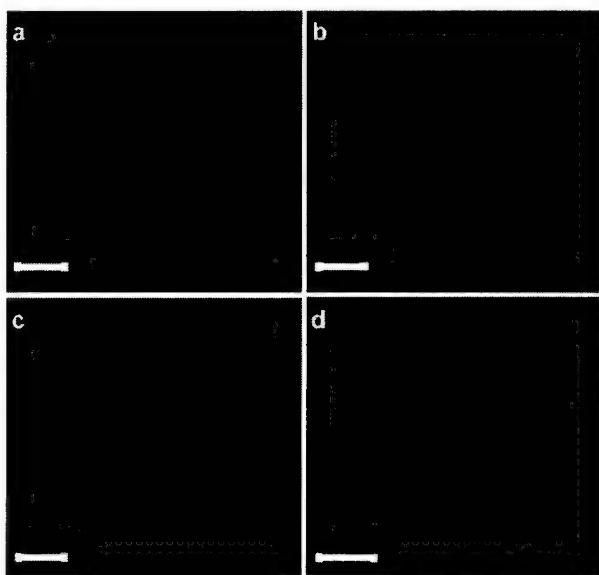


Figure 5. Glycosaminoglycan-deficient cells bind and internalize F3. FITC-F3 is internalized by the glycosaminoglycan-deficient pgsA-745 cells and transported into the nucleus. (a) pgsA-745 cells incubated with FITC-F3 and stained with DAPI to visualize the nuclei. (b and c) The same field as in panel a viewed separately for the F3 fluorescence (b) or the nuclear DAPI staining (c). (d) A FITC-labeled control peptide is not internalized by the pgsA-745 cells. The images were obtained by confocal microscopy. Bars, 10 μ m.

Circulating antinucleolin antibodies selectively localize in angiogenic blood vessels

The F3 peptide, when expressed on the surface of phage, or labeled with fluorescein or quantum dots, selectively homes to tumor blood vessels and vessels in a matrigel angiogenesis

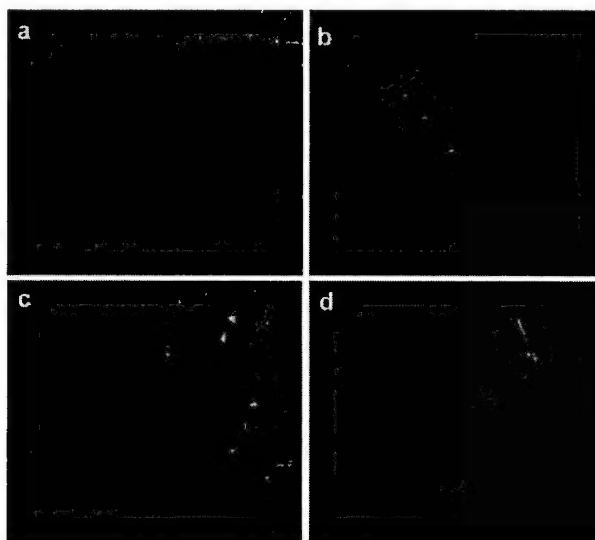


Figure 6. Intravenously injected antinucleolin antibody accumulates in tumor blood vessels. An affinity-purified rabbit antinucleolin antibody (NCL3) was injected into the tail vein of mice bearing MDA-MB-435 xenograft tumors. The tumor and various organs were removed 1 h after the injection, sectioned, and examined for the presence of rabbit IgG using Alexa-594 anti-rabbit IgG (red). Blood vessels were stained with anti-CD31 antibody (green), and nuclei were counterstained with DAPI (blue). The antinucleolin antibody has bound to tumor blood vessels (a and b), but is not seen in the skin (c). Rabbit IgG injected similarly as a control does not bind to tumor blood vessels (d).

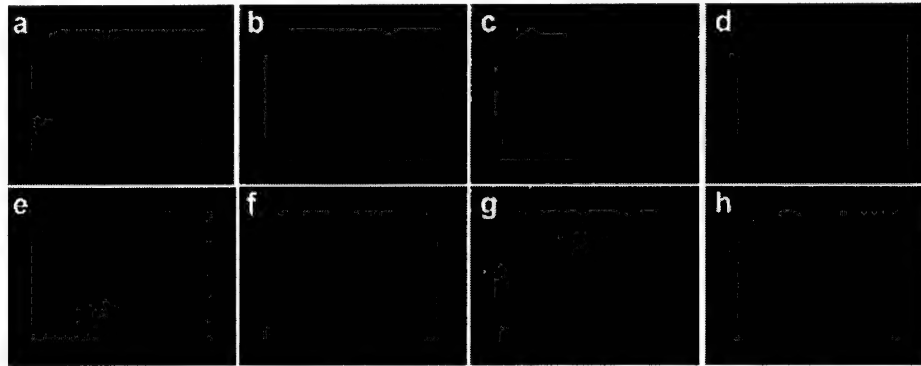


Figure 7. Cell surface nucleolin is expressed in angiogenic blood vessels. Balb/c *nu/nu* mice were subcutaneously injected with matrigel supplemented with bFGF. 8 d later, an antinucleolin antibody (NCL3) or control IgG was injected into the tail vein of the mice. The matrigel plugs were removed 1 h after the injection, sectioned, and examined for the presence of rabbit IgG using Alexa-594 anti-rabbit IgG (red). Blood vessels were stained with anti-CD31 antibody (green), and nuclei were counterstained with DAPI (blue). The injected NCL3 colocalizes the blood vessel staining in the matrigel plugs (a), but no injected rabbit IgG is detected in the plugs (e). No specific NCL3 accumulation over the IgG control is seen in any of the tissues examined: b and f, skin; c and g, heart; or d and h, brain. b–d, NCL3; f–h, IgG.

model but not to normal blood vessels. (Akerman et al., 2002; Porkka et al., 2002; Joyce et al., 2003).

To determine whether antinucleolin would similarly accumulate in tumor vessels and/or tumor cells, we intravenously injected the NCL3 antibody into mice bearing MDA-MB-435 tumors. Tissues collected 60 min after injection showed selective accumulation of the antibody in tumor blood vessels (Fig. 6, a and b). No antibody was detected in association with the tumor cells. About 70% of the tumor vessels were positive for the antibody, whereas no positive vessels were seen in the blood vessels of the normal tissues tested (skin and lung; shown for skin subcutaneous tissue in Fig. 6, c). Purified rabbit IgG, injected as a control, was not detected in tumor blood vessels (Fig. 6, d).

Next, we examined the binding of antinucleolin antibodies to angiogenic blood vessels in a nonmalignant tissue (matrigel plugs impregnated with basic FGF as an angiogenesis inducer). Intravenously injected NCL3 antibodies selectively accumulated in 70% of the blood vessels of subcutaneously implanted matrigel plugs (Fig. 7, a). Control IgG was not detectable in the matrigel plug vessels (Fig. 7, e), and NCL3 was not detectable in the blood vessels of various control organs (Fig. 7, b–d). Thus, nucleolin appears to be selectively expressed on the cell surface of angiogenic blood vessels but not on blood vessels of other tissues *in vivo*.

Discussion

Here, we show that the tumor-homing F3 peptide, which binds to and is internalized by endothelial and tumor cells (Porkka et al., 2002), interacts with nucleolin. We also show that antinucleolin antibodies detect nucleolin at the surface of cultured tumor cells and endothelial cells of angiogenic vessels *in vivo*. These results support the previously proposed role for nucleolin as a shuttle molecule between the nucleus and the cell surface, and they define cell surface nucleolin as a novel vascular marker for angiogenic endothelium.

Several approaches were used to identify the binding molecule for the F3 peptide as nucleolin. First, nucleolin and histones were identified as the main cellular proteins that

specifically bound to immobilized F3 peptide. Cell surface labeling indicated that the bound nucleolin was derived from the surface of intact cells, whereas the histones were not labeled and, therefore, likely originated from dead cells. Second, inhibition of F3 uptake into cultured cells by an antinucleolin antibody that is internalized into the nucleus provides additional evidence for the specificity of the F3–nucleolin interaction and its occurrence in intact cells. Third, the specific binding of injected antinucleolin antibodies to tumor blood vessels extends the association of F3 binding and cell surface nucleolin expression to an *in vivo* animal model.

The nucleolin polypeptide consists of a negatively charged NH₂-terminal domain, an RNA-binding domain, and a COOH-terminal domain rich in RGG motifs. The main functions of nucleolin relate to rRNA maturation and ribosome assembly (Ginisty et al., 1999; Srivastava and Pollard, 1999). Although nucleolin was originally described as a nuclear and cytoplasmic protein, a number of studies show that it can also be expressed at the cell surface (Deng et al., 1996; Larrucea et al., 1998; Said et al., 2002; Sinclair and O'Brien, 2002). Recent results also ascribe additional functions to nucleolin as a shuttle protein between the cytoplasm and the nucleus (Borer et al., 1989; Yu et al., 1998), and between the cell surface and the nucleus (Schmidt-Zachmann and Nigg, 1993; Said et al., 2002; Shibata et al., 2002). The localization of nucleolin within the cell may be regulated by phosphorylation of its NH₂ terminus (Schwab and Dreyer, 1997). Our results provide additional evidence for the cell surface localization and shuttle function of nucleolin.

The expression of nucleolin at the cell surface seems to correlate with growth and metabolic activity of cells. Both the uptake of the F3 peptide and the staining of intact cells with antinucleolin antibodies were suppressed in serum-starved cells. This may be a proliferation-related effect. An association of cell surface nucleolin expression with cell proliferation *in vitro* has been described previously (Hovanessian et al., 2000). Other factors besides proliferation may contribute to the regulation of cell surface nucleolin expression. We found only modest levels of cell surface nucleolin on actively proliferating

erating endothelial cells *in vitro*, whereas antinucleolin binding to angiogenic endothelium was readily detectable *in vivo*. The differentiation state of the cells may be a factor contributing to nucleolin regulation, as cultured human leukemia-60 cells induced to differentiate into nonproliferating macrophages lose their ability to bind F3 (unpublished data). The restricted expression of cell surface nucleolin and the cell-type specificity of the expression may explain why some investigators have not been able to document the presence of nucleolin at the cell surface (Yu et al., 1998). A similar explanation may apply to the heterogeneity of the cell surface nucleolin expression in the vasculature of tumors and matrigel plugs; local variation in endothelial cell proliferation is likely to occur in angiogenic lesions *in vivo*.

F3-displaying phage selectively homes to tumor vasculature *in vivo*, and fluorescein-tagged F3 also binds to and is taken up by endothelial cells in tumor vasculature. However, the peptide also spreads to tumor cells, and it appears in a few individual nonvascular cells in the skin and the gut (Porkka et al., 2002). Intravenously injected antinucleolin antibody was only detected in angiogenic vessels of tumors as well as of matrigel plugs. The restricted distribution of the antibody resembles that of the phage, probably because the size of phage and antibody limit their access to tissues, whereas the relatively small molecular mass of the peptide conjugate (~5 kD) may permit wider distribution. Nonetheless, each of these reagents demonstrates the specificity of cell surface nucleolin for angiogenic vessels within the vasculature.

F3 is rich in basic amino acids and binds to cell surface heparan sulfate. However, our demonstration that CHO cells lacking heparan sulfate (and other glycosaminoglycans) internalize F3 excludes a direct role of heparan sulfate as the internalizing molecule. Indeed, binding and antibody inhibition studies show that F3 internalization is mediated by cell surface nucleolin. El-Sheikh et al. (2002) have described a peptide from the heparin-binding domain of vascular endothelial growth factor that selectively homes to tumor vasculature. The authors attributed the tumor homing to affinity of the peptide for heparan sulfate. It will be interesting to see whether this peptide might also bind to nucleolin.

The internalization of the F3 peptide and NCL3 antibody may reflect a physiological function of cell surface nucleolin. Midkine is a 13-kD cytokine that, like F3, contains a high proportion of basic amino acids (Said et al., 2002). It plays a role in neurite outgrowth and neuronal differentiation, and its mRNA is up-regulated in several human carcinomas (Tsutsui et al., 1993). The internalization of midkine by cells has been reported to be nucleolin dependent (Said et al., 2002), although lipoprotein receptor-related protein can also serve as the internalizing receptor for midkine (Shibata et al., 2002). The binding site for midkine in nucleolin has been localized to the RGG domain of nucleolin (Said et al., 2002), whereas our antibody inhibition results implicate the domain rich in acidic amino acids as the binding site for F3. Cell surface nucleolin may also be involved in the activities of basic FGF, which has been shown to bind to nucleolin in nuclear extracts (Bonnet et al., 1996). Thus, F3, midkine, and possibly basic FGF, might be internalized by a nucleolin-dependent mechanism, but distinct binding sites on nucleolin may exist to mediate the uptake.

A highly basic peptide derived from the HIV Tat protein also binds to cells and is internalized by them. The Tat peptide allows internalization of conjugated proteins and is commonly used as a cell-penetrating agent (Fawell et al., 1994; Langel, 2002). It is unlikely that the Tat peptide would use nucleolin for its internalization and nuclear transport. First, the internalization of Tat is independent of the cell type, even *in vivo*, whereas our results show that cell surface nucleolin is limited, it is expressed in angiogenic endothelium but not in the blood vessels in normal tissues. Second, treatment of cells with heparinase to remove heparan sulfates inhibits internalization of the Tat peptide (Suzuki et al., 2002), whereas we found that lack of heparan sulfates did not affect F3 uptake. Third, Tat internalization is independent of temperature and does not require energy, and several other cell-penetrating peptides are similar to Tat in this regard (Langel, 2002). In contrast, F3 uptake is blocked at 4°C (Porkka et al., 2002). Finally, our antibody inhibition data also suggest that Tat peptide internalization is independent of nucleolin because an antinucleolin antibody inhibited the uptake of F3 but not of the Tat peptide.

Our laboratory has recently described yet another type of a cell-penetrating peptide, LyP-1, which is also rich in basic amino acids (Laakkonen et al., 2002). This peptide specifically homes to the endothelium of tumor lymphatics and the tumor cells in certain, but not all, tumors. The internalization of this peptide is not affected by antinucleolin antibodies (unpublished data). Thus, several different internalization mechanisms for basic peptides appear to exist, both universal and cell-type specific.

Cell-penetrating peptides rich in basic amino acids are transported into the nucleus after internalization (Langel, 2002). This is also the case with F3 and LyP-1 (Laakkonen et al., 2002; Porkka et al., 2002). Nucleolin is thought to be responsible for the nuclear transport of midkine (Shibata et al., 2002), and the same may be the case with F3. It is also possible that the multiple basic amino acids in F3 form one or more independent nuclear localization signals.

The selective *in vivo* homing of the two nucleolin-binding reagents, the F3 peptide and the NCL3 antibody, to angiogenic blood vessels establishes cell surface nucleolin as a new angiogenesis marker. Tumor blood vessels undergo angiogenesis (Hanahan and Folkman, 1996) and have specific markers in common with other angiogenic vessels (Ruoslahti, 2002). Future studies will determine whether cell surface nucleolin might play a role in angiogenesis, possibly by binding and internalizing growth factors such as midkine and bFGF. The restricted expression of cell surface nucleolin in angiogenic vessels and in tumor cells *in vivo*, and its ability to internalize molecules bound to it, make nucleolin an attractive potential target for the development of agents for vascular therapy of tumors.

Materials and methods

Cells and antibodies

MDA-MB-435 cells were grown in RPMI 1640 medium with 10% FCS and 1% Glutamine Pen-Strep (Irvine Scientific). CHO-K1 and pgsA-745 cells were grown in α MEM Earle's salt with 10% FCS and 1% Glutamine Pen-Strep. The antibodies used were mouse monoclonal antinucleolin (IgG₁; MS-3; Santa Cruz Biotechnology, Inc.) and rabbit polyclonal antibodies

raised against peptides synthesized according to the nucleolin sequence. NCL2 and NCL3 were raised against amino acids 43–51 and 221–232 of human nucleolin, respectively. The peptides were coupled to keyhole limpet hemocyanin and used to immunize rabbits according to the manufacturer's instructions. Antibodies were affinity purified from the sera on the appropriate synthetic peptide immobilized on a SulfoLink Column (Pierce Chemical Co.; 2 mg of peptide covalently coupled/column). Bound antibodies were eluted with a glycine-hydrochloride buffer, pH 2.5, and neutralized with 1 M Tris-HCl, pH 8. Each antibody immunoblotted the same 110-kD nucleolin band in cell extracts as the monoclonal antinucleolin.

F3 affinity chromatography and mass spectroscopy

Affinity purification of nucleolin from MDA-MB-435 detergent extracts was performed as described previously (Christian et al., 2001b). In brief, 6×10^6 cells were pelleted and lysed in 60 ml of RIPA buffer (1% Triton X-100, 0.5% deoxycholic acid, 0.1% SDS, 10 mM Tris-HCl, pH 7.6, 150 mM NaCl, and 1% protease inhibitor cocktail for mammalian cells; Sigma-Aldrich). The lysate was incubated with 20 μ l F3 (AKVKDEPQRSARLSAKPAPPKPEPKPKAPAKK) affinity matrix (2 mg of peptide covalently coupled to 1 ml of affigel 10). Control fractionation was performed on a 34-amino acid peptide that represents a scrambled version of F3. The matrix beads were washed three times with 0.025% Triton X-100, 50 mM Tris-HCl, pH 8.4, 150 mM NaCl, 1 mM CaCl₂, and 0.02% azide; washed twice with 25 mM Tris-HCl, pH 8.4, and 250 mM NaCl; and the bound proteins were eluted with 30 μ l SDS gel sample buffer. The affinity-purified proteins were reduced with 50 mM DTT and separated on an 8–20% polyacrylamide gel and visualized by colloidal blue staining (Invitrogen). The molecular masses of the gel bands were determined by comparing to the standards in an Alphamanager instrument (Alpha Innotech Corp.). Bands that appeared in the F3 eluate, but not in the control, were cut out, digested with trypsin, and analyzed by mass spectroscopy using a matrix-assisted laser desorption/ionization, time of flight instrument (model Voyager DE-PRO; Applied Biosystems) using an α -cyano-4-hydroxycinnamic acid/nitrocellulose matrix.

Immunoblot analysis

Cell extracts or affinity-purified samples were separated on an SDS-PAGE and transferred onto nitrocellulose membranes for 1 h at 100 V. The membranes were blocked overnight at 4°C with 5% milk powder in TBS-T (140 mM NaCl, 10 mM Tris-HCl, pH 7.4, and 0.05% Tween) and incubated with mouse monoclonal or rabbit polyclonal antinucleolin antibody (10 μ g/ml in TBS-T) for 1 h at RT. After extensive washing, the membranes were incubated with peroxidase-coupled rabbit anti-mouse or goat anti-rabbit antibody, and bound antibody was detected with ECL (Amersham Biosciences) and exposure to Biomax MR (Kodak).

Cell surface biotinylation

For cell surface expression analysis, MDA-MB-435 cells (5×10^6 cells) were washed three times with cold PBS on a cell culture plate and incubated with biotinylation buffer (20 mM HEPES, pH 7.45, 5 mM KCl, 130 mM NaCl, 0.8 mM MgCl₂, 1 mM CaCl₂, and 0.5 mg/ml EZ link Sulfo-NHS-Biotin; Pierce Chemical Co.) for 1 h at 4°C. After the removal of the reagent, the cells were washed three times with wash buffer (50 mM Tris, pH 7.5, 150 mM NaCl, 1 mM MgCl₂, and 1 mM CaCl₂) and lysed in 1% Triton X-100 lysis buffer for 1 h. The lysates were centrifuged for 15 min at 15,000 g. F3 binding proteins were isolated by affinity chromatography as described above, separated on SDS-PAGE, and transferred to nitrocellulose. The nitrocellulose membranes were incubated after blocking with Extravidin-peroxidase conjugates diluted at 1:5,000 (Sigma-Aldrich) for 1 h at RT. Bands were detected after incubation with ECL reagent and exposure to Biomax MR.

FACS analysis of cell surface nucleolin

For FACS[®] analysis, MDA-MB-435 or HUVEC were detached with EDTA and 10^6 cells/sample were incubated with either polyclonal rabbit antinucleolin antibody NCL3 (10 μ g/ml) or monoclonal antinucleolin antibody MS-3 (Santa Cruz Biotechnology, Inc.; 10 μ g/ml) for 45 min on ice. Cells were washed with ice-cold PBS and incubated with Alexa-488 (Molecular Probes) secondary antibody (1:50 in PBS). As a negative control, the cells were incubated with 10 μ g/ml of rabbit IgG or with 10 μ g/ml monoclonal anti-c-myc antibody (Santa Cruz Biotechnology, Inc.), followed by the secondary antibody. As a positive control, the cells were incubated with 10 μ g/ml of mouse monoclonal anti- β_2 -integrin (CBL 479; Cymbus Biotechnology Ltd.). The antibody-treated cells were washed and resuspended in 50 μ l PBS containing 2 μ g/ml propidium iodide to distinguish between live and dead cells, and 10,000 cells per sample were analyzed using a FACSCalibur flow cytometer.

Detection of peptides and antibodies in cells and tissues

For internalization experiments, cells were incubated with 1 μ M of fluorescein-conjugated peptide for 2 h at 37°C. The cells were washed with PBS, fixed with 4% PFA in PBS, and analyzed by confocal microscopy. The cell-penetrating basic peptide from the human immunodeficiency virus Tat protein (GRKKRRQRRR; Fawell et al., 1994) was used as a positive control in the internalization experiments. To detect nucleolin, cells were fixed with 4% PFA in PBS and stained with 10 μ g/ml antinucleolin antibodies either directly or after permeabilization with Triton X-100. Bound antibodies were detected with Alexa-594-labeled anti-rabbit antibody (Molecular Probes) and visualized by fluorescence microscopy.

In vivo distribution of circulation-accessible cell surface nucleolin was examined in mice bearing xenograft tumors or basement membrane (matrigel) plugs. Xenograft tumors were generated by subcutaneously injecting exponentially growing MDA-MB-435 human breast cancer cells (10^6 cells in 200 μ l of culture media) into the mammary fat pad area of 2-mo-old Balb/c *nu/nu* mice (Animal Technologies). The animals were used for experiments 8 wk after injection. Nontumor angiogenesis was studied in matrigel plugs (Fulgham et al., 1999; Ngo et al., 2000). 2-mo-old Balb/c *nu/nu* mice were subcutaneously injected with 100 μ l of Matrigel (Becton Dickinson) at two or three locations in the abdominal area. Each 100- μ l plug contained 100 ng of recombinant human bFGF as an angiogenesis stimulant (R&D Systems). The animals were used for antibody injection experiments 8 d after the implantation.

In vivo distribution of antibodies was studied by intravenously injecting mice with 200 μ g of polyclonal rabbit antinucleolin antibody or rabbit IgG. 1 h after the injection, the mice were anesthetized, perfused through the heart with 10 ml PBS, and killed by infusing 10 ml of 4% PFA in PBS. Tumors or matrigel plugs, along with various control tissues were removed, fixed in 4% PFA, and frozen in OCT embedding medium (Tissue-Tek). All procedures were performed under anesthesia induced by intraperitoneal injection of 2,2,2-tribromoethanol (Avertin) at a dosage of 0.4–0.75 mg/gram of body weight (500–700 μ l/mouse). All animal experiments were approved by the Animal Review Committee of the Burnham Institute.

For histological analyses, 5- μ m sections were cut. The injected rabbit antinucleolin antibody and anti-CD31 antibody (10 μ g/ml; BD Biosciences) applied on the tissue sections were detected with Alexa-594- and Alexa-488-conjugated secondary antibodies, respectively. The sections were examined under an inverted fluorescent microscope (Nikon) or a confocal microscope (Bio-Rad Laboratories). Nuclei were counterstained using DAPI (Vector Laboratories).

We thank Dr. Ed Monosov, Jennifer Freund, and Jeff Nickel for their help with microscopy; Dr. Fernando Ferrer for peptide synthesis; and Tristan Williams for mass spectroscopy.

This work was supported by grants from the National Cancer Institute (CA82713), the Department of Defense (DAMD 17-02-1-0315; given to E. Ruoslahti), and the Cancer Center (CA30199). S. Christian is supported by a fellowship from the Deutsche Forschungsgemeinschaft.

Submitted: 24 April 2003

Accepted: 7 October 2003

References

- Akerman, M.E., W.C. Chan, P. Laakkonen, S.N. Bhatia, and E. Ruoslahti. 2002. Nanocrystal targeting in vivo. *Proc. Natl. Acad. Sci. USA* 99:12617–12621.
- Arap, W., R. Pasqualini, and E. Ruoslahti. 1998. Cancer treatment by targeted drug delivery to tumor vasculature in a mouse model. *Science* 279:377–380.
- Bergers, G., R. Brekken, G. McMahon, T.H. Vu, T. Itoh, K. Tamaki, K. Tanzawa, P. Thorpe, S. Itohara, Z. Werb, and D. Hanahan. 2000. Matrix metalloproteinase-9 triggers the angiogenic switch during carcinogenesis. *Nat. Cell Biol.* 2:737–744.
- Bonnet, H., O. Filhol, I. Truchet, P. Brethenou, C. Cochet, F. Amalric, and G. Bouche. 1996. Fibroblast growth factor-2 binds to the regulatory beta subunit of CK2 and directly stimulates CK2 activity toward nucleolin. *J. Biol. Chem.* 271:24781–24787.
- Borer, R.A., C.F. Lehner, H.M. Eppenberger, and E.A. Nigg. 1989. Major nucleolar proteins shuttle between nucleus and cytoplasm. *Cell* 56:379–390.
- Brooks, P.C., S. Silletti, T.L. von Schalscha, M. Friedlander, and D.A. Cheresh. 1998. Disruption of angiogenesis by PEX, a noncatalytic metalloproteinase fragment with integrin binding activity. *Cell* 92:391–400.
- Christian, S., H. Ahorn, A. Koehler, F. Eisenhaber, H.P. Rodi, P. Garin-Chesa, J.E. Park, W.J. Rettig, and M.C. Lenter. 2001a. Molecular cloning and

- characterization of endosialin, a C-type lectin-like cell surface receptor of tumor endothelium. *J. Biol. Chem.* 276:7408–7414.
- Christian, S., H. Ahorn, M. Novatchkova, P. Garin-Chesa, J.E. Park, G. Weber, F. Eisenhaber, W.J. Rettig, and M.C. Lenter. 2001b. Molecular cloning and characterization of EndoGlyx-1, an EMILIN-like multisubunit glycoprotein of vascular endothelium. *J. Biol. Chem.* 276:48588–48595.
- Deng, J.S., B. Ballou, and J.K. Hofmeister. 1996. Internalization of anti-nucleolin antibody into viable HEp-2 cells. *Mol. Biol. Rep.* 23:191–195.
- El-Sheikh, A., C. Liu, H. Huang, and T.S. Edgington. 2002. A novel vascular endothelial growth factor heparin-binding domain substructure binds to glycosaminoglycans in vivo and localizes to tumor microvascular endothelium. *Cancer Res.* 62:7118–7123.
- Eliceiri, B.P., and D.A. Cheresh. 1999. The role of alphav integrins during angiogenesis: insights into potential mechanisms of action and clinical development. *J. Clin. Invest.* 103:1227–1230.
- Esko, J.D., T.E. Stewart, and W.H. Taylor. 1985. Animal cell mutants defective in glycosaminoglycan biosynthesis. *Proc. Natl. Acad. Sci. USA.* 82:3197–3201.
- Fawell, S., J. Seery, Y. Daikh, C. Moore, L.L. Chen, B. Pepinsky, and J. Barsoum. 1994. Tat-mediated delivery of heterologous proteins into cells. *Proc. Natl. Acad. Sci. USA.* 91:664–668.
- Ferrara, N., and K. Alitalo. 1999. Clinical applications of angiogenic growth factors and their inhibitors. *Nat. Med.* 5:1359–1364.
- Fulgham, D.L., S.R. Widhalm, S. Martin, and J.D. Coffin. 1999. FGF-2 dependent angiogenesis is a latent phenotype in basic fibroblast growth factor transgenic mice. *Endothelium.* 6:185–195.
- Ginisty, H., H. Sicard, B. Roger, and P. Bouvet. 1999. Structure and functions of nucleolin. *J. Cell Sci.* 112:761–772.
- Hanahan, D., and J. Folkman. 1996. Patterns and emerging mechanisms of the angiogenic switch during tumorigenesis. *Cell.* 86:353–364.
- Harms, G., R. Kraft, G. Grelle, B. Volz, J. Dornedde, and R. Tauber. 2001. Identification of nucleolin as a new L-selectin ligand. *Biochem. J.* 360:531–538.
- Hood, J.D., M. Bednarski, R. Frausto, S. Guccione, R.A. Reisfeld, R. Xiang, and D.A. Cheresh. 2002. Tumor regression by targeted gene delivery to the neovasculature. *Science.* 296:2404–2407.
- Hovanessian, A.G., F. Puvion-Dutilleul, S. Nisole, J. Svab, E. Perret, J.S. Deng, and B. Krust. 2000. The cell-surface-expressed nucleolin is associated with the actin cytoskeleton. *Exp. Cell Res.* 261:312–328.
- Hynes, R.O. 2002. A reevaluation of integrins as regulators of angiogenesis. *Nat. Med.* 8:918–921.
- Joyce, J.A., P. Laakkonen, M. Bernasconi, G. Bergers, E. Ruoslahti, and D. Hanahan. 2003. Stage-specific vascular markers revealed by phage display in a mouse model of pancreatic islet tumorigenesis. *Cancer Cell.* In press.
- Laakkonen, P., K. Porkka, J.A. Hoffman, and E. Ruoslahti. 2002. A tumor-homing peptide with a targeting specificity related to lymphatic vessels. *Nat. Med.* 8:751–755.
- Langel, Ü. 2002. Cell-Penetrating Peptides: Processes and Applications. CRC Press, Boca Raton, FL. 406 pp.
- Larrucea, S., C. Gonzalez-Rubio, R. Cambroner, B. Ballou, P. Bonay, E. Lopez-Granados, P. Bouvet, G. Fontan, M. Fresno, and M. Lopez-Trascasa. 1998. Cellular adhesion mediated by factor J, a complement inhibitor. Evidence for nucleolin involvement. *J. Biol. Chem.* 273:31718–31725.
- Ngo, C.V., M. Gee, N. Akhtar, D. Yu, O. Volpert, R. Auerbach, and A. Thomas-Tikhonenko. 2000. An in vivo function for the transforming Myc protein: elicitation of the angiogenic phenotype. *Cell Growth Differ.* 11:201–210.
- Nilsson, F., H. Kosmehl, L. Zardi, and D. Neri. 2001. Targeted delivery of tissue factor to the ED-B domain of fibronectin, a marker of angiogenesis, mediates the infarction of solid tumors in mice. *Cancer Res.* 61:711–716.
- Pasqualini, R., E. Koivunen, R. Kain, J. Lahdenranta, M. Sakamoto, A. Stryhn, R.A. Ashmun, L.H. Shapiro, W. Arap, and E. Ruoslahti. 2000. Aminopeptidase N is a receptor for tumor-homing peptides and a target for inhibiting angiogenesis. *Cancer Res.* 60:722–727.
- Porkka, K., P. Laakkonen, J.A. Hoffman, M. Bernasconi, and E. Ruoslahti. 2002. A fragment of the HMG2 protein homes to the nuclei of tumor cells and tumor endothelial cells in vivo. *Proc. Natl. Acad. Sci. USA.* 99:7444–7449.
- Roghani, M., and D. Moscatelli. 1992. Basic fibroblast growth factor is internalized through both receptor-mediated and heparan sulfate-mediated mechanisms. *J. Biol. Chem.* 267:22156–22162.
- Ruoslahti, E. 2002. Specialization of tumour vasculature. *Nat. Rev. Cancer.* 2:83–90.
- Said, E.A., B. Krust, S. Nisole, J. Svab, J.P. Briand, and A.G. Hovanessian. 2002. The anti-HIV cytokine midkine binds the cell surface-expressed nucleolin as a low affinity receptor. *J. Biol. Chem.* 277:37492–37502.
- Schmidt-Zachmann, M.S., and E.A. Nigg. 1993. Protein localization to the nucleolus: a search for targeting domains in nucleolin. *J. Cell Sci.* 105:799–806.
- Schwab, M.S., and C. Dreyer. 1997. Protein phosphorylation sites regulate the function of the bipartite NLS of nucleolin. *Eur. J. Cell Biol.* 73:287–297.
- Shibata, Y., T. Muramatsu, M. Hirai, T. Inui, T. Kimura, H. Saito, L.M. McCormick, G. Bu, and K. Kadomatsu. 2002. Nuclear targeting by the growth factor midkine. *Mol. Cell. Biol.* 22:6788–6796.
- Sinclair, J.F., and A.D. O'Brien. 2002. Cell surface-localized nucleolin is a eukaryotic receptor for the adhesin intimin-gamma of enterohemorrhagic *Escherichia coli* O157:H7. *J. Biol. Chem.* 277:2876–2885.
- Srivastava, M., and H.B. Pollard. 1999. Molecular dissection of nucleolin's role in growth and cell proliferation: new insights. *FASEB J.* 13:1911–1922.
- St Croix, B., C. Rago, V. Velculescu, G. Traverso, K.E. Romans, E. Montgomery, A. Lal, G.J. Riggins, C. Lengauer, B. Vogelstein, and K.W. Kinzler. 2000. Genes expressed in human tumor endothelium. *Science.* 289:1197–1202.
- Suzuki, T., S. Futaki, M. Niwa, S. Tanaka, K. Ueda, and Y. Sugiyama. 2002. Possible existence of common internalization mechanisms among arginine-rich peptides. *J. Biol. Chem.* 277:2437–2443.
- Tsutsui, J., K. Kadomatsu, S. Matsubara, A. Nakagawara, M. Hamanoue, S. Takao, H. Shimazu, Y. Ohi, and T. Muramatsu. 1993. A new family of heparin-binding growth/differentiation factors: increased midkine expression in Wilms' tumor and other human carcinomas. *Cancer Res.* 53:1281–1285.
- Yu, D., M.Z. Schwartz, and R. Petryshyn. 1998. Effect of laminin on the nuclear localization of nucleolin in rat intestinal epithelial IEC-6 cells. *Biochem. Biophys. Res. Commun.* 247:186–192.

Drug Identification through in vivo Screening of Chemical Libraries

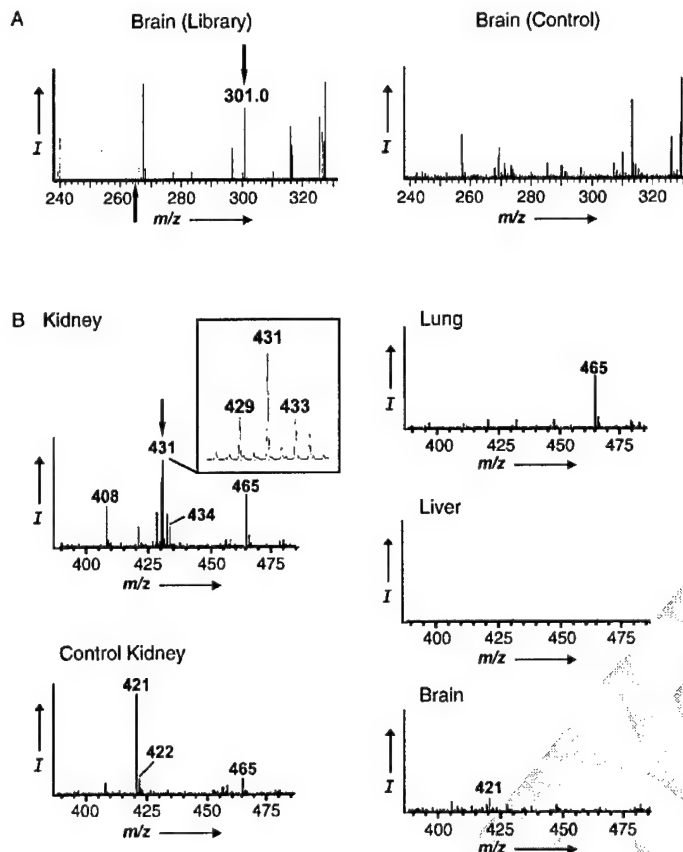
Darren M. Brown, Maurizio Pellecchia, and
Erkki Ruoslahti^{*[a]}

Specific cell-surface molecules can direct leukocytes and certain tumor cells to particular organs.^[1–3] Recent work by our group has shown that peptides, selected by using the in vivo phage-screening approach, are also capable of mediating selective in vivo localization of phages to individual organs as well as tumors.^[4–6] To develop our targeting technology beyond peptide-based systems, we investigated the feasibility of screening a chemical library to identify small molecules other than peptides that possess a preferential affinity for particular organs or tissues. As a proof of principle, we screened two different chemical libraries in vivo and identified three compounds that preferentially accumulated in individual organs: a pharmacologically active benzodiazepine localized in the brain, another compound specifically homed in on the liver, and the third on the kidneys. These results show that it is possible to use in vivo chemical-library screening to identify compounds that distribute themselves to specific sites in the body. Such knowledge can focus drug discovery on compounds with promising pharmacokinetic and tissue specificity profiles.

For in vivo screening of chemical libraries, we injected mixtures of small molecules into the circulation of mice, harvested selected organs in organic solvent to precipitate proteins, and detected the presence of compounds from the library in the soluble phase by mass spectrometry. We initially tested a library of ten compounds. Mass-spectrometric analysis of extracts from organs harvested 10 min after the intravenous injection of the library showed that one compound preferentially accumulated in the brain (Figure 1A). Breaking the code for the compounds revealed this 301 Da compound to be a benzodiazepine known as Oxazepam.^[7] A biologically inactive 265 Da benzodiazepine also present in the library was not detected in the brain (Figure 1A). Thus, it appeared possible to obtain organ-targeting small molecules by screening chemical libraries in vivo. We also learned from these early studies that it was easier to detect library compounds and differentiate them from endogenous tissue molecules in organic extracts analyzed by electrospray mass spectrometry when the library molecules had molar masses greater than 300 Da.

To test a larger library, we assembled a mixture of 75 compounds with molar masses between 300 and 600 Da and screened for compounds that home in on the brain, liver, lungs, or kidneys. Mass spectrometry performed on organ extracts from library-injected mice identified ten molecules as candidate organ-homing compounds. These ten compounds

[a] Dr. D. M. Brown, Prof. M. Pellecchia, Prof. E. Ruoslahti
Cancer Research Center, The Burnham Institute
10901 North Torrey Pines Road, La Jolla, CA 92037 (USA)
Fax: (+1) 858-646-3198
E-mail: ruoslahti@burnham.org



were tested individually for their ability to specifically target individual organs. Compounds 5862461 and 6074428 were found to accumulate in the kidneys (Figure 1B and C). The other tissues tested negative for these two compounds. Compound 5343617 was found primarily in the liver and, to a lesser extent, the lungs and kidneys (Figure 1D). The spectral patterns of compounds 5862461 and 5343617 were particularly distinct because these compounds contain bromine, which exists as two equally abundant natural isotopes,^[8] and causes a characteristic two-mass-unit split in the spectral peak (Figure 1B, inset). One compound accumulated in the lungs, kidneys, and liver, but not the brain; and another localized to the brain, kidneys, and liver, but not the lungs (data not shown). These compounds are likely to bind to receptors that are expressed in more than one tissue, but the varying tissue selectivity of these compounds clearly indicates tissue-specific homing. Extracts from the organs of control-injected mice confirmed that no molecules matched the spectral pattern of the homing compounds. Two other candidate organ-homing compounds localized to all four tested organs. These compounds might bind to molecules present in all tissues, but it is also possible that their concentration in blood remaining in tissues is high enough to allow detection. As these compounds did not show any tissue-specific homing, we did not study them further. For three compounds, the specific organ homing could

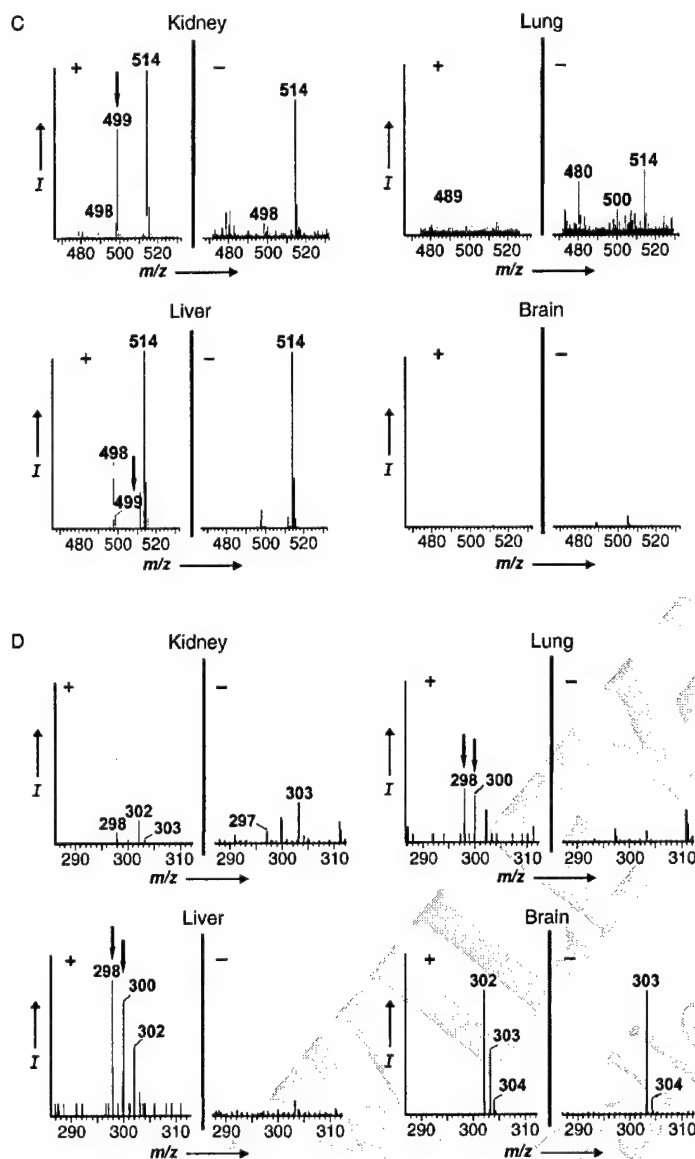


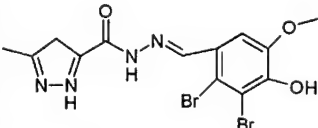
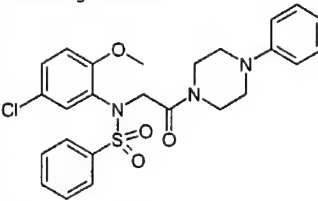
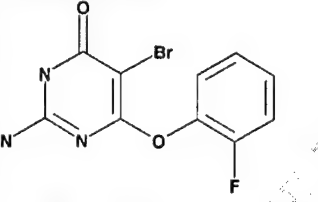
Figure 1. In vivo targeting of small molecules to particular organs. A) Detection of the benzodiazepine, Oxazepam, in the brain 10 min after intravenous injection with a ten-compound library. "Control" mice were injected with vehicle alone. The downward pointing arrow denotes the spectral peak for Oxazepam. The arrow below the axis denotes the m/z of the biologically inactive benzodiazepine in the library. No peak is seen at this position. B–D) Mice were intravenously injected with individual compounds from the 75-member library, and tissues were analyzed 10 min later by mass spectrometry. B) Detection of compound 5862461 in the kidneys after intravenous injection and circulation for 10 min. "Control" denotes mice injected just with DMSO. C) Compound 6074428 targets the kidneys ■■ or lungs? ■■■. D) Compound 5343617 targets the liver and lungs. Compound peak heights are shown as relative signal intensity (I). A "+" denotes compound-injected mice and "-" denotes DMSO-injected mice. The downward pointing arrows mark the spectral peaks for the organ-homing compounds.

not be confirmed in individual testing. The remaining 68 compounds were not detected in any tissue, apparently because they did not sufficiently accumulate in any of the test tissues to bring the concentration above the detection limit.

We next quantified the organ accumulation of the three compounds with the most promising organ-homing proper-

ties. We used the mass spectrometer to compare the relative amounts of targeting compound in extracts of different organs. Compound 6074428 was at least 30-fold more concentrated in the lungs ■■or kidneys?■■ than in the liver, kidneys, and brain (Table 1). At least 2.4 times more compound

Table 1. Homing specificity of compounds and their accumulation in target organs. The structure, target organ, and homing activity of the three organ-homing compounds are shown. The quantity of homing compound in the target organs 10 min after an intravenous injection of individual compounds was determined as described in the Experimental Section. The accumulation of targeting compound was expressed as normalized signal intensity level relative to the detection limit.

Organ-targeting Compound	Target Organ(s)	Signal Intensity ^[a] (fold higher than detection limit)
 ChemBridge 5862461	kidney	2.4-fold (± 0.6)
 ChemBridge 6074428	kidney	32-fold (± 5.4)
 ChemBridge 5343617	■■lung?■■ liver lung	67-fold (± 2.1) 8.2-fold (± 0.6)
	kidney	1.2-fold (± 0.3)

[a] Accumulation data is represented as mean percentage (\pm standard deviation) for two experiments per variable.

5862461 localized to the kidneys than to the liver, lungs, and brain. Compound 5343617 accumulated very strongly in the liver; about 55-fold higher levels were detected in the liver than in the kidneys, which contained a trace amount of the compound. This compound was also present at moderate levels in the lungs, but was not detectable in the brain. As each of these three compounds accumulated in different tissues ■■see above■■, their organ-selective homing is clearly specific and not due to the presence of blood or unspecific trapping in the target organs.

We then measured two parameters that influence the sensitivity of in vivo chemical-library screening. First, we used the mass spectrometer to analyze the spectral intensity of nine different compounds added to organ extracts, and found that the smallest amount of an individual compound that could be

detected in a tissue extract was between 34 and 215 pmol. For the second parameter, we determined the smallest amount of homing compound that could be injected and still detected in our *in vivo* screening system. For this analysis, the signal intensity of compound 6074428 in kidney extracts from mice injected with various amounts (2 to 125 nmol) of the compound was determined by mass spectrometry. The spectral peak at m/z 499 from compound 6074428 was detectable in kidney extracts from mice injected with as little as 7.8 nmol of targeting compound (Figure 2). In the initial library screen with 75

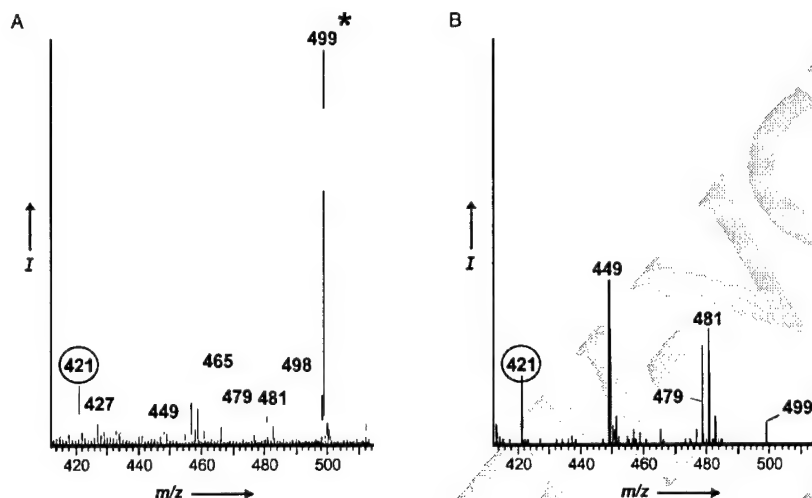


Figure 2. The lower detection limit of *in vivo* chemical-library screening. Mass-spectrometric analysis of kidney extracts from mice injected with either A) 125 nmol or B) 7.8 nmol of compound 6074428. The peak intensities were normalized to the height of an endogenous tissue molecule at m/z 421 that was consistently detected in kidney extracts (circled). The asterisk denotes the spectral peak for the kidney-homing compound, 6074428. The spectral peak intensities of other endogenous tissue molecules (e.g. the molecules at m/z 449 and 481) varied between experiments; as a result, they were not used to normalize the spectral peak intensities of compound 6074428. Compound peak heights are shown as relative signal intensity (I).

compounds, about 33 nmol of each molecule was present in the injected library mix. Therefore, it is likely that 300 compounds could be tested in a single screening round for organ-targeting compounds. Given the ease and simplicity of this screening technique, a library of 10 000 compounds could be screened *in vivo* in a few weeks with a relatively small-scale effort.

We encountered some limitations with *in vivo* chemical-library screening that will be addressed in future studies. The volume of library injected into the mice (25 μ L) was limited by the toxicity of the solvent, dimethyl sulfoxide (DMSO). With a less toxic solvent, it should be possible to inject up to 200 μ L of library and screen potentially as many as 3600 compounds in one round. Emulsifying agents like Cremophor® EL, Emulphor®, polysorbate 80, Solutol® HS15, or solvents containing *N*-methylpyrrolidone could be used as an alternative to DMSO when solubilizing the chemical library before *in vivo* screening. In addition, only 1% of the organ extract could be analyzed by mass spectrometry due to the presence of various endogenous tissue compounds in the acetone extracts. A more selective ex-

traction and prepurification method could increase the sensitivity of the compound detection by mass spectrometry.

The biological basis for the targeting activity of some of the compounds identified in the screen has yet to be determined. However, it seems likely that binding to benzodiazepine receptors mediated the brain-homing activity of the pharmacologically active benzodiazepine, as the related inactive compound did not accumulate in the brain. The kidney-homing compound, 6074428, contains a benzenesulfonamide group that is known to have diuretic properties; perhaps this group mediates the kidney-homing activity of this compound.

This work provides the first demonstration that it is possible to conduct large-scale screening of chemical libraries *in vivo*. Such screening can identify targeted small molecules for use in a variety of applications and has some advantages over previous methods. *In vivo* phage screening primarily targets the vascular endothelium. Low-molecular-weight chemical compounds can target the vasculature, but are also likely to gain access to parenchymal cells in tissues. That parenchymal cells can be targets is suggested by our recovery of a benzodiazepine as a brain-homing molecule, as most receptors for these compounds are on the neurons. As an additional advantage, this screening approach does not require encoded or tagged library compounds. This is an improvement over other approaches that require separate chemistries for coupling different small molecules to synthetic or genetically engineered tags such as bacteriophages.^[9] In addition, the absence of compound tags eliminates the possibility of interference by the tag with the *in vivo* homing activity.

The localization of selective molecules to specific "addresses" on the endothelium suggests that each tissue puts a specialized signature on its vasculature.^[10] Organ-specific vascular molecules are attractive targets for the delivery of therapeutics to particular sites. By conjugating targeting moieties to drugs, diseases such as cancer can be treated with increased efficacy and fewer side effects;^[11,12] phage-derived homing peptides and peptidomimetics have been used in this manner to target malignant tumors.^[11–15] Organ-homing compounds isolated from chemical libraries are likely to be useful for similar purposes.

In vivo screening may also identify small molecules that have pharmacological effects at the target organ. The identification of a neuroactive compound and a potential diuretic as brain- and kidney-homing molecules, respectively, suggests that this may be possible. Thus, *in vivo* screening has the potential to advance drug discovery; it allows pharmacokinetics and specificity of action to be studied among large numbers of candidate compounds, or even from completely random libraries. Such approaches may accelerate the discovery and development of new drugs.

Experimental Section

A library of ten small molecules with molecular weights between 200 and 300 Da was prepared by a person not involved in the *in vivo* experimentation and was tested blindly. The ten-compound library was prepared in phosphate buffer (40 mM, pH 7.2) with each

molecule at a final concentration of 1 mM. A larger library of small molecules was prepared from 75 organic molecules (purchased from ChemBridge, San Diego, CA) with molecular weights between 300 and 600 Da. The library compounds were randomly selected from a 420 000-member ChemBridge library, with each compound satisfying the following criteria: 1) the partition coefficient, expressed numerically as $\log P$, was less than 5 and 2) the molecular weights of the compounds differed from each other by at least 4 Da. There was high structural diversity in the library, given that the only limitation was the compounds selected from the 420 000-member parent library needed to fit the parameters described above. The 75-compound library was resuspended in DMSO, with each molecule at a final concentration of 1.33 mM.

To identify molecules that localize to particular organs, two-month-old female Balb/c mice were anesthetized with avertin ($0.15 \mu\text{L g}^{-1}$) administered intraperitoneally. In experiments with the ten-compound library, 200 μL of library solution (200 nmol per compound) was intravenously injected into the tail vein. With the 75-compound library, 25 μL of library solution (33 nmol per compound) was intravenously injected into the tail-vein. After 10 min of circulation, the lungs, liver, kidneys, and brain were removed. We found 5–15 min to be optimal for the screening of intravenously injected phage for homing to individual tissues and tumors,^[16] and we wanted to keep the time short enough to prevent metabolism of the injected compounds, which would change their mass-spectrometric signature.

The organs were washed with PBS (5 mL) to remove excess blood and weighed. Each organ was mixed with acetone (5 mL) and then homogenized with a Handishear hand-held homogenizer (Virtis, Gardiner, NY). For certain organ homogenates, a control compound (ChemBridge 5116670, molar mass 340 Da, 0.25–2.5 nmol) was added as a reference to quantify the amount of homing compound in target organs. The organ/acetone homogenates were transferred to 15 mL centrifuge tubes and incubated at -80°C for 12 h to precipitate the proteins. Following centrifugation for 30 min at 3000 g and 4°C , the supernatants were recovered and dried in a Speed Vac. A set of control organ extracts was also prepared from mice that were injected with pure DMSO (25 μL).

The dried organ extracts were resuspended in methanol (100 μL), spun in a vortex for about 10–20 min, and separated in a centrifuge to give pellet debris and supernatant. The supernatants were recovered, further diluted 1:20 in methanol, and the diluted sample (20 μL) was analyzed on a Waters Micromass[®] LCT mass spectrometer (Milford, MA) at The Scripps Research Institute (La Jolla, CA). The mobile phase of the liquid chromatography was run with methanol/water/acetonitrile (90:9:1). By comparing the masses of the individual compounds and the molecules in the organ extracts of mice injected with DMSO to the molecules in the organ extracts from the mice injected with the library, we were able to identify molecules in the library that localized to a particular organ.

The accumulation of compounds in organs was measured as follows:

We first measured the signal intensities of the targeting compounds using the mass spectrometer and compared them to the signal intensity of a standard compound that was added to the organ extracts; this enabled us to normalize the intensity value of compound peaks from experiments performed on different days. We then determined the smallest amount of an individual compound that could be detected in a tissue extract using mass spectrometry by measuring the spectral intensity of nine different compounds added in small amounts to organ extracts. The detection

limit was defined as the spectral intensity level halfway between the background noise and the spectral intensity level generated from the smallest detectable amount of compound in organ extracts (averaged from nine different compounds whose spectra were analyzed and displayed with a scanning window of m/z 290–610). The normalized intensity values for homing compounds were compared to the detection limit to determine the degree of enrichment of compound in target organs relative to background levels. These enrichment values were not comparable from compound to compound, since each compound has a different ionization efficiency and stability on the mass spectrometer.

The Burnham Institute Animal Research Committee approved the animal experimentation in compliance with the relevant US laws.

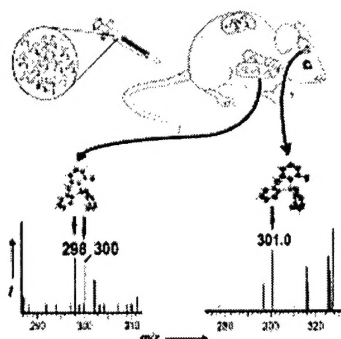
Acknowledgements

This work was supported by the U.S. National Cancer Institute (P01 CA82713 and P30 CA30199) and the U.S. Department of Defense (DAMD17-02-1-0315). D.M.B. was supported by Post-doctoral training grant T32 CA09579 from the U.S. National Cancer Institute. We thank Dr. Eva Engvall for her valuable comments on the manuscript, and Roslind Varghese for editing.

Keywords: drug delivery • in vivo screening • mass spectrometry • tissue-specificity

- [1] I. J. Fidler, *Surg. Oncol. Clin. North Am.* **2001**, *10*, 257.
- [2] A. Müller, B. Horney, H. Soto, N. Ge, D. Catron, M. E. Buchanan, T. McClanahan, E. Murphy, W. Yuan, S. N. Wagner, J. L. Barrera, A. Mohar, E. Verastegui, A. Zlotnik, *Nature* **2001**, *410*, 50.
- [3] E. J. Kunkel, E. C. Butcher, *Immunity* **2002**, *16*, 1.
- [4] R. Pasqualini, E. Ruoslahti, *Nature* **1996**, *380*, 364.
- [5] D. Rajotte, W. Arap, M. Hagedorn, E. Koivunen, R. Pasqualini, E. Ruoslahti, *J. Clin. Invest.* **1998**, *102*, 430.
- [6] P. Laakkonen, K. Porkka, J. A. Hoffman, E. Ruoslahti, *Nat. Med. (N.Y. U.S.)* **2002**, *8*, 751.
- [7] *title?* **11th rev. ed.** (Eds.: K. Z. Bezchlibnyk-Butler, J. J. Jeffries), Huber, Seattle, **2001**, p. 273.
- [8] *title?* **84 ed.** (Ed.: D. R. Lide), CRC Press, Boca Raton, **2003**, p. 11.
- [9] T. F. Woiwode, J. E. Haggerty, R. Katz, M. A. Gallop, R. W. Barrett, W. J. Dower, S. E. Cwirla, *Chem. Biol.* **2003**, *10*, 847.
- [10] E. Ruoslahti, *Nat. Rev. Cancer* **2002**, *2*, 83.
- [11] W. Arap, W. Haedicke, M. Bernasconi, R. Kain, D. Rajotte, S. Krajewski, H. M. Ellerby, D. E. Bredesen, R. Pasqualini, E. Ruoslahti, *Proc. Natl. Acad. Sci. USA* **2002**, *99*, 1527.
- [12] F. Curnis, A. Sacchi, L. Borgna, F. Magni, A. Gasparri, A. Corti, *Nat. Biotechnol.* **2000**, *18*, 1185.
- [13] J. D. Hood, M. Bednarski, R. Frausto, S. Guccione, R. A. Reisfeld, R. Xiang, D. A. Cheresh, *Science* **2002**, *296*, 2404.
- [14] D. Hallahan, L. Geng, S. Qu, C. Scarfone, T. Giorgio, E. Donnelly, X. Gao, J. Clanton, *Cancer Cell* **2003**, *3*, 63.
- [15] W. Arap, R. Pasqualini, E. Ruoslahti, *Science* **1998**, *279*, 377.
- [16] J. A. Hoffman, P. Laakkonen, K. Porkka, M. Bernasconi, E. Ruoslahti in *Phage Display: A Practical Approach* (Eds.: T. Clackson, H. Lowman), Oxford University Press, Oxford, **2004**.

Received: November 19, 2003 [Z300824]



D. M. Brown, M. Pellecchia,
E. Ruoslahti*

■■ - ■■

Drug Identification through
in vivo Screening of
Chemical Libraries

Drug discovery process stood on its head? A proof-of-principle study has shown that large numbers of chemical compounds can be tested for selective accumulation in individual tissues in live mice. The picture shows how the site of accumulation of the tail-vein-injected molecules could be determined by mass spectrometry. The process picks drug candidates based on tissue specificity and pharmacokinetics rather than defined activity, which is the usual starting point of drug discovery.